GULF GENERAL ATOMIC

Gulf-GA-A12599

HTGR BASE PROGRAM
QUARTERLY PROGRESS REPORT
FOR THE PERIOD ENDING
MAY 31, 1973

Prepared under
Contract AT(04-3)-167
Project Agreement No. 17
for the
San Francisco Operations Office
U.S. Atomic Energy Commission

Gulf General Atomic Project 317

Date Published - June 29, 1973

GULF GENERAL ATOMIC COMPANY
P.O. BOX 81608, SAN DIEGO, CALIFORNIA 92138

QUARTERLY REPORT SERIES

GA-4072-December, 1962, through February, 1963
GA-4350-March, 1963, through May, 1963
GA-4569-June, 1963, through August, 1963
GA-4937-September, 1963, through November, 1963
GA-5104-December, 1963, through February, 1964
GA-5366-March, 1964, through May, 1964
GA-5618-June, 1964, through August, 1964
GA-5866-September, 1964, through November, 1964
GA-6113-December, 1964, through February, 1965
GA-6418-March, 1965, through May, 1965
GA-6671-June, 1965, through August, 1965
GA-6869-September, 1965, through November, 1965
GA-7010-December, 1965, through February, 1966
GA-7181-March, 1966, through May, 1966
GA-7396-June, 1966, through August, 1966
GA-7553-September, 1966, through November, 1966
GA-7801-December, 1966, through February, 1967
GA-7981-March, 1967, through May, 1967
GA-8200-June, 1967, through August, 1967
GA-8356-September, 1967, through November, 1967
GA-8530-December, 1967, through February, 1968
GA-8662-March, 1968, through May, 1968
GA-8860-June, 1968, through August, 1968
GA-9090-September, 1968, through November, 1968
GA-9227-December, 1968, through February, 1969
GA-9372-March, 1969, through May, 1969
GA-9660-June, 1969, through August, 1969
GA-9815-September, 1969, through November, 1969
GA-9944-December, 1969, through February, 1970
GA-10088-March, 1970, through May, 1970
GA-10288-June, 1970, through August, 1970
GA-10399-September, 1970, through November, 1970
GA-10501-December, 1970, through February, 1971
GA-10661-March, 1971, through May, 1971
Gulf-GA-A10784-June, 1971, through August, 1971
Gulf-GA-A10930-September, 1971, through November, 1971
Gulf-GA-A10999-December, 1971, through February, 1972
Gulf-GA-A12150-March, 1972, through May, 1972
Gulf-GA-A12222-June, 1972, through August, 1972
Gulf-GA-A12422-September, 1972, through November, 1972
Gulf-GA-A12515-December, 1972, through February, 1973

ABSTRACT

This publication continues the quarterly report series on the HTGR Base Program. The Program covers items of the base technology of the High-Temperature Gas-cooled Reactor (HTGR) system. The development of the HTGR system will, in part, meet the greater national objective of more effective and efficient utilization of our national resources. The work reported here includes studies of basic fission-product distribution mechanisms, recycle fuel studies (including designing and testing of recycle test elements) and exploration of head-end reprocessing methods (as part of a national recycle plan and of a recycle fuel plan), and physics and fuel management studies. Materials studies include irradiation and analysis of fuel particles in capsules to evaluate fuel systems, and basic studies of control materials and of carbon and graphite. Experimental procedures and results are discussed and, where appropriate, the data are presented in tables, graphs, and photographs. More detailed descriptions of experimental work are presented in topical reports, and these are listed at the end of the report for those concerned with the field.

INTRODUCTION

This report covers the work performed by Gulf General Atomic under U.S. Atomic Energy Commission Contract AT(04-3)-167, Project Agreement No. 17. This Project Agreement calls for support of basic technology associated with gas-cooled, nuclear power reactor systems. The program is based on the concept of the High-temperature Gas-cooled Reactor (HTGR) developed by Gulf General Atomic.

Large HTGR systems will be placed in operation starting in the late 1970's following the operation of the 330-MW(e) prototype in 1973. Characteristics of these advanced systems include:

1. A single-phase gas coolant allowing generation of high-temperature, high-pressure steam with consequent high-efficiency energy conversion and low thermal discharge.

2. A prestressed concrete reactor vessel (PCRV) offering advantages in field construction, primary system integrity, and stressed member inspectability.

3. Graphite core material assuring high-temperature structural strength, large temperature safety margins, and good neutron economy.

4. Thorium fuel cycle leading to U-233 fuel which allows good utilization of nuclear resources and minimum demands on separative work.

CONTENTS

FIGURES

TABLES

TASK IV
FISSION PRODUCT MECHANISMS

FIPER CODE DEVELOPMENT

The FIPER codes are used to calculate metallic fission product release from an HTGR core. The release calculation is for a basically simple physical problem, and an effort is being made to demonstrate, in simple form, the important parameters that govern fission product release. A grasp of the overall transport process is very useful for a simple preliminary evaluation of the effect of changing reactor operating conditions or of changes in any of the input parameters (by uncertainties in their values or by new measurements). A great utility also lies in more easily determining the effect of changes in core design characteristics or in indicating fruitful directions for product improvement efforts.

A very simple and straightforward approach has worked quite well. To date, attention has been focused on cesium release. The diffusion coefficient used for cesium diffusion through graphite is sufficiently large so that steady-state concentration profiles are established in times which are short compared with the fuel block service length in-core. To a good approximation, it can then be assumed that the time evolution of release occurs while maintaining at all times a steady-state concentration profile across the graphite web. This is not true for the lowest temperature blocks, but it is true for the sufficiently large fraction of the blocks which dominate the release.

Figure 4-1 shows the results of FIPER calculations where the fuel blocks are ordered according to their release. The curves show that a relatively few blocks are the source of most of the released cesium. One curve was calculated by use of the FIPER S code, which has a relatively

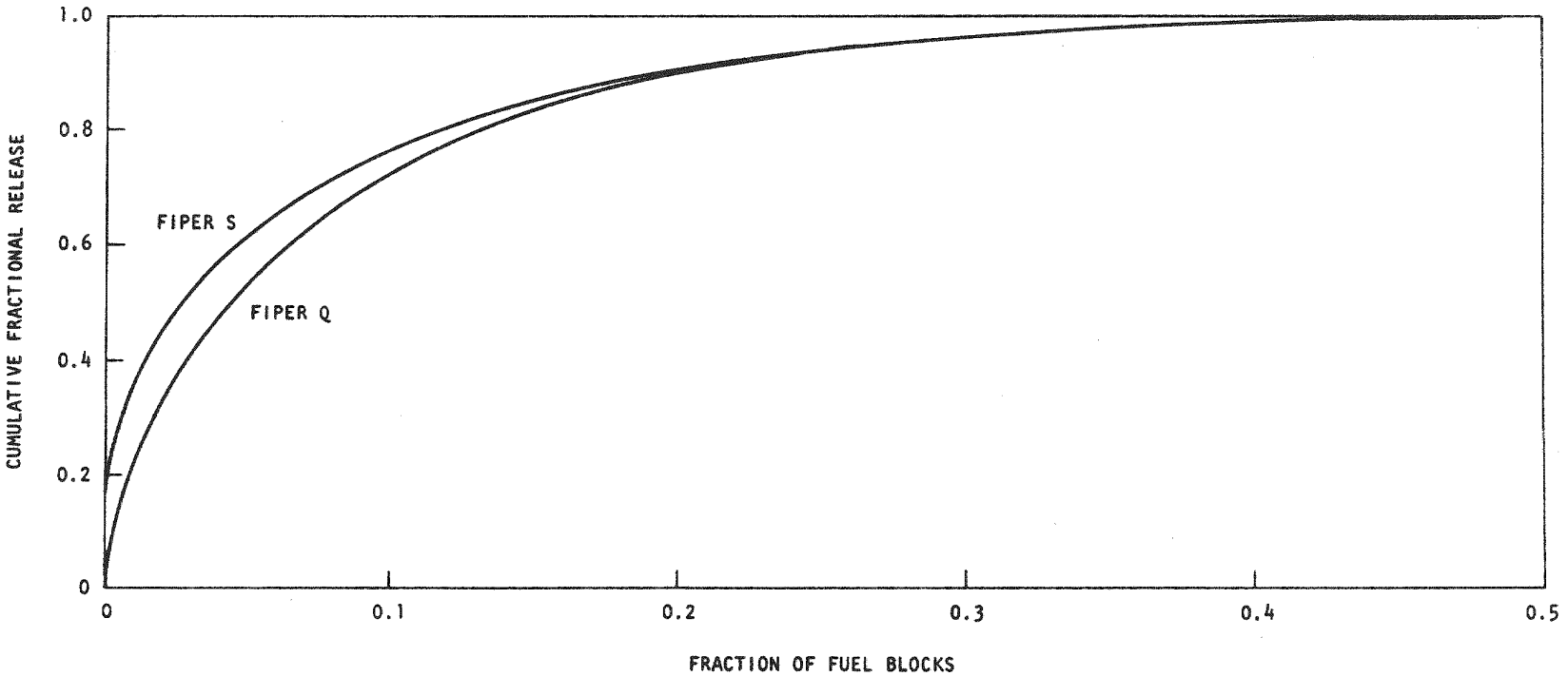

Fig. 4-1. Release distribution from core for the case of blocks ordered according to their release

short computing time obtained by incorporating various approximations into the code. The other curve is estimated from the first and correlates with what would be expected for a more time-consuming FIPER Q calculation; it is closer to the actual distribution since FIPER S is known to overestimate.

A derivation of the release rate follows. Initially, the power (fission rate), temperature, and helium flow are assumed constant, and the fractional release to the helium coolant is assumed small.

FIPER S assumes linear fuel particle failure with time, i.e.,

$$f = \alpha t \quad .$$

It does not distinguish between fissile and fertile particles and, therefore, the fission product content of each particle is assumed to be

$$i = \beta t \quad ,$$

where β is proportional to power. Release from failed particles is rapid, so that the fuel rod concentration of fission product is

$$c = fi = \alpha\beta t^2 \quad .$$

The inner graphite concentration is simply

$$C_i = \frac{c}{\phi} = \frac{\alpha\beta}{\phi} t^2 \quad .$$

The next step, to determine C_o, the outside surface concentration, is not quite so simple, but can be managed as follows.

The flux across the graphite is

$$j(G) = D\frac{\Delta C}{\Delta X} \equiv \delta(C_i - C_o) \quad ,$$

where D is the diffusion coefficient. The flux through the helium boundary layer film is

$$j(He) = Kv \equiv \varepsilon C_o^n \quad ,$$

where K is the mass transfer coefficient and v is the cesium vapor concentration in equilibrium with the condensed phase concentration C_o; ε is temperature and helium flow dependent, and n is temperature dependent with values n = 1.7 or 2.0 at 1000° or 800°C.

Equating these two fluxes, since they must be equal at steady state,

$$\delta(C_i - C_o) = \varepsilon C_o^n \quad ,$$

and C_o can be determined in terms of C_i by simple means. Figure 4-2 is a plot showing the ratio C_o/C_i.

It is clear that there are two limiting cases to consider. These are when the release is rate limited either by diffusion across the graphite ($C_o \simeq o$) or, on the other hand, by transport through the helium boundary layer film at the graphite surface ($C_o \simeq C_i$). The continuation of the derivation now diverges into two paths.

The graphite diffusion flux is rate limiting for high temperatures and high cesium concentrations. To a first approximation the release flux is

$$J = j(G) = \delta(C_i - C_o) \simeq \delta C_i = \frac{\alpha\beta\delta}{\phi} t^2 \quad .$$

The total release from time zero is

$$G = \int_o^\tau J \, dt = \frac{\tau}{3} J_f \quad ,$$

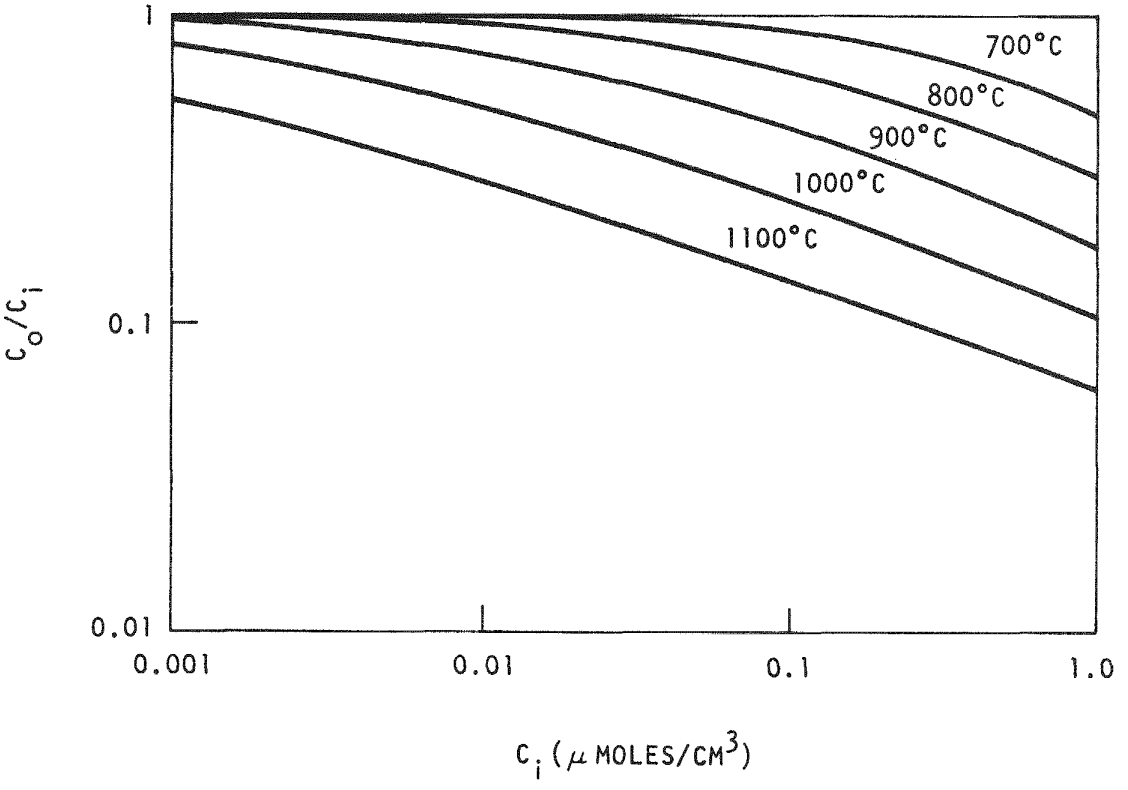

Fig. 4-2. Effect of temperature and concentration on C_o/C_i, where C_o and C_i are outer and inner graphite concentrations

where J_f is the final value of the flux at time τ. The time average release is

$$J_{ave} = \frac{1}{3} J_f \quad .$$

J_f is easily evaluated, and the average flux is simply 1/3 of this final value.

For the film limiting case (low temperature and low concentration), in a similar manner

$$J_{ave} = \frac{1}{2n + 1} J_f \quad .$$

Since n is the range 1.7 to 2.0, 1/(2n + 1) is in the range 1/4.4 to 1/5. This result differs by less than a factor of two from that for the graphite limiting case, and estimating the correct factor for the transition region cannot introduce much error.

Reduction of the FIPER computer code calculation to a simple desk-top calculation allows for some relatively easy parametric studies (for example, failure fraction or temperature variations). These may be accomplished analytically if the time variation of the parameter permits integration of the flux or, if not, graphical integration will permit essentially any variation. An example is given in Fig. 4-3 where release rates and cumulative release are shown for two different linear temperature variations with time and are compared with curves for a constant temperature case. All three histories represent the same average operating temperature.

FISSION PRODUCT DEPOSITION LOOP STUDIES

Work on the fission product deposition loop has continued. The objectives of this work are to obtain plateout distribution data and to obtain liftoff data by subjecting sections of the loop to conditions of higher

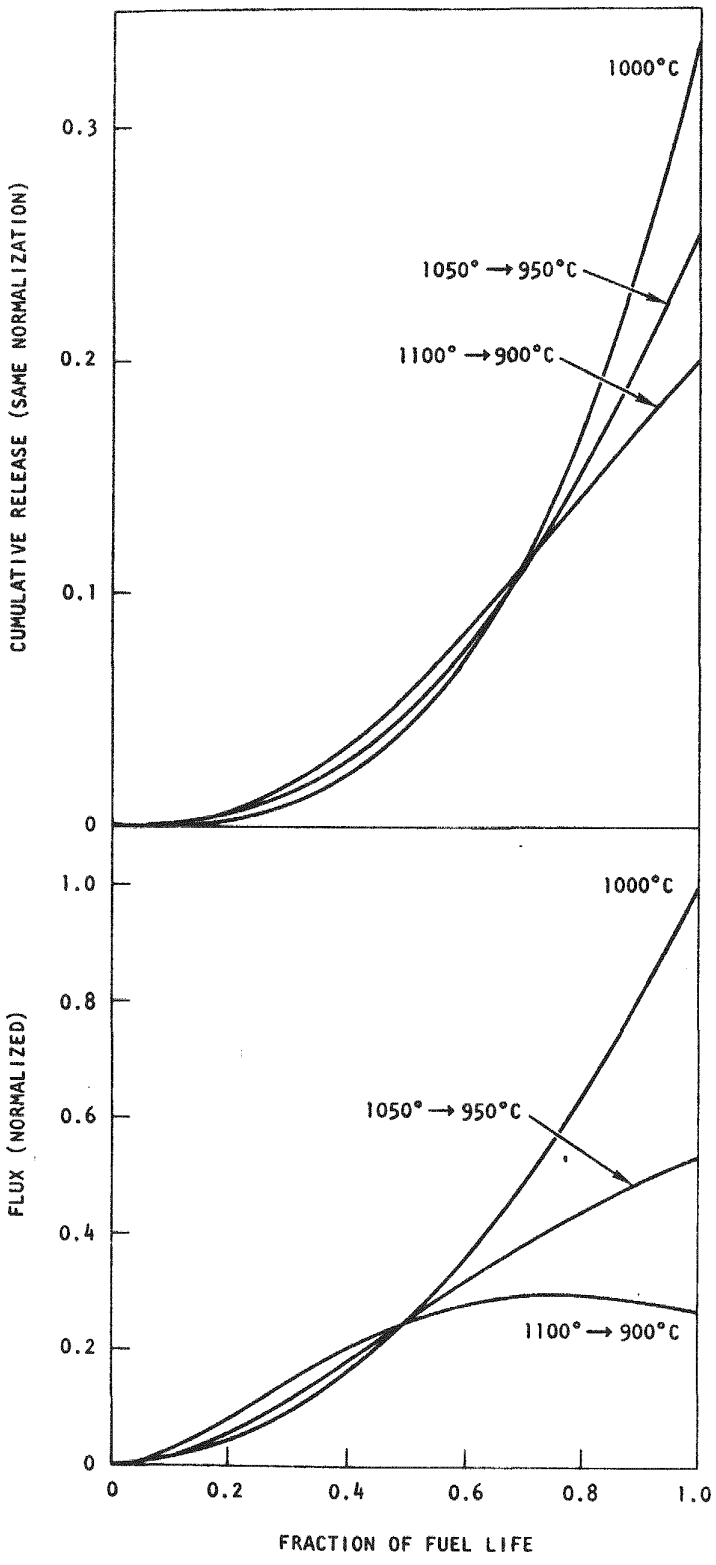

Fig. 4-3. Effect of temperature variations on release rates and cumulative release

shear ratios than obtained in the loop. The plateout data are used to test and refine the PAD code, which has been developed at Gulf General Atomic for predicting the fission product plateout distribution in an HTGR primary coolant circuit. The liftoff data are used for safety analyses associated with HTGR depressurization accidents.

The deposition loop, described in an earlier Quarterly Progress Report (GA-10399), is mounted in a 5-ft, high-pressure, high-temperature autoclave. Helium at 350 psia circulates in the loop with Reynolds numbers in the range of 15,000 and temperatures varying from 150° to 320°C. The type of steel used for the loop tubing is representative of steel used in the steam generators of HTGRs. Surface temperatures in the loop vary from 150° to 400°C. The source of fission products in the loop is obtained by heating graphite crucibles within the loop that are loaded with the fission products sorbed on graphite matrix material. Four loop experiments have been conducted.

The data obtained so far in the loop experiments are being evaluated, and a report is in preparation which will provide a complete description of the methods and results of the first four deposition loop experiments.

Experimental work on deposition loop experiment No. 4 is nearing completion. The depositing nuclide was cesium tagged with Cs-137. Since the chilled section of the loop was not operative during this experiment, relatively higher loop temperatures (300° to 400°C) were obtained. The plateout distribution obtained clearly showed the effect of flow disturbers and generally an exponential decrease in activity with distance from the source; however, the reported activities (cpm/cm) for the two legs of the loop differed by as much as a factor of three. A possible explanation is spurious behavior of the counting system. A number of samples are to be recounted to check this possibility. The liftoff and wipedown tests are about 50% completed, and the results to date indicate very low blowdown fractions.

In order to augment the results obtained from the deposition loop and to assist in the verification of the PAD code, a review of the available

plateout literature has been conducted. Numerous researchers have explored this subject, particularly those at ORNL, BMI, and Dragon. Dragon efforts have included the disassembly of primary heat exchangers from the Dragon reactor for measurement of the plateout of fission products such as I-131 and Cs-137. Since large portions of these data are available in Dragon Project reports, this information could be of considerable assistance in interpretation of deposition loop results.

A PAD model of the Dragon reactor has been prepared and is now operational. The model was constructed from material gleaned from Dragon reports, but many assumptions were necessary. The model could be considerably improved if more detailed information, such as circuit geometry and coolant transit times, were in hand . Efforts are also compromised by the scanty amount of sorption isotherm data available to describe the behavior of cesium and iodine on steels. Using this approximate PAD model, efforts are under way to calculate Dragon plateout activity distributions for comparison with observed data.

VAPOR PRESSURE STUDIES

The vapor pressure of cesium sorbed on H-327 graphite is being studied using the Knudsen cell mass spectrometric method. The objective of this work is to extend the vapor pressure data to low concentrations (below 10 ppm), comparable to presently predicted end-of-life concentrations of cesium in fuel element graphite at the graphite-helium interface. The low concentration data are important for use in refining predicted releases of cesium nuclides in HTGR systems.

Cesium isotherms are measured by integrating the observed rate of cesium effusion from a Knudsen cell to give a pressure versus concentration description. Mass spectrometric signals and a description of cesium content before and after sample depletion are required for the determination of effusion rates.

The cesium vapor pressure studies have yielded a surprising result. The vapor pressure data (or isotherms) have shown a downward pressure break at about 5 ppm cesium. A systematic investigation is being directed toward determining if this pressure break is real. If this investigation demonstrates that the break is real, it can lead to a significant reduction in the predicted release of cesium nuclides in HTGR systems.

A mass spectrometric experiment utilizing a two-compartment Knudsen cell has been devised to study the pressure break. The two-compartment Knudsen cell is illustrated in Fig. 4-4. Compartment A is supplied with a normal sample (or with a sample partially depleted in cesium), while compartment B is supplied with an undoped graphite sample. The progress of cesium loss from the normal sample can be followed by observing the effusate from its outer orifice, while progress of the cesium loss (and therefore cesium pressure) from the second cell can be followed by observing the effusate from its outer orifice. The undoped graphite during the experiment is loaded at a measured rate through an orifice connecting the two Knudsen cell compartments. Loading and unloading isotherms are derived from these data. If the loading and unloading isotherms are consistent with the anticipated observed cesium pressure break in the unloading isotherm, the break will be proven to originate from thermodynamic properties of the system; if they are not consistent, a kinetic problem would be inferred. This study constitutes no more than the classical experiment of approaching a supposed equilibrium situation from concentrations both higher and lower than the projected equilibrium values to prove that true equilibrium exists.

In preparation for this study, the effusion properties of the three orifices have been determined by experiments with silver contained in either and both of the compartments.

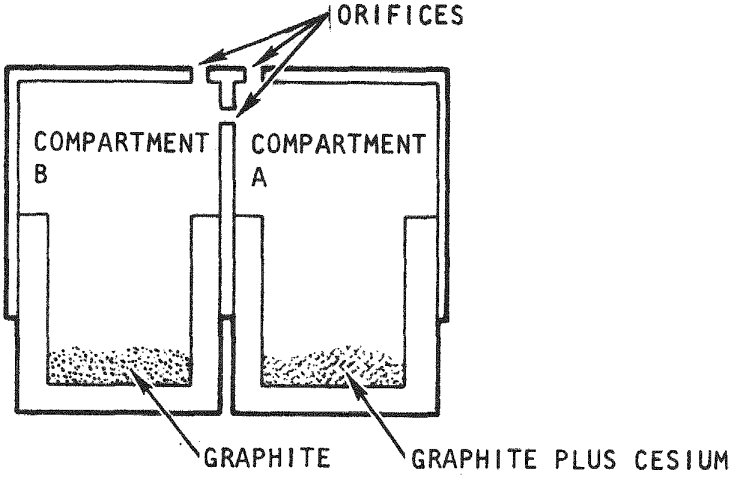

Fig. 4-4. Two-compartment Knudsen cell

TASK V
RECYCLE FUEL STUDIES

HTGR FUEL RECYCLE PLANT STUDY

Plant cross-section elevation drawings have been prepared from the preliminary layout drawing for the 45,000-MW(e) economy recycle plant shown in Fig. 5-1, Sheet 1. Drawings with the basic elevations for each area of the plant have now been completed (Fig. 5-1, Sheets 2-6).

Reference fuel element definitions were compiled for the spent fuel element going into reprocessing and for the refabricated recycle fuel element. The element definitions were developed using current 1160-MW(e) HTGR mass flow data for the selective recycle fuel system. The data assumed elements irradiated for a full 4-year cycle followed by a decay period after removal from the reactor of 6 months. In the selective recycle fuel system, U-235 is used twice in the reactor, the first time as virgin makeup U-235 and the second time, recycled after recovery and refabrication of the partially spent U-235. As makeup U-235 and recycle U-235, the uranium is not diluted with fertile material, and the fuel particle is TRISO coated. The TRISO coating is required for selective separation from the BISO coated U-233 fuel stream in the HTGR fuel reprocessing plant.

Afterheat generation data were calculated for the reference spent fuel element and the refabricated fuel element. A total afterheat generation of 1400 Btu/hr, at the end of a 6-month decay period, was calculated for the average spent fuel element. The U-235 containing TRISO coated fissile particle fraction contributes 550 Btu/hr, with the remaining 850 Btu/hr occurring from the BISO coated recycle fissile particles plus the fertile particles. Forty percent of the total afterheat is due to the

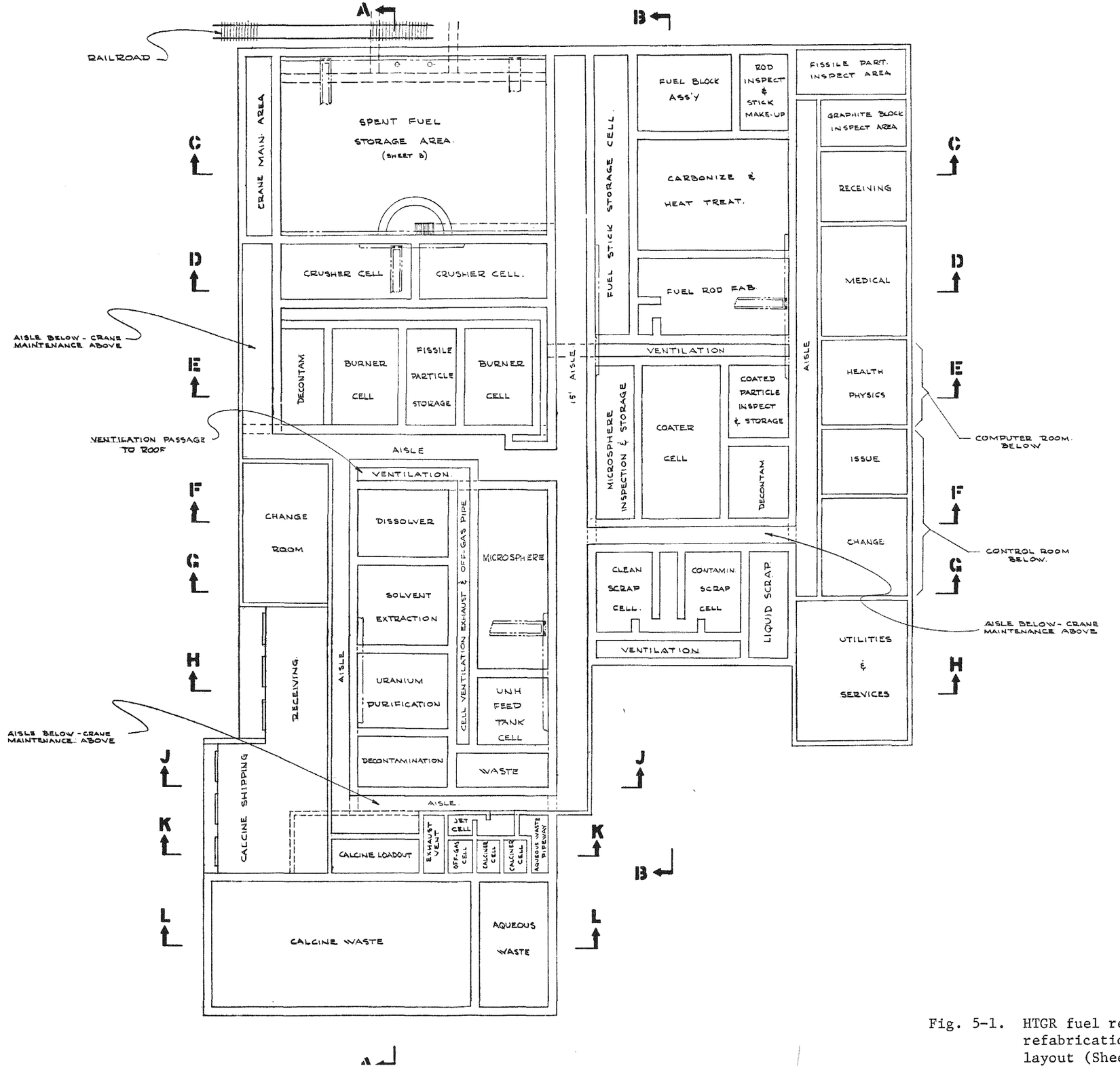

Fig. 5-1. HTGR fuel reprocessing-refabrication plant layout (Sheet 1 of 6)

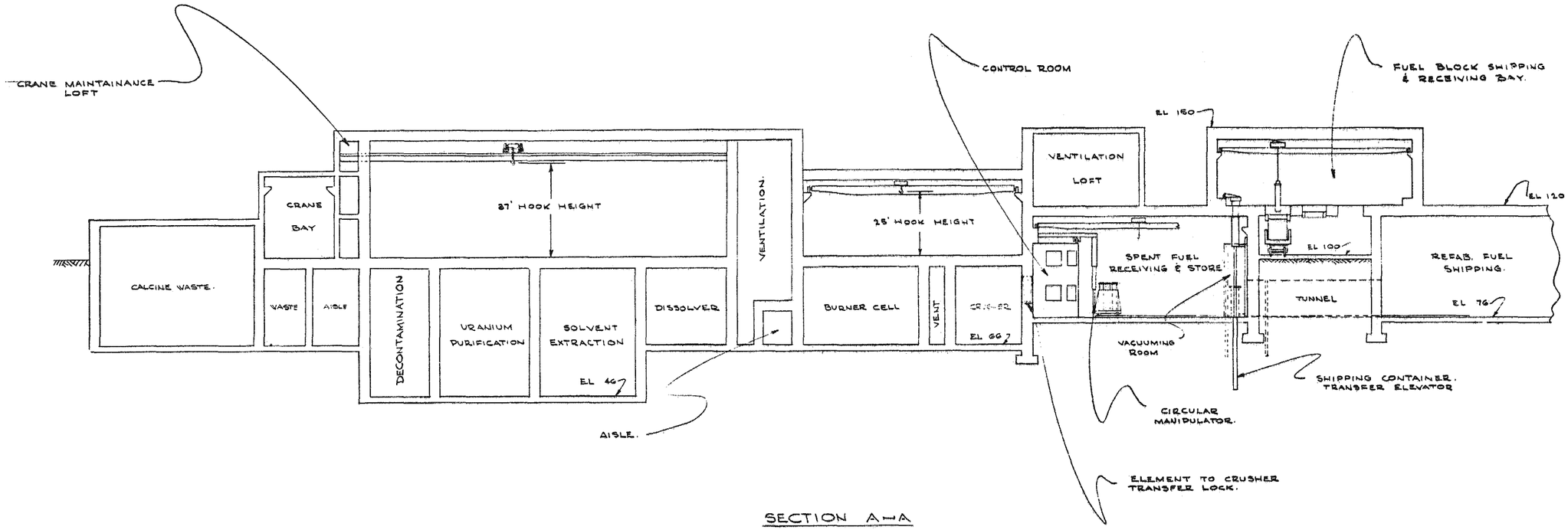

SECTION A-A

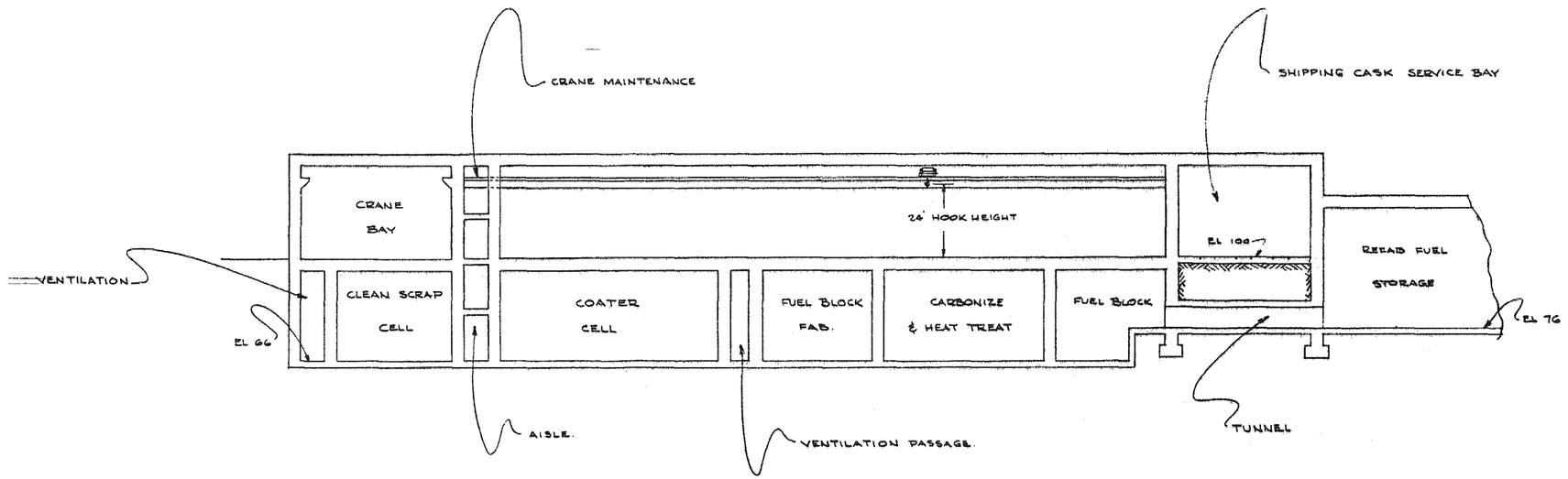

SECTION B-B

Fig. 5-1. HTGR fuel reprocessing-refabrication plant layout (Sheet 2 of 6)

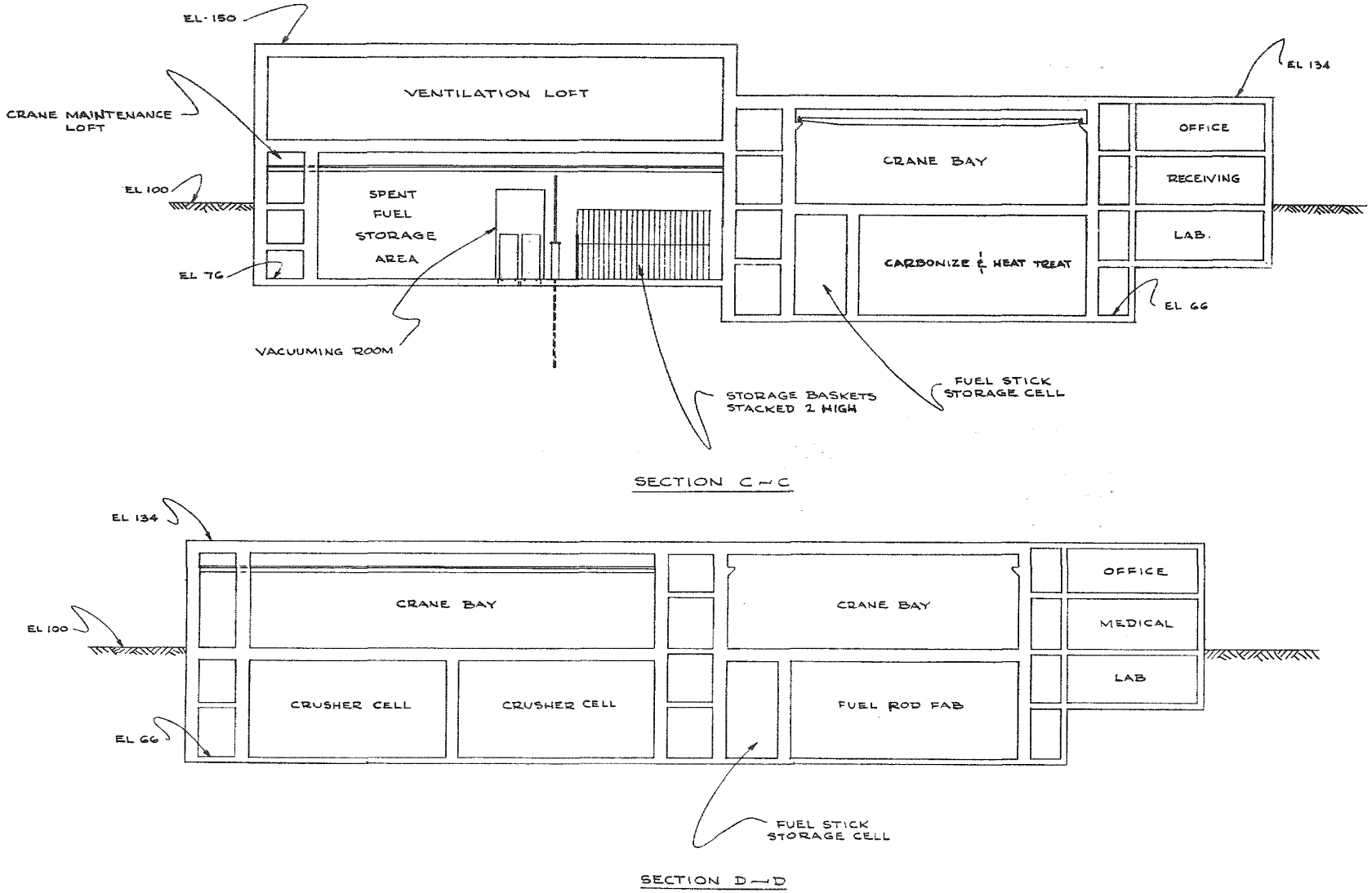

Fig. 5-1. HTGR fuel reprocessing-refabrication plant layout (Sheet 3 of 6)

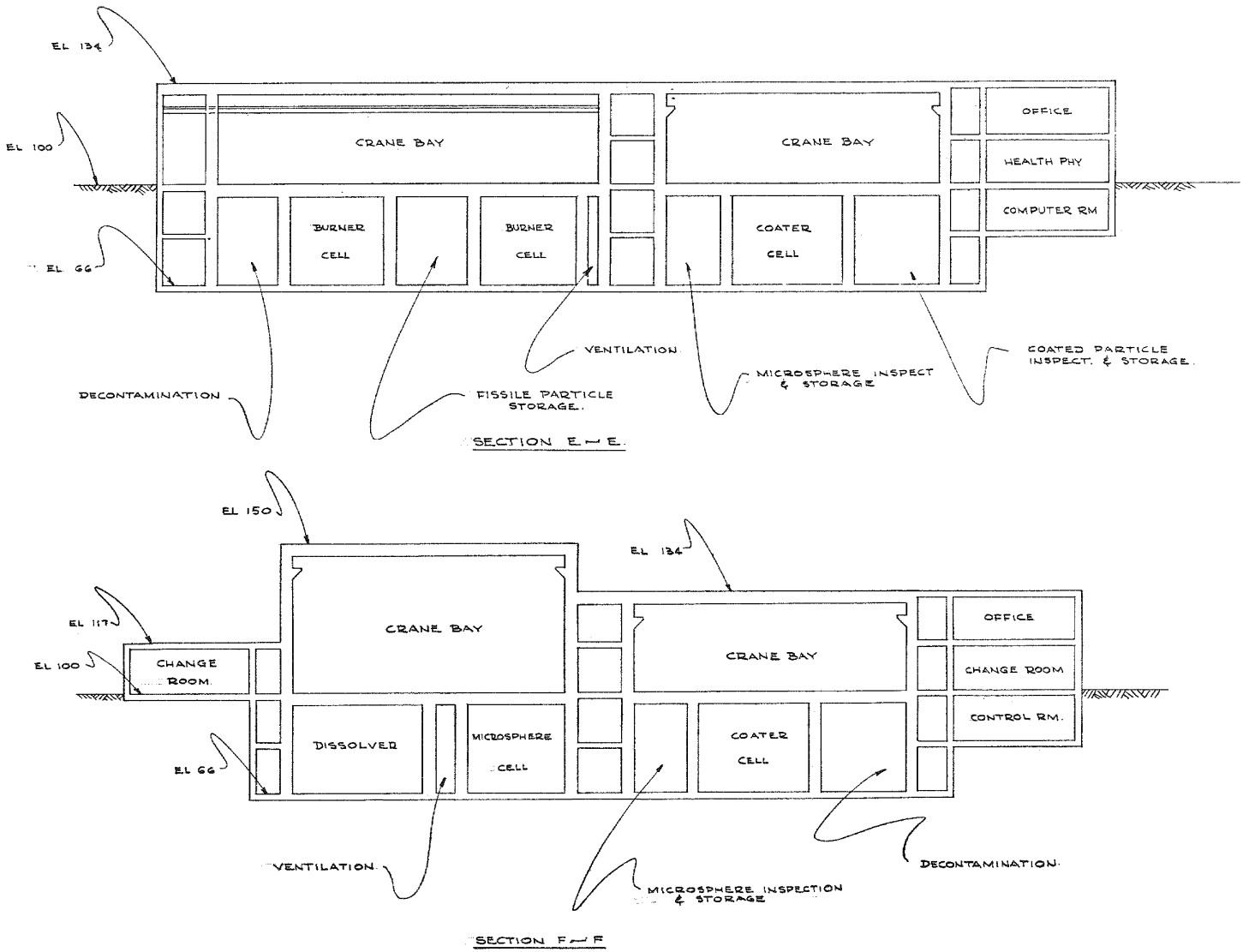

Fig. 5-1. HTGR fuel reprocessing-refabrication plant layout (Sheet 4 of 6)

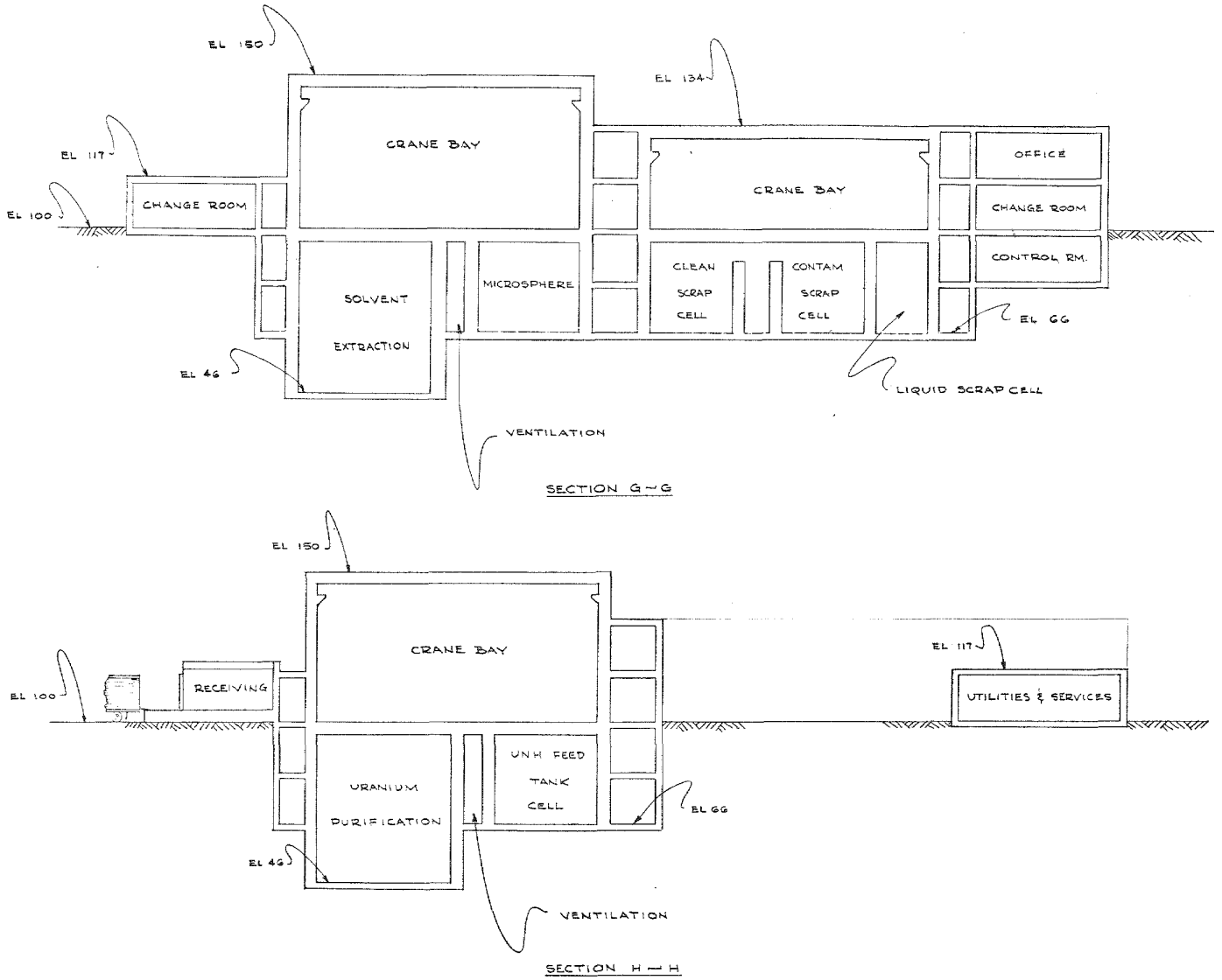

Fig. 5-1. HTGR fuel reprocessing-refabrication plant layout (Sheet 5 of 6)

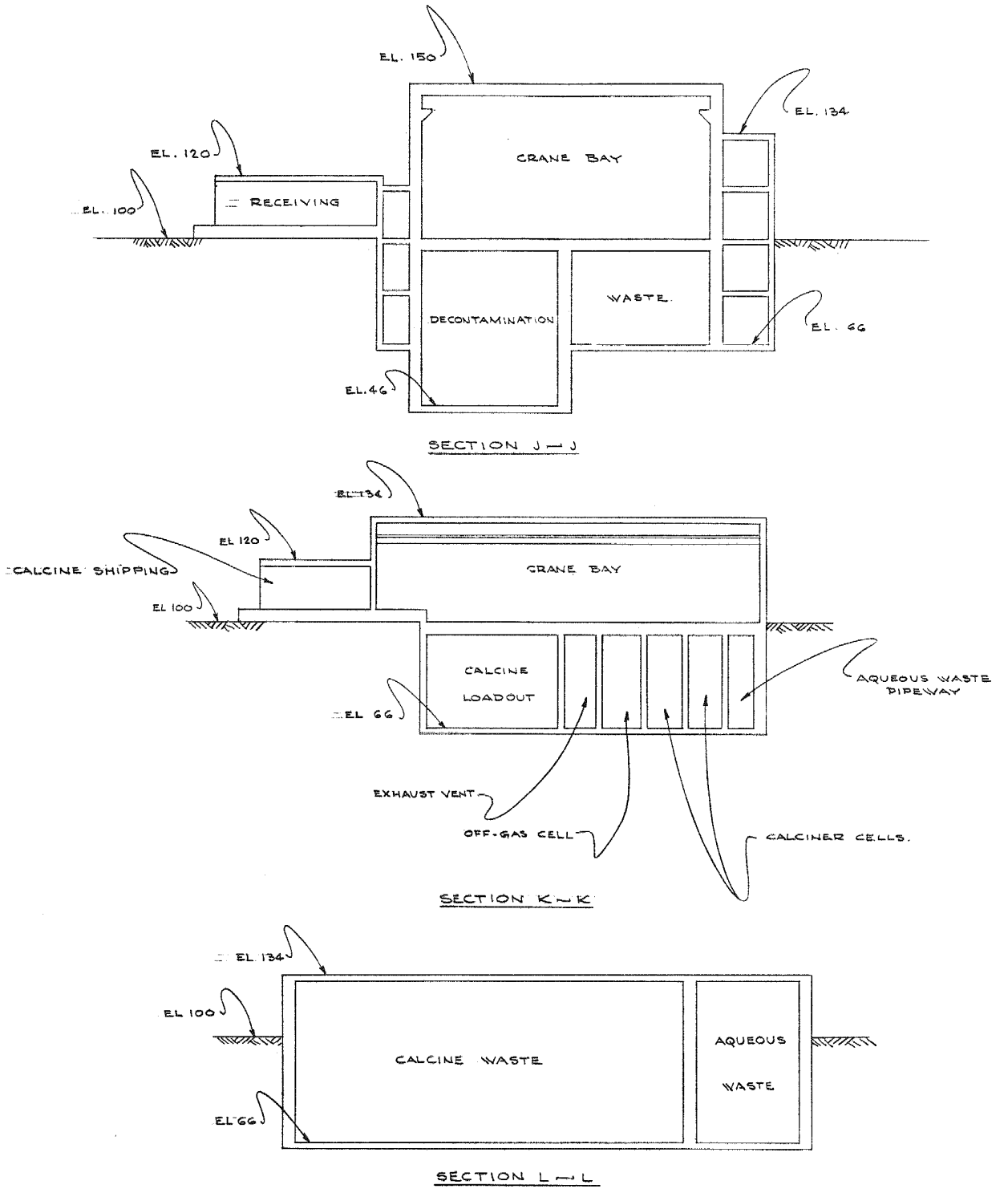

Fig. 5-1. HTGR fuel reprocessing-refabrication plant layout (Sheet 6 of 6)

Ce-144, Pr-144 decay; 25% from the Zr and Nb-95 chain; and 15% from Cs-134. The principal sources for the remaining 20% of the afterheat are about equally divided among Sr-89, Y-90, Y-91, Rb-106, and Pa-233.

Afterheat generation in the refabricated fuel elements is a function of the degree of cleanup of the recovered recycle uranium feed. For the HTGR refabricated fuel elements as defined for the AEC Base Program study, the decay of Th-228 and its daughters is responsible for the 2 to 4 Btu/hr afterheat generation. The Th-228 may be present from the partitioning between thorium and uranium and the decay of U-232 present in the uranium. For design purposes, a value of 500 ppm U-232 (compared to about 350 ppm actual) has been used in conjunction with an elapsed time period of 100 days following purification of the uranium. In terms of afterheat generation, these conditions would result in 2.3 Btu/hr per fuel element.

Summary process descriptions were prepared for receiving-shipping, crushing, burning, dissolution and extraction, ventilation off-gas system, microsphere preparation, coating, rod fabrication, scrap recovery, and waste processing.

The solvent extraction system for this study has been changed from that used previously to a tandem two-cycle acid Thorex process for decontamination and partitioning of the thorium and uranium. In the first cycle partial decontamination is done using an acidic feed to suppress the formation and precipitation of zirconium oxide hydrates at the feed adjustment step. Final decontamination and partitioning are done in the second cycle using the standard Thorex flow sheet with an acid deficient feed. The partial removal of zirconium by the first cycle is sufficient to prevent hydrate formation when the second cycle feed is adjusted to the acid deficient condition.

Detailed process descriptions, schematic flow sheets, and basic material balance data preparation are in work for the fuel dissolution and the extraction-purification systems for spent fuel reprocessing.

A detailed process description was completed for the refabrication processes. A process modification has been made for in-block carbonization and heat treatment of the fuel rods. Process schematic flow sheets are being updated to include this process change.

Equipment sizing for the refabrication plant (all three plant sizes -- 15,00-, 30,000-, and 45,000-MW(e) economies) has continued through this reporting period and is about 85% complete.

Meetings were held with ORNL to update and review laboratory programs related to fuel recycle for the HTGR. The technical status of the following three programs was reviewed in detail:

1. The Krypton Absorption with Liquid Carbon dioxide (KALC) fuel reprocessing head-end off-gas processing program.

2. The Concentrated Uranium Sol Preparation (CUSP) and the SOLEX processes for oxide microsphere preparation. Results of the HTGR recycle economic evaluation task were reviewed.

3. Proposed hot cell work on recycle test elements. This work will involve quiescent burning followed by dissolution, with fission products being traced through the process. The tracing of tritium is considered one of the most important aspects of this work.

The following drafts were reviewed at the ANSI Subcommittee meeting: "Design Objectives for Highly Radioactive Material Handling and Storage," "The Decommissioning of Nuclear Fuel Reprocessing Plants," and sections covering dry receiving, storage, and crane design.

HEAD-END REPROCESSING

Summary

The primary crusher has been completely assembled and successfully operated. Two full-size Fort St. Vrain fuel elements have been reduced through both the primary and secondary crushers.

Vendor quotations are being obtained on a specification for a pneumatic solids transport system. An air classifier has been ordered and two fixed-gap roll crushers are being designed for primary burner product separation and crushing.

A 103-hour primary burner run with top feed and no fines recycle yielded information on fines carryover rates and burner control characteristics. Work on primary burner distributor plates has been halted until a satisfactory startup technique is demonstrated by ICPP. After several flameouts due to fallback of fines, the off-gas heat exchanger was replaced with a 5-cm pipe. No further flameouts have occurred.

A smaller furnace and larger cooling jacket were installed on the 10-cm secondary burner, yielding higher peak burn rates. Hot batch dumping systems are being seriously considered.

A leaching system consisting chiefly of two air-sparged leachers and a batch centrifuge has been constructed and instrumented. It was successfully operated from a "remote" control room during eleven equipment shakedown runs. Steam-jet transfer tests indicate the need for a higher-pressure steam supply.

Crushing and Solids Handling

Primary Crusher

The primary crusher has been completely assembled and is totally operational. As shown in Fig. 5-2, the length of the crushing cavity extends from the frame bottom to the centerline of the shaft on which the Pitman assembly is supported. The cavity has a length of 58 in. and a nip angle of 18°. Two standard Fort St. Vrain fuel elements and several half-lengths of Fort St. Vrain control rod elements have been successfully reduced in this machine.

Secondary Crusher

The crushed product obtained from the reduction of Fort St. Vrain fuel and control rod elements in the primary crusher was successfully reduced in the secondary crusher.

Solids Handling

A set of specifications has been issued to several vendors of pneumatic conveying equipment to obtain quotations for a conveying system. The system will consist of three branches, namely:

1. Crusher product to primary burners.
2. Primary burner product to secondary burner.
3. Secondary burner product to leachers.

As an intermediate operation, the primary burner product is intended to be air classified, that is, fertile particles separated from fissile particles. Following particle separation it is intended that several optional modes of particle crushing be effected using double-roll crushers. A vendor survey has been completed on air classifiers, and the roll crushers are presently being designed.

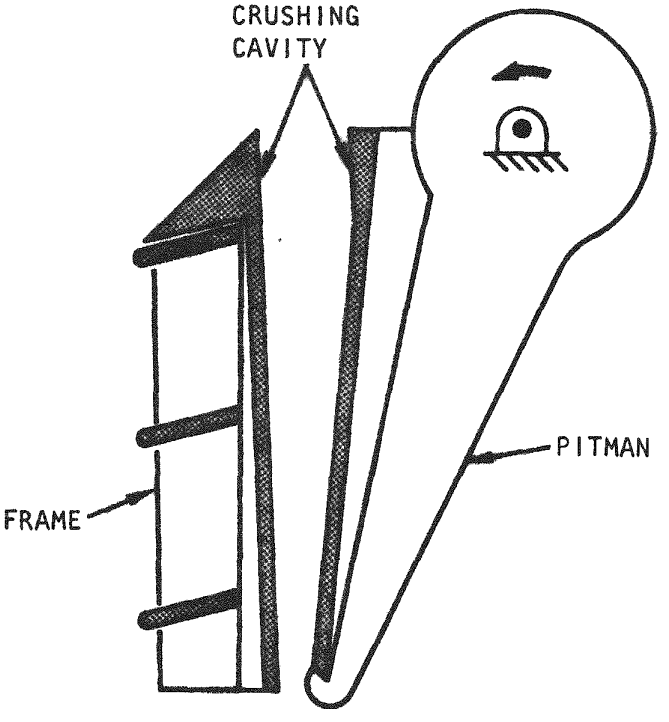

Fig. 5-2. Crushing cavity

Burning

During the past quarter the burner development program has concentrated on the 10-cm primary and secondary burners. This program is aimed at obtaining processing and design data. The program complements work being performed at ICPP and is being performed with direct communications between GGA and ICPP.

Primary Fluidized-Bed Burner Development

During the past quarter emphasis has shifted away from work on operation with distributor plates. The agglomeration problem observed with distributor plates occurred during startup when particles were exposed to high local temperatures. With the configuration of our burner (see Fig. 5-3), the CO-O_2 flame (flame temperature ∿2000°C) was directed toward the distributor plate and apparently was hot enough to melt the SiC coatings if any particles were present. Successful startup using a distributor plate was only possible when the burner was completely emptied by removing the distributor and cleaning out the bottom feed auger. Based on this experience, the distributor plate was removed. The runs reported in this report were made with a cone gas distributor, which will be used until a satisfactory startup technique is demonstrated by ICPP for perforated plate distributors. ICPP and GGA development personnel agree that a distributor is not significant in a 10-cm fluid bed because of the large wall effects.

Before this series of runs was made, the heat exchanger was removed from the top of the burner. Figure 5-4 shows the present 10-cm primary burner configuration. This change was made after two runs were extinguished by a fines fall-back flameout, which occurred when fines built up on the heat exchanger walls and then fell back into the reactor (∿500 g fines), rapidly cooling the bed. When this happens the off-gas CO concentration makes a rapid peak, followed by a rise in the O_2 concentration. Under those conditions, the run cannot be brought back to stable operation, the temperature drops below 800°C, and the run is no longer self-sustaining. A 5-cm-diameter section was installed in place of the heat exchanger to maintain

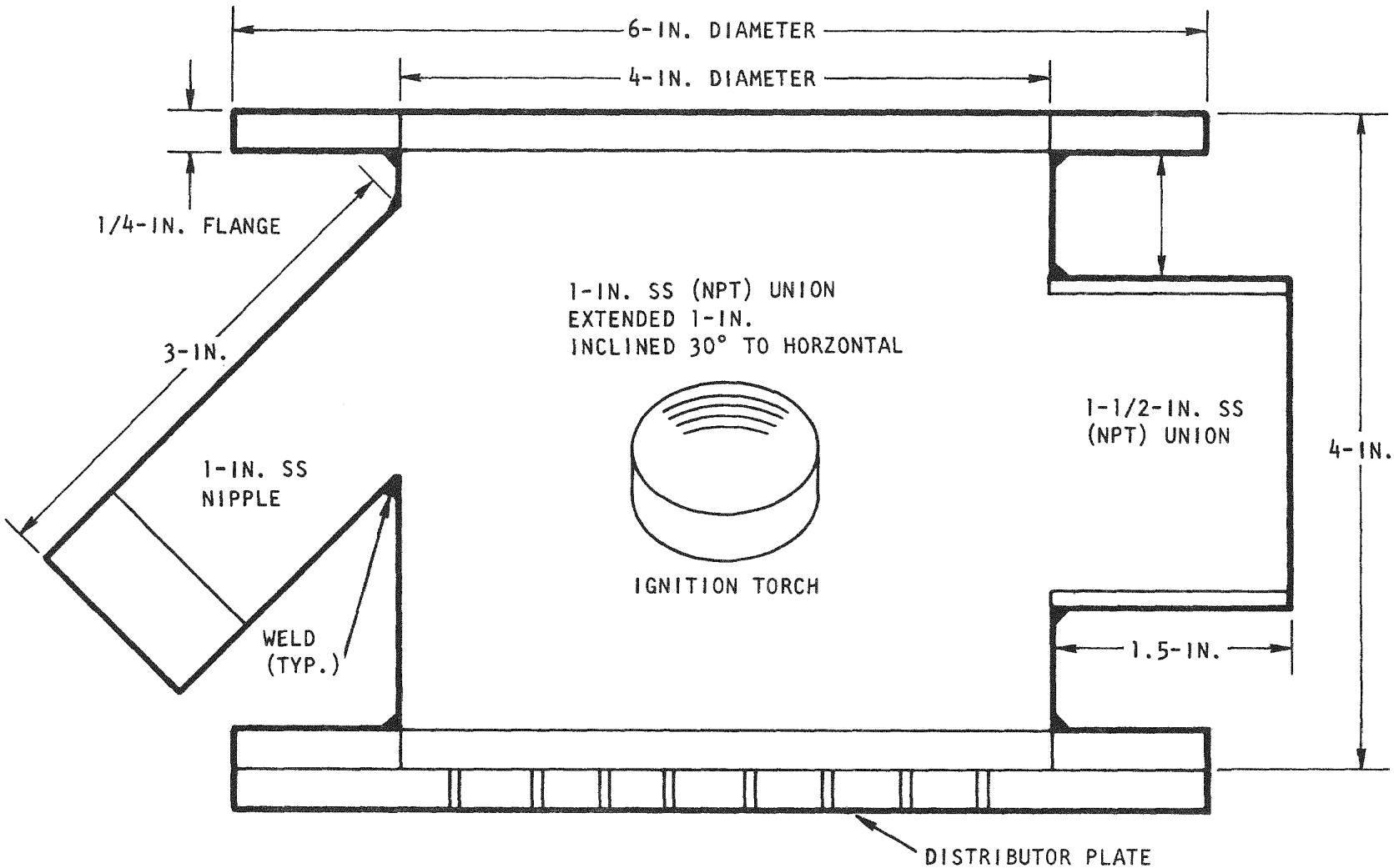

Fig. 5-3. Spooled piece for 10-cm primary burner

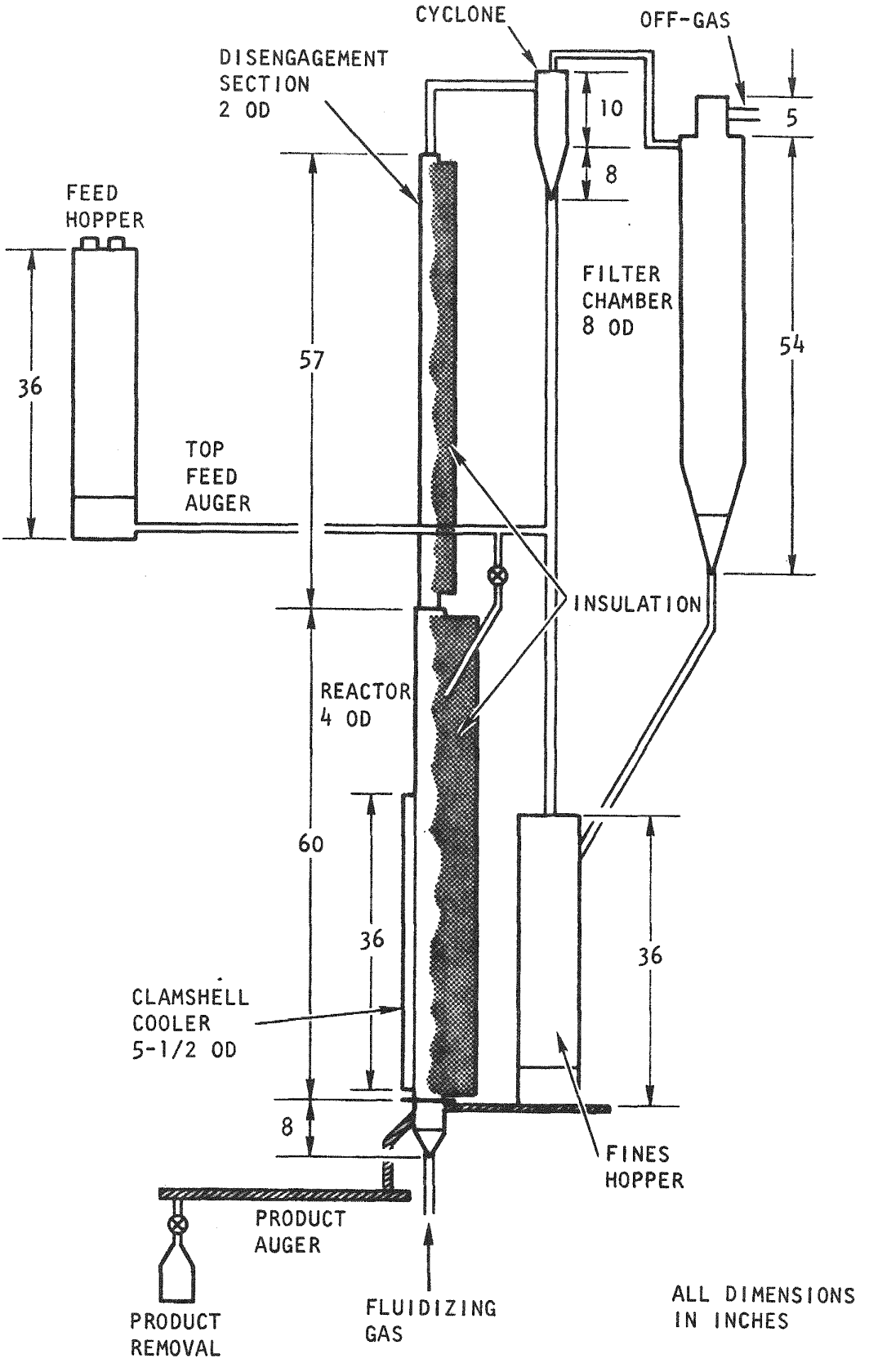

Fig. 5-4. 10-cm primary burner

a high velocity through that section and to prevent any fines problem. The 10-cm-diameter section is considered to have a sufficient disengagement length.

Run F4B-M16 was made with top feed and no recycle of elutriated fines. The run was made to demonstrate burner operability over an extended period of time (103 hours) and to collect operating data on this burner configuration. Table 5-1 shows the average run conditions for this run. Figure 5-5 shows the product, fines, and final bed size distribution. It should be noted that the fines distribution remained constant throughout the run, although the elutriation rate varied with the gas rate. This indicates that the present burner configuration has a sufficient disengagement section; the 10-cm-diameter burner section is 162 cm long and the bed height varied between 28 and 36 cm during this run. The product distribution was also fairly constant with run conditions. The bed has a higher fraction of large particles than the product and a smaller fraction of fine material (<600 μm). The product is withdrawn through an auger, which breaks particles, accounting for the difference between the product and final bed size distributions. The larger concentration of large material is accounted for by large pieces of graphite floating on top of the bed. This stratification of the bed was further investigated in Run F4B-M20 and is discussed later.

Two important operating parameters were defined for top feed, no fines recycle run conditions. The ratio of fines elutriation to burn rate was 0.43 g/g of carbon burned; the reduction in carbon was 70%. Operating in this manner would require either a separate fines burner or increasing the load on the secondary burner to burn all of the graphite. Table 5-2 summarizes the material properties measured during this run. It was observed that the cyclone fines (elutriated material) had a tendency to bridge, causing problems when dumping the collection vessel. This material might exhibit similar bridging problems in a pneumatic system and would have to be taken into account in the design of any fines storage hoppers.

Table 5-3 summarizes empirical correlations obtained from the run data at the 95% confidence level. The two correlations of greatest interest are

TABLE 5-1
AVERAGE RUN CONDITIONS FOR RUN F4B-M16,
103 HOURS OF OPERATION

Feed rate, g/min	55.0
Burn rate, g/min	31.5
Product rate, g/min	9.1
Cyclone fines rate, g/min (96.4% of the elutriated fines)	13.2
Filter fines rate, g/min	0.5
O_2 flow, liters/min at STP	61.9
Air flow, liters/min at STP	22.4
Superficial velocity, cm/sec (980°C, 4.7-kg bed)	66.1
(g C)/(g particles) in feed	4.88
(g C)/(g particles) in product and fines	1.47
(g fines)/(g product)	1.42
(g fines)/(g C burned)	0.43

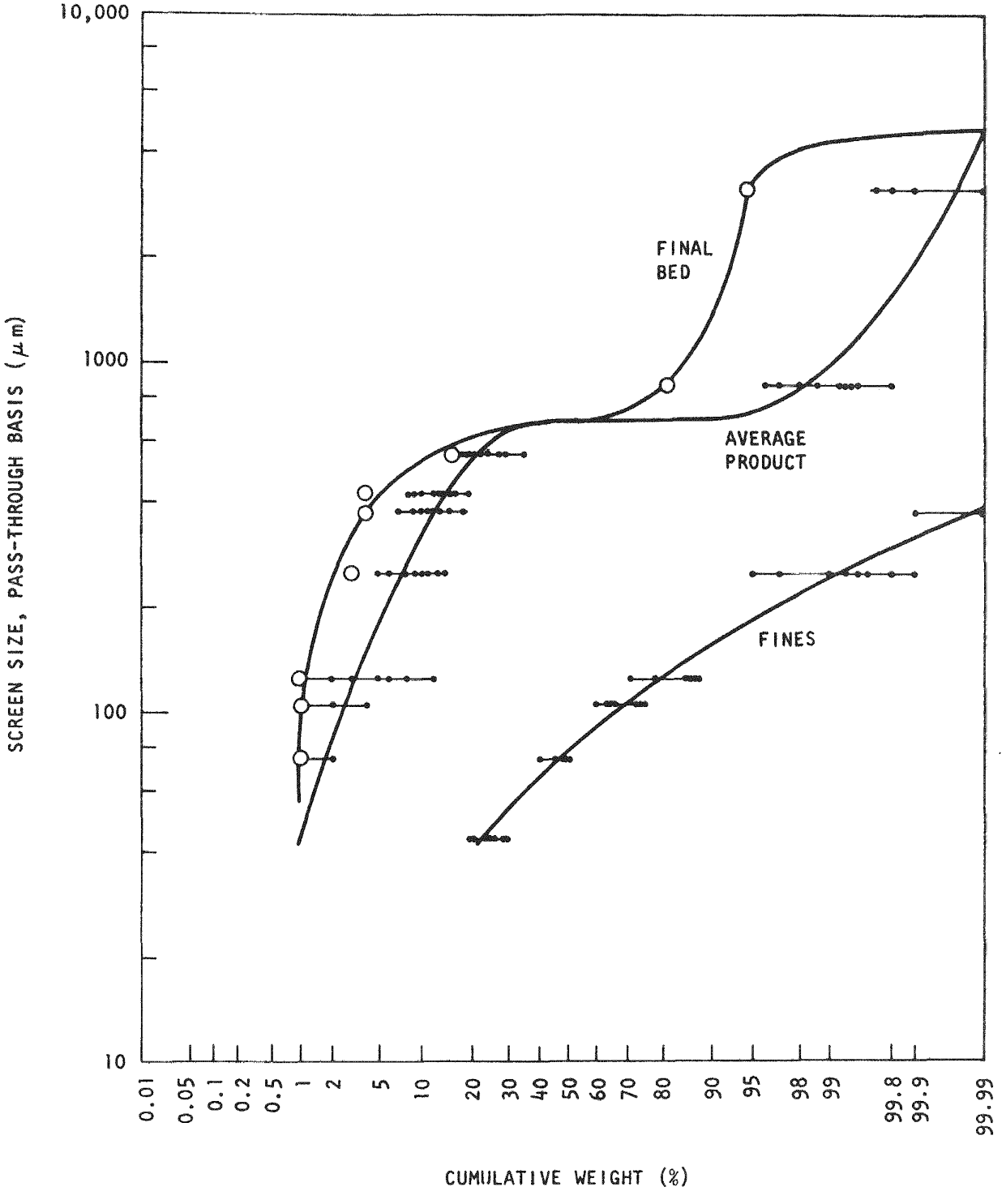

Fig. 5-5. Product and fines size distribution

TABLE 5-2
MATERIAL PROPERTIES

	Top Density (g/cm^3)	Angle of Repose (degrees)	Particle Size, $\overline{d}_p$ [a] (μm)
Feed	1.15 - 1.25	35	860
Product	2.3	27	690 ($d_{sv} = 485$) [b]
Cyclone fines	0.7	36	80

[a] 50% of the material is less than $\overline{d}_p$.

[b] $$d_{sv} = \frac{1}{\sum_i} \frac{(Wt\ \%)_i}{(\text{Average screen size})_i}$$

TABLE 5-3
EMPIRICAL CORRELATIONS
(SIGNIFICANT AT 95% CONFIDENCE LEVEL)

Burn Rate

$$g/min = -3.28 + 0.393(\%\ O_2\ in) + 0.484(V_1,\ cm/sec) - 0.0309(T_1,\ °C) \pm 0.5$$

$$r^2 = 0.920$$

Meets 99% confidence level

Fines Rate

$$g/min = 89.2 - 0.1064(T_1,\ °C) + 0.6112(V_5,\ cm/sec) \pm 2.4$$

$$r^2 = 0.809$$

Carbon in the Bed

$$g\ C = -340.0 + 27.8(fines,\ g/min) + 17.5(liters/min) - 71.8(\%\ rpm) \pm 80.7$$

$$r^2 = 0.832$$

$$\%\ burnable\ C = -69.0 + 7.879(bed\ size,\ kg) + 263.6\ e^{-T/100} - 374.4\left[\frac{Bed\ wt,\ kg}{Burn\ rate,\ g\ C/min}\right] \pm 1.8$$

$$r^2 = 0.819$$

Oxygen Concentration, Off-Gas

$$\%\ O_2 = -4.0 - 0.377(\%\ CO\ out) + 0.139(\%\ O_2\ in) \pm 0.4$$

$$r^2 = 0.920$$

Carbon Monoxide Concentration, Off-Gas

$$\%\ CO = 15.6 - 2.00(\%\ O_2) - 0.301(V_1,\ cm/sec) + 0.691\ (burn\ rate,\ g\ C/min) \pm 1.1$$

$$r^2 = 0.890$$

the fines rate and the off-gas CO concentration. The CO concentration did not have any significant correlation with the carbon content of the bed (grams carbon or percent carbon). This would indicate that the feed control loop will not work as expected. The fines rate has an empirical correlation with the bed temperature and the superficial velocity at the top of the 10-cm burner section. In operations with fines recycle, the fines rate will be larger since the size distribution of the feed will favor the small-sized material which elutriates (<400 μm).

Four runs were made with fines recycle and bottom feed. When operating in this manner, the elutriated fines and the fresh feed (-3/16 in. ring size graphite mixed 4:1 with fertile particles) are both fed to the bottom hopper (shown in Fig. 5-4) and are then fed to the bottom of the burner. The auger speeds are adjusted to maintain a constant bottom hopper level. Table 5-4 summarizes the four runs made with fines recycle as well as the extended run made without fines recycle. Three earlier run attempts (Runs F4B-M13, F4B-M14, and F4B-M15) were terminated due to fines fall-back flameouts, as discussed previously; the decision to remove the heat exchanger was based on these earlier runs.

Run F4B-M17 was a shakedown run made after reassembly of the burner following operation without fines recycle. During this run the bottom auger operated intermittently due to a mismatch between the electronics of the motor control (a ratiotrol) and a new auger motor (which required an SCR controller).

One of the important operating parameters is the fines elutriation rate. As shown on Table 5-4, the fines elutriation rate when operating with recycle appears to be about four times the rate when operating without fines recycle.

Runs F4B-M18, F4B-M19, and F4B-M20 were made to investigate burner operations with bottom feed of mixed feed and fines. The feed and fines were mixed by maintaining a continuous flow of fresh feed into the bottom

TABLE 5-4
SUMMARY OF PRIMARY BURNER OPERATION

	F4B-M16[a]	F4B-M17	F4B-M18	F4B-M19	F4B-M20
Burn rate, g/cm^2-sec	23	22	23	28	38
Superficial velocity, cm/sec	66	66	64	78	85
Bed size per unit area, g/cm^2	58	42	52	53	59
Bed temperature, °C	980	960	1015	995	975
Oxygen concentration, %	79	77	87	88	91
Fines carryover rate, g/g burned	0.43		1.04	2.15	2.13
Off-gas concentrations, %:					
O_2	3	0.2	0.0	0.0	0.0
CO	7	2.2	4.5	8.0	8.2
CO_2	76	74	83	80	82
Final bed properties:					
d_{sv}, μm	485	532	600	580	655
Carbon, %	10.2	3.7	6.3	10.9	23.2
Broken particles, %[b]			3.2	0.8	1.5

[a] Run made with top feed, no fines recycle.

[b] Percent of nonburnable material less than 420 μm.

hopper along with the fines, which blow over continuously. Previous burner operation had used on-off control of the top auger to control the bottom hopper level. The on-off control produced layered feed for the bottom auger, providing varying feed rates to the burner due to the different auger delivery characteristics of the fresh feed (-4760-μm ring size) and fines (-125 μm). The off-gas concentration varied considerably (for example, cycled over a range from 6 to 12%) while operating with on-off control of the top auger. By operating with mixed feed the burner operation was more constant; bed temperatures were more constant and the off-gas CO concentration was less cyclical (8 to 10%).

All three of these runs demonstrated small fractions (1 to 3%) of broken particles in the bed. The measured broken particle content of the feed varies between 0.5 and 2.0%. Some particle breakage occurs in the top and bottom feed augers. A significant fraction is broken by the product takeoff auger. Product from this auger typically runs 13 to 15% broken particles. The present product takeoff auger acts as a metering device; the takeoff is a wier removing product from the middle of the bed at a rate controlled by the product auger. The present auger will be modified to lower particle breakage of the product. A rotary valve will be used on the 20-cm burner. On the 10-cm burner, the present auger (30 cm long, 24 cm in diameter) will be shortened and supported by bearings at both ends. (Presently it is supported by a double bushing at one end.) The top feed hopper will be moved to a position above the bottom hopper, considerably shortening the top auger (which only needs to act as a metering device), which should help reduce any particle breakage caused by this auger. Negotiations have begun to have core-type augers, which break fewer particles, manufactured to our requirements based on earlier auger performance tests. When these are procured, the auger system will be modified to better achieve auger-cone alignment. A pneumatic feed system is being built for the 20-cm burner which will allow evaluation of an alternative feed system. A rotary valve will be used to control the product removal rate on the 20-cm burner. Using the pneumatic system and a rotary product valve, particle breakage should be less of a problem.

The final beds from Runs F4B-M19 and F4B-M20 were removed in layers. Analysis of these data indicates stratification of carbon in the bed. Table 5-5 and Fig. 5-6 summarize the data on Run F4B-M20. The top and middle sections were augered out; the bottom was dumped. As shown by these data, the top 5% of the bed had a high carbon content and a large fraction of large particles (10% > 3800 μm). The middle of the bed (the next lower 33%) had a carbon content that was higher than the bottom 62% of the bed, but it had a lower content of large particles than the top 5% of the bed. The segregation of larger, lighter pieces on top of a bed of dense material has been documented by several investigators.*

Figures 5-7 and 5-8 show the temperature profiles for Run F4B-M19. During this run the bed height was ∿39 cm from the check valve. The bed temperature remains fairly constant. Overall heat transfer coefficients for the top and bottom sections were calculated at 47.7 kcal/m^2-°C-hr (9.8 Btu/ft^2-°F-hr) and 56.6 kcal/m^2-°C-hr (11.6 Btu/ft^2-°F-hr). A higher heat transfer coefficient for the bottom section might be expected due to the presence of the particles in the fluidized bed. However, only ∿15 cm of the bed is in the clamshelled area, which is 46 cm long. Also the limiting resistance for heat transfer is probably in the wall and cooling-air side. Calculations for the clamshell give a gas coefficient of 55.1 kcal/m^2-°C-hr (11.3 Btu/ft^2-°F-hr).

In summary, primary burner operation has been demonstrated for an extended period (103 hours). Operations with top feed and no fines recycle were investigated during this run period. The data from the run indicate that using the CO concentration to control the feed rate will not work as anticipated. Operations since that time have demonstrated that improved burner operation is achieved by using "mixed" fresh feed and recycled fines when using an auger feed system. The fines elutriation rate, when recycling fines, is about four times the level when fines are not recycled.

---

*Strijbos, S., "Motion and Distribution of Large Particles Suspended in a Fluidized Bed," Powder Technology 6, 337 (1972).

TABLE 5-5
BED CHARACTERIZATION BY SECTIONS, RUN F4B-M20

Top, Augered

d_{sv}, μm	842
% carbon	71
% broken particles	8.5 (% < 420 μm)
% of bed	5

Middle, Augered

d_{sv}, μm	430
% carbon	33
% of bed	33

Bottom, Dumped

d_{sv}, μm	655
% carbon	14
% broken particles	1.5 (% < 420 μm)
% of bed	62

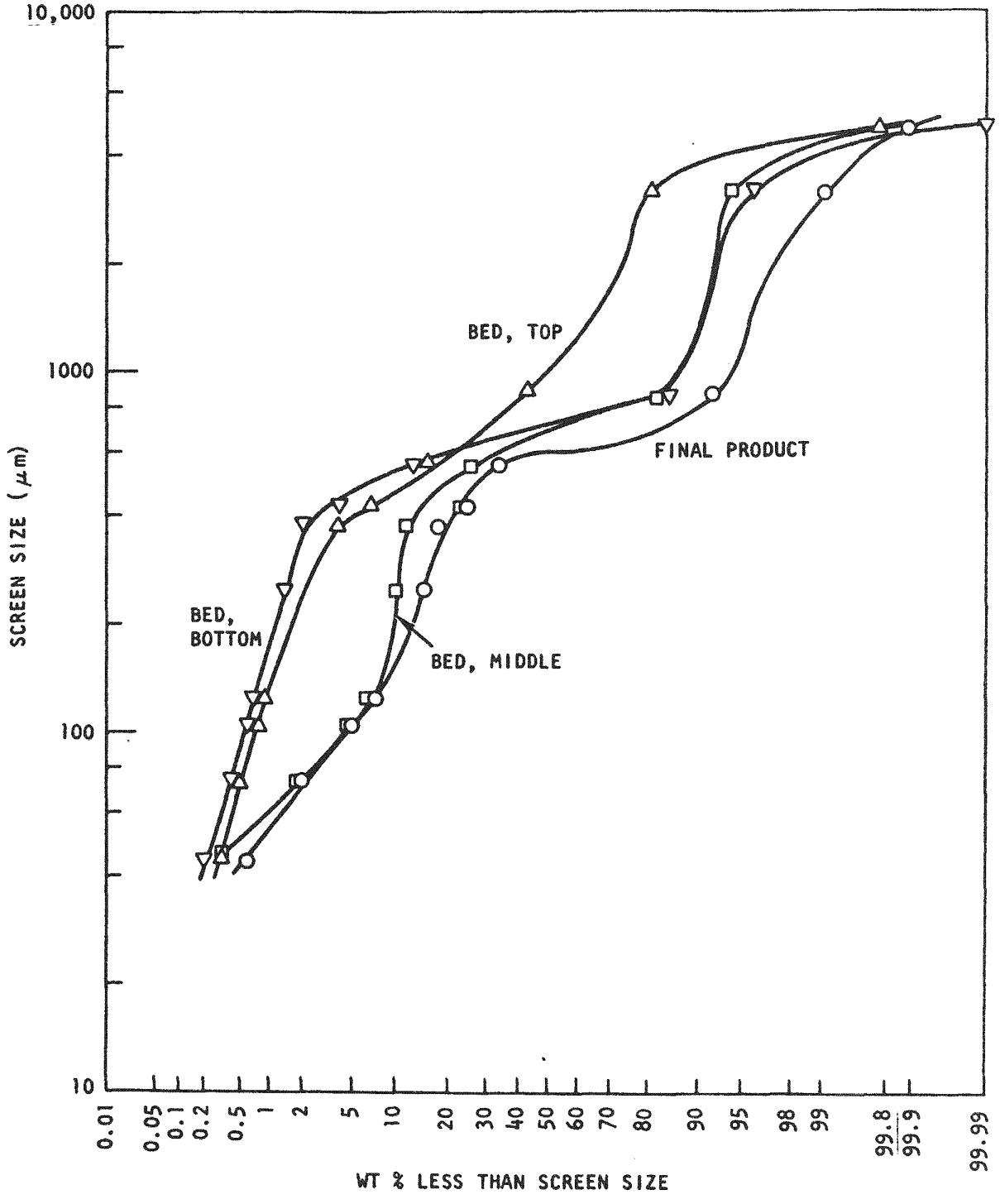

Fig. 5-6. Size distribution, Run F4B-M20

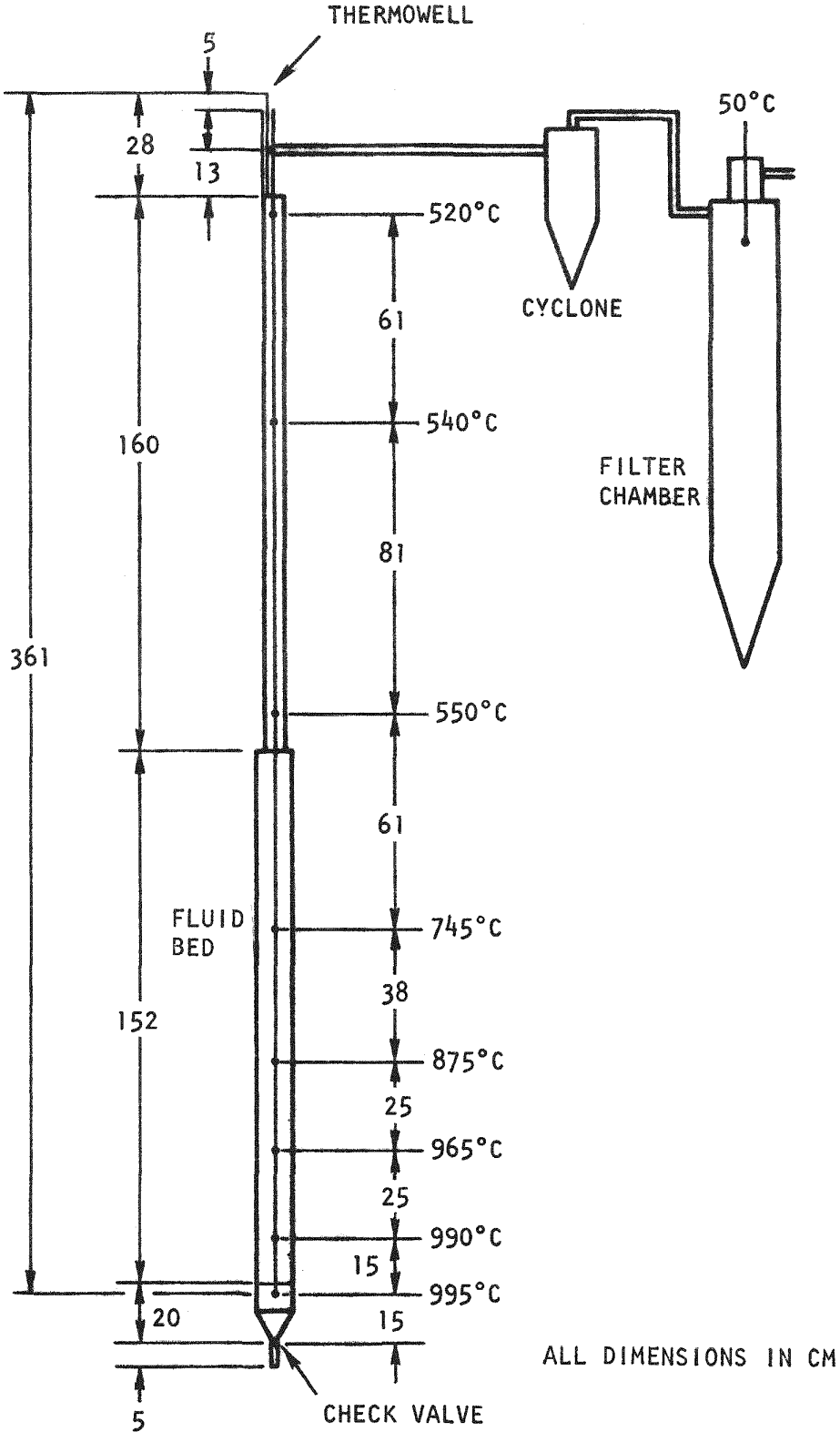

Fig. 5-7. Temperature profile for 10-cm primary burner, Run F4B-M19

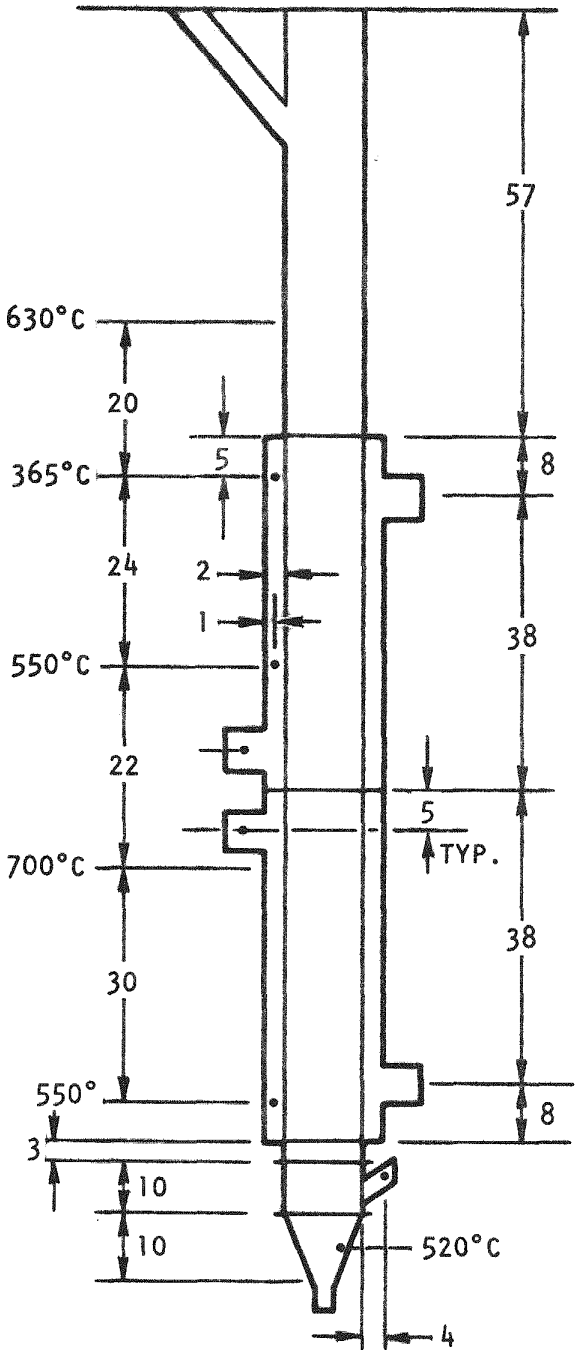

Fig. 5-8. Wall temperatures, 10-cm primary burner, Run F4B-M19

Secondary Fluidized-Bed Burner Development

After modifying the heating and cooling systems (see Fig. 5-9), four batches of crushed TRISO fertile particles were burned in the 10-cm secondary burner. These runs are summarized in Table 5-6.

The previous 48-in.-high furnace was replaced with a 22-in.-high furnace. This allowed more reactor tube area for an additional air cooling jacket, yielding increased peak burn rates.

A system was installed that recycles burner off-gas through the filter blowback ventures. This cuts down the volume of off-gas and reduces the spikes in off-gas analyses that accompanied the former practice of blowing back with air.

Shutdown conditions are still being varied in each run to define those conditions that yield acceptable product. Additional temperature and gas flow measurements are being taken to determine heat balances for each run. Burner fines (<44 μm) have been analyzed for size distribution to better define the average bed particle size.

Tests are in progress on the pulsed pneumatic feeding system to determine feed rate as a function of gas velocity and pulse frequency and to examine the effect of varying feeder geometries.

Many conceptual hot batch dump schemes have been considered, the requirements being to have a distributor plate and to be able to completely empty the burner in a short time. Several of these will be tried in order of their expected probability of success. A large portion of effort on this burner is now being directed toward this end, since it is necessary for both automation of the burner and interfacing with the proposed pneumatic product transport system.

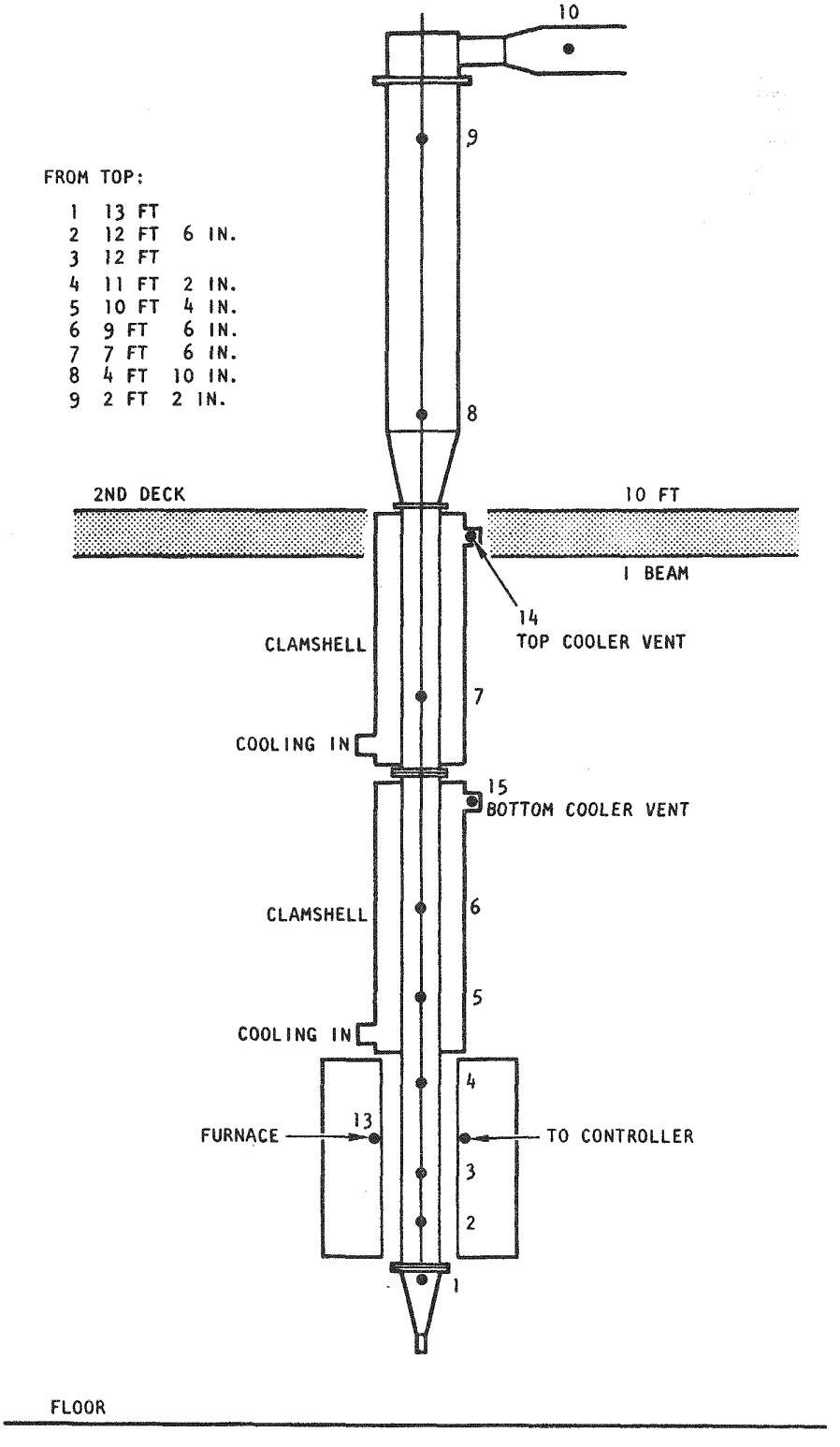

Fig. 5-9. Heating and cooling systems and thermocouple locations, 10-cm secondary burner

TABLE 5-6
SUMMARY OF SECONDARY BURNER OPERATION

	Run No. 20	Run No. 21	Run No. 22	Run No. 23
Type Feed	Crushed TRISO fertile	45% crushed TRISO fertile, 55% whole TRISO fertile	Crushed TRISO fertile	Crushed TRISO fertile
Feed, % burnable C[(a)]	30.4	16.5	26.8	24.8
Feed d_{sv}, μm	134	235	134	140
Bed temperature, °C	980	1000	1000	1000
Total flow, liters/min[(b)]	120	100	140	100
Average O_2 in, %	73	56	87	92
Average burn rate, g/min	45	22	38	40
Peak burn rate, g/min	68	58	62	62
Product, % burnable C	4.1	1.5	0.5	1.2
Product d_{sv}, μm	50	81	27	21
Shutdown, % CO_2/% O_2	(c)	3%/29%	2%/21%	1%/21%

(a) Includes carbon present as graphite, particle coatings, and ThC_2.

(b) During exothermic portion of run.

(c) Shutdown conditions were obscured by carbon fines reentering burner from filter chamber.

Leaching

A leaching system has been constructed for operation at 10 to 20% of the expected capacity of the "hot" demonstration facility at ICPP (see Fig. 5-10). Basically, this system consists of (1) two air-sparged leachers that are operated as single batch or in a countercurrent series manner, (2) a batch centrifuge for centrifugal filtration or centrifugal sedimentation of solids from liquid phases, (3) steam-jet ejectors for transfer of liquids and slurries, and (4) sufficient auxiliary tankage for storage of reagents and products.

A layout of the 13-cm-diameter leacher is given in Fig. 5-11. This vessel was fabricated from 5-in.-diameter, schedule 40, 304L stainless steel pipe. It is heated with four tubular band heaters (Chromalox HBT-55, 950 watts). The condenser being utilized is a spiral heat exchanger (American Heat Reclaiming Corporation, Type I-V, 5 ft^2 of surface). A layout of the 20-cm-diameter leacher is given in Fig. 5-12. This vessel was fabricated from 8-in.-diameter, schedule 40, 304L stainless steel pipe. It is heated with three tubular band heaters (Chromalox HBT-85, 1425 watts). The condenser being utilized is a single-pass, shell and tube heat exchanger (American Standard 03024, 7.3 ft^2 of surface). Both of these vessels have a bottom cone section (60° included angle) and are air-sparged (see Fig. 5-13). The centrifuge being utilized is a 12-in.-diameter ($\sim$30 cm) batch DeLaval/A.T.M. basket centrifuge. A 1-hp d.c. variable speed motor allows a centrifuge operating range of 0 to 1550 g. The layout for a typical storage tank is given in Fig. 5-14. These storage tanks were fabricated from 8-in.-diameter, schedule 40, 304L stainless steel pipe. All welding on 304L stainless steel was done with 308 ELC welding wire.

This system is instrumented and is operated on a "remote basis" from a central control room. Solenoid valves are used to initiate and terminate the transfer of liquids using steam-jet ejectors. All tankage is equipped with nitrogen purge systems and differential pressure transmitters to allow determination of liquid levels and specific gravities. A simplified diagram of the purgerator system layout is given in Fig. 5-15.

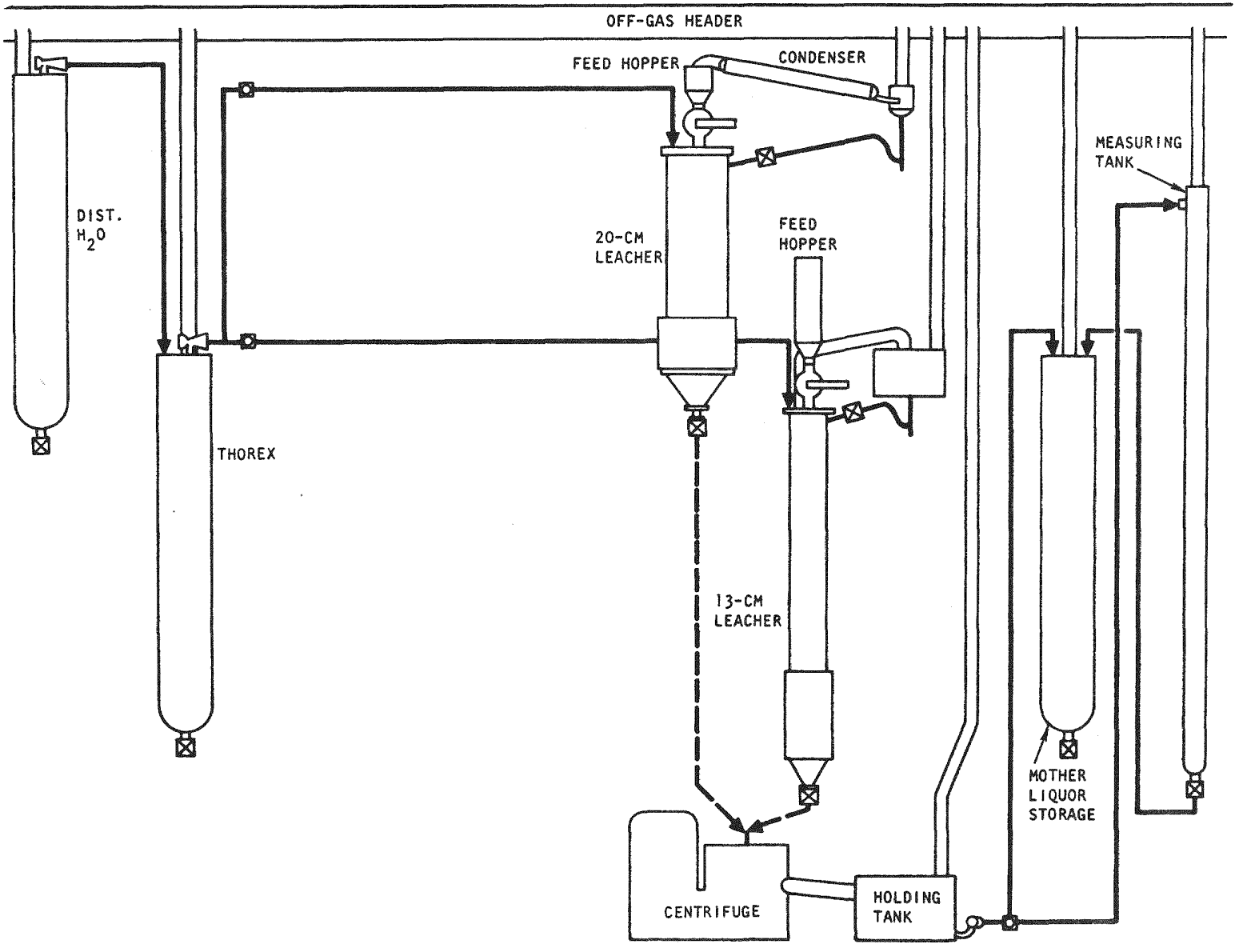

Fig. 5-10. Equipment layout for leaching system

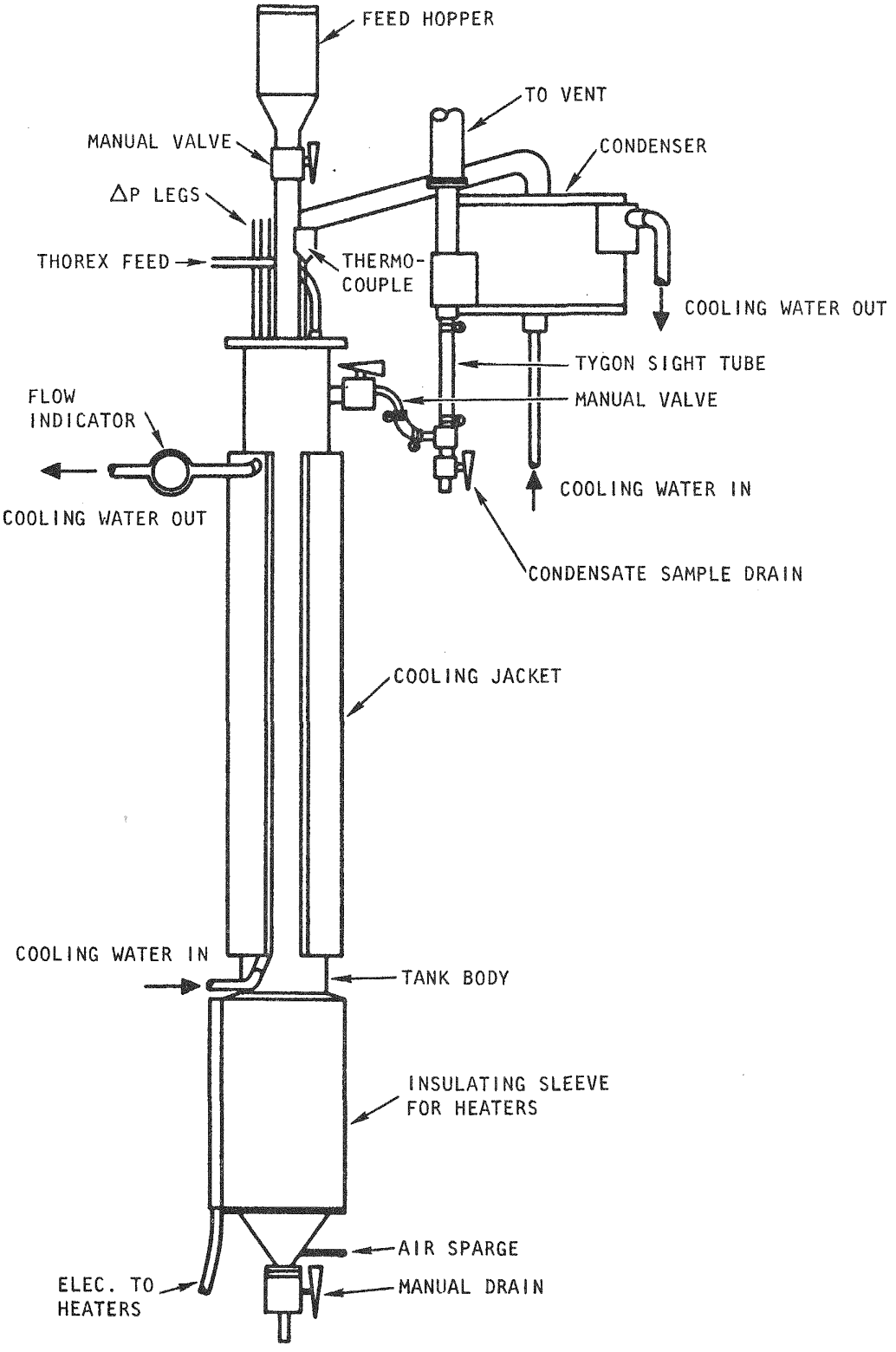

Fig. 5-11. 13-cm leacher

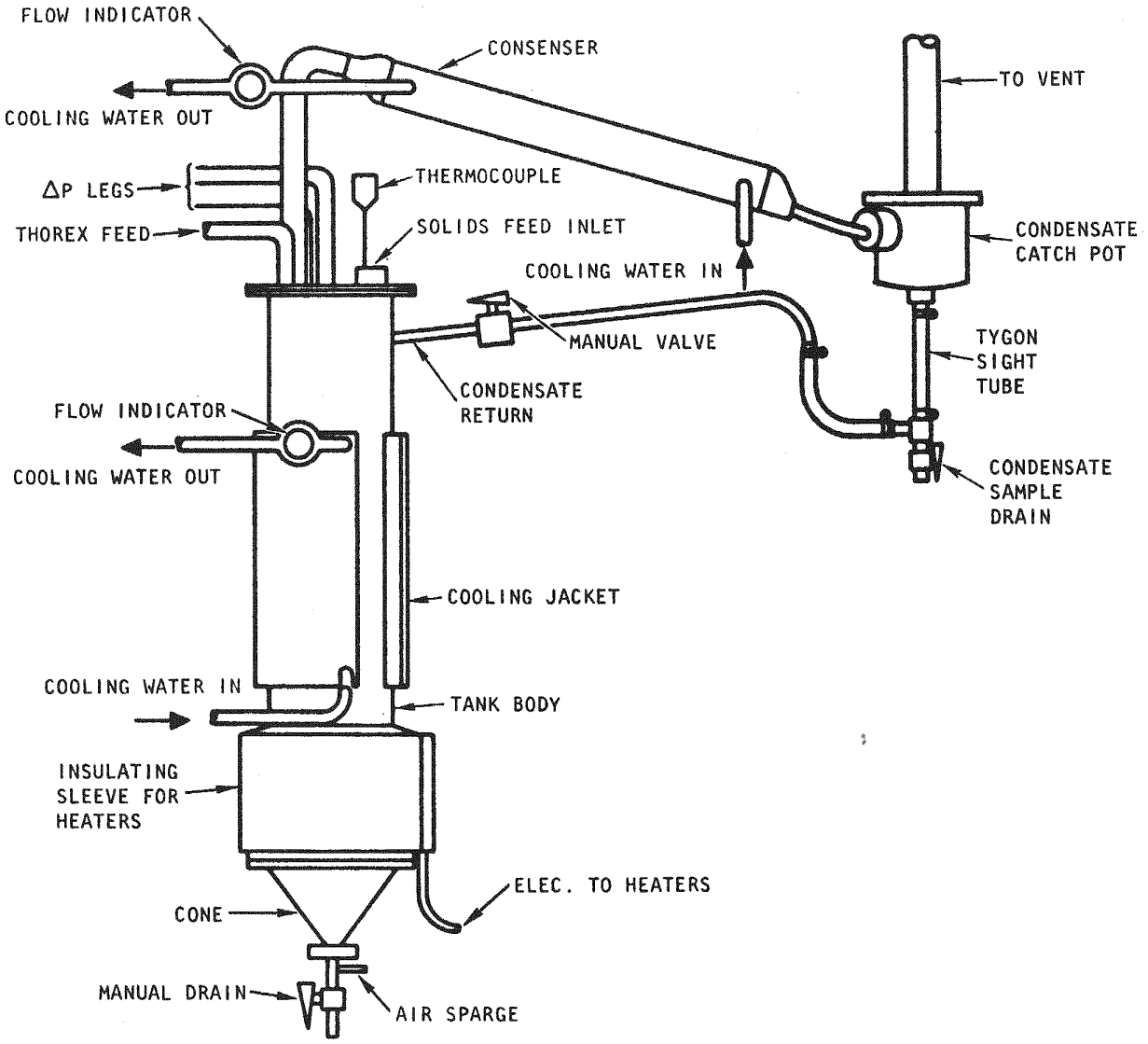

Fig. 5-12. 20-cm leacher

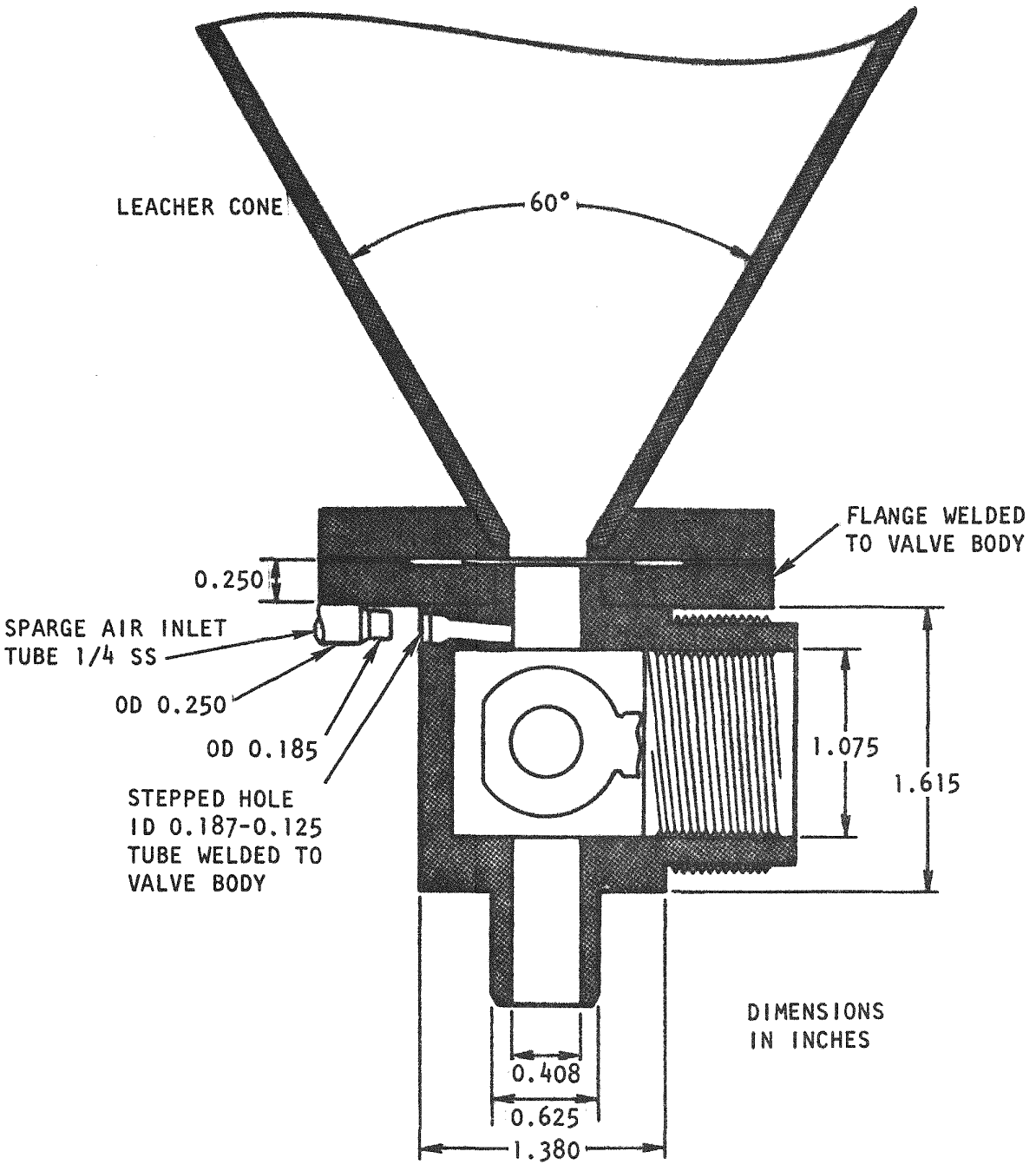

Fig. 5-13. Leacher dump valve for 13- and 20-cm leachers

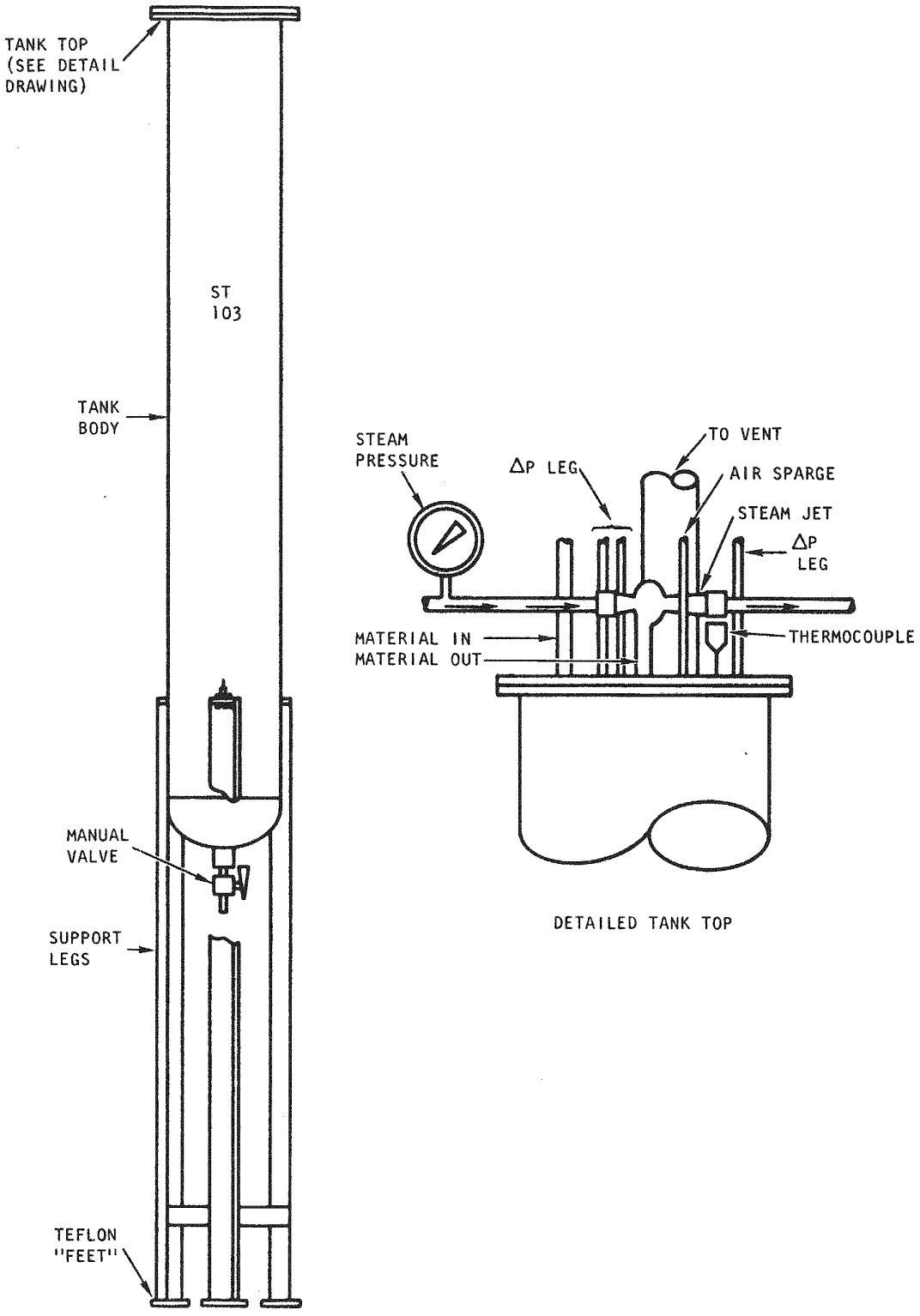

Fig 5-14. Typical storage tank

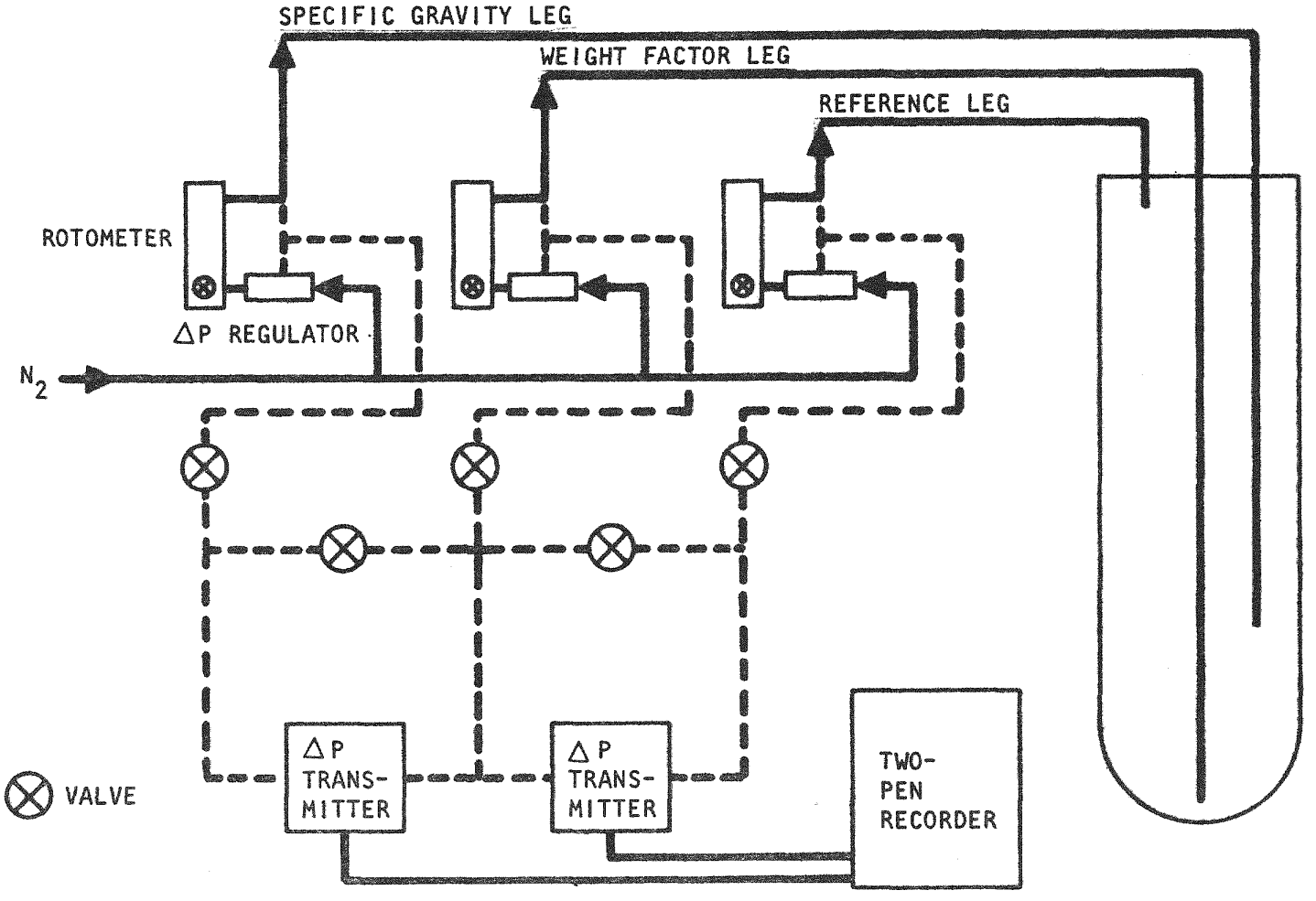

Fig. 5-15. Purgerator system for determination of liquid level and specific gravity

Prior to making leaching runs, an attempt was made to steam-jet transfer a simulated slurry from the leaching vessels. A Schutte and Koerting Type 217-60 ejector and a steam supply of 30 psig were used for this test. Under these conditions, it was impossible to transfer the slurry from the leacher. Thus for initial testing, it was decided to remove the leacher contents from the bottom of the cone using gravity. A few shakedown runs of the centrifuge were tried under these conditions. For initial testing, a perforate basket with a polypropylene cloth having 6- to 7-μm openings was selected. It was discovered that a gravity dump of the leacher produced an initial feed to the centrifuge containing over 80 wt % solids. This initial high concentration of solids occasionally produced "off-loading" and excessive vibration of the centrifuge. To remedy this situation, a "dilution" tube was placed in the leacher (see Fig. 5-16). This dilution tube allowed liquid from the upper part of the leacher to mix with the concentrated slurry at the bottom of the leacher, which reduced the solids concentration of the feed to the leacher to between 30 and 40 wt %. No problems were encountered in centrifugal separation of this material.

Leaching Runs

Eleven leaching runs (leach Runs 38 through 48) were made with this equipment during this quarter to check the operability and reliability of the new equipment. All material transfers were automatically recorded and remotely monitored from the control room. In general, the shakedown was smooth and highly successful.

All tests were made utilizing secondary burner product, resulting from burning crushed fertile particles. Data on burner ash fed to the leachers are included in Tables 5-7 and 5-8. All test runs were conducted with approximately 3.2 liters of Thorex [13M HNO_3/0.05M HF/0.1M $Al(NO_3)_3$] per kilogram of burner ash for about 1 hour dissolution at 116°C. Operating data for the leachers are included in Tables 5-9 and 5-10. The liquid-solid separation of leacher product was accomplished with the batch-basket centrifuge. Centrifuge operating data for all runs are as follows:

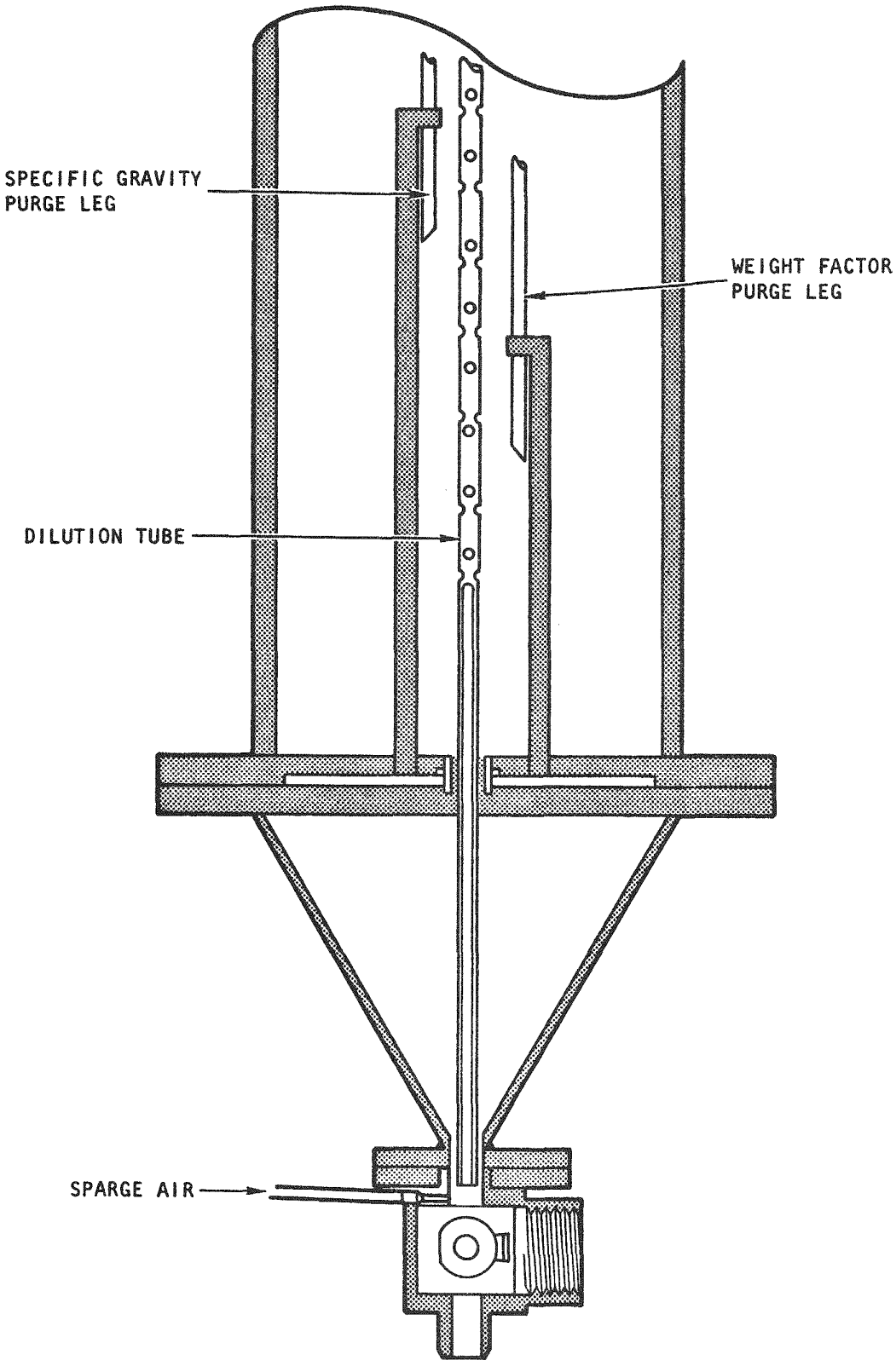

Fig. 5-16. Location of leacher dilution tube and spider

TABLE 5-7
BURNER ASH FED TO LEACHERS, LEACH RUNS 38 THROUGH 41

	13-cm Leacher	20-cm Leacher		
Secondary burner run number	F4RHB-M19	F4RHB-M19	F4RHB-M13	F4RHB-M18
Ash fed to leacher, kg	2.5	5.82	7.0	7.0
Burnable carbon in ash, wt %	0	0	0.2	0.3
Th in ash, wt %	70.67	70.67	73.59	75.80
Screen analysis, cumulative wt %				
<44 μm	41	41	26	28
<76 μm	63	63	70	58
<124 μm	79	79	88	86
<250 μm	97	97	99	97
<450 μm	98.5	98.5	99.8	99

TABLE 5-8
BURNER ASH[(a)] FED TO LEACHERS, LEACH RUNS 42 THROUGH 48

Secondary burner run number	F4RHB-M6	F4RHB-M7	F4RHB-M8	F4RHB-M9
Burner ash product, kg	7.668	7.487	7.612	9.735
Burnable carbon in ash, wt %	0	1.1	0.4	0.2
Screen analysis, cumulative wt %				
<44 μm	46	14	43	45
<76 μm	71	46	76	78
<124 μm	89	82.5	90.2	91.5
<250 μm	99.3	97.7	99.5	99.6
<450 μm	99.9	99.9	99.9	99.9

[(a)]The ash from all four burner runs was mixed to form the feed material for leach runs 42 through 48.

TABLE 5-9
OPERATING DATA FOR LEACH RUNS 38 THROUGH 41

	13-cm Leacher	20-cm Leacher		
	38	39	40	41
Burner ash charged, kg	2.5	5.82	7.0	7.0
Thorex charged, liters	8.19	18.62	22.61	22.78
Air sparge rate, liters/min	11.33	28.32	28.32	51.92
Leaching time at boiling point, hr	1.0	1.0	1.0	1.0
Insolubles after leach (dry wt), kg	0.462	1.019	2.169	1.202
Mother liquor, liters	9.533[(a)]	18.40	22.94	23.186
Wash water, liters	2.83	1.71	3.0	2.942

[(a)] Includes some wash water and steam-jet transfer dilutions.

TABLE 5-10
OPERATING DATA FOR LEACH RUNS 42 THROUGH 48

	13-cm Leacher			20-cm Leacher			
	42	44	46	43	45	47	48
Burner ash charged, kg	4.0	2.38[a]	4.0	6.0	6.0	6.0	6.0
Thorex charged, liters	12.71	11.21	12.9	19.3	19.3	19.7	19.5
Air sparge rate, liters/min	17.5	17.5	16.52	27.0	27.0	30.68	33.04
Leaching time at boiling point, hr	1.5	1.0	1.5	1.5	1.5	1.5	1.5
Insolubles after leach[b] (dry wt), kg	2.380	0.956	0.914	1.375	3.035	1.373	1.371
Mother liquor,[c] liters	12.88	15.64	13.265	19.46	19.59	20.713	19.578

[a] Insolubles from Run 42.

[b] Estimated based on feed and insolubles analysis.

[c] Includes some wash water.

1. 30-cm-diameter perforate basket
2. Polypropylene filter bag (6- to 7-μm openings)
3. 682 g purging force at basket sheet (2000 rpm)
4. After washing filter cake, spin dry for about 5 min

Analyses of samples taken for each leach run are given in Tables 5-11 and 5-12. These data were utilized in material balance calculations (see Tables 5-13 and 5-14).

Steam-Jet Ejectors

Steam-jet transfer of liquid from the Thorex storage tank to the leacher was tried in Run 38. It was found (as expected) that the suction lift provided with available 28-psig steam was not sufficient. A pump was therefore used to charge Thorex to the leacher in all of the eleven runs. (Prior to these tests an Inquiry for Quote for a 90- to 100-psig steam generator was made.) This problem will be eliminated as soon as the new steam supply system is available.

In Runs 38 through 41, the transfer of liquid from the centrifuged-liquid holding tank to the mother liquor storage tank was sucessfully accomplished by a steam-jet ejector. In Runs 39 through 41, a pump was first used to transfer liquid to a special 3-in.-diameter measuring tank and then to the mother liquor storage tank so that a comparison of the quantity and specific gravity of the undiluted mother liquor could be obtained. This liquid was transferred by pump back to the centrifuge holding tank. Run 38 mother liquor was only steam-jet transferred directly to the mother liquor storage tank. Thus, only an estimate of the quantity of undiluted mother liquor is available from the quantity of slurry contained in the 13-cm leacher. These data for dilution of mother liquor by steam-jet transfer are included in Table 5-15. The high dilution that occurred in Run 38 is not completely understood. It could be the result of steam condensate that was not removed from the steam lines. This will be checked in future runs.

TABLE 5-11
SAMPLE ANALYSIS RESULTS[a] FROM LEACH RUNS 38 THROUGH 41

	13-cm Leacher	20-cm Leacher		
	38	39	40	41
Burner ash, wt % Th	70.67	70.67	73.59	75.80
Insolubles, wt % Th	0.08	0.24	51.42	1.69
Mother liquor, g Th/liter	177.05	219.0	152.06	222.88
Wash water, g Th/liter	2.84	117.2	58.87	96.52

[a]Based on gravimetric determination by oxalate precipitation.

TABLE 5-12
SAMPLE ANALYSIS RESULTS[a] FROM LEACH RUNS 42 THROUGH 48

	13-cm Leacher			20-cm Leacher			
	42	44	46	43	45	47	48
Burner ash, wt % Th	68.38	68.38	68.38	68.38	68.38	68.38	68.38
Insolubles, wt % Th	54.61	3.99	0.15	0.40	48.63	0.32	0.13
Mother liquor,[b] g Th/liter	120.2	73.9	217.7	210.9	132.3	213.0	211.0

[a]Based on gravimetric determination by oxalate precipitation.

[b]Includes some wash water.

TABLE 5-13
THORIUM MATERIAL BALANCE RESULTS, LEACH RUNS 38 THROUGH 41

	13-cm Leacher	20-cm Leacher		
	38	39	40	41
Thorium input, g				
Burner ash	1752.75	4079.0	5151.3	5282.0
Thorium output, g				
Mother liquor	1687.82	4084.6	3488.1	5167.8
Insolubles	3.70	2.44	1115.3	20.3
Wash water	8.04	200.0	176.6	284.0
Total output	1699.56	4287.04	4780.0	5472.1
Material balance closure,[(a)] wt %	96.96	105.0	92.7	103.6
Thorium recovery,[(b)] wt %	99.78	99.94	76.66	99.63

[(a)] Output/input.

[(b)] Based on outlet quantities.

TABLE 5-14
THORIUM MATERIAL BALANCE RESULTS, LEACH RUNS 42 THROUGH 48

	13-cm Leacher			20-cm Leacher			
	42	44	46	43	45	47	48
Thorium input, g							
Burner ash	2735	1299[a]	2735	4105	4106	4103	4103
Thorium output, g							
Mother liquor[b]	1548	1156	2888	4104	2592	4412	4131
Insolubles	1299	38	1.4	5.5	1476	4.4	1.8
Total output	2847	1194	2889	4110	4068	4416	4133
Material balance closure,[c] wt %	104.0	91.9	105.6	100.1	99.1	107.6	100.7
Thorium recovery,[d] wt %	54.37	96.8	99.96	99.84	63.7	99.91	99.95

[a] Insolubles from Run 42.
[b] Includes some wash water.
[c] Output/input.
[d] Based on outlet quantities.

TABLE 5-15
DILUTION OF MOTHER LIQUOR BY STEAM-JET EJECTOR

	Leach Run 38	Leach Run 39	Leach Run 40	Leach Run 41
Quantity of liquid before steam-jet transfer, kg	13.03[a]	29.56	34.10	36.99
Quantity of liquid after steam-jet transfer, kg	15.17	30.57	34.48	37.72
Dilution, wt %	14.1	3.30	1.10	1.93

[a]Estimate.

The steam-jet ejector system was not used for transfer of liquids in Runs 42 through 48. All liquid transfers were accomplished with a peristaltic pump.

Feed Hoppers

Solids were charged by gravity to the leachers from a feed hopper (see Fig. 5-17). When the feed valve was first opened, the purge leg readings (recorded in the control room) frequently indicated that solid feed did not enter the leacher. It was necessary to tap the side of the feed hopper before the flow of solids would start. The feed line and valve were electrically heated and maintained at about 170°C. Thus, the problem is not thought to be a result of wet solids buildup. It is felt that bridging of solids in the hopper or feed line caused the problem. To try and eliminate this problem in subsequent runs (42 through 48), an insert was fitted along the sides of the hopper (from top to bottom) to provide an unsymmetrical surface area inside the hopper. However, this did not eliminate the problem. It is felt that increasing the hopper outlet line diameter will eliminate this problem. A separate feed hopper test setup will be assembled in a fume hood on an "as-time-permits" basis. When a successful system is developed, it will be installed on the leaching equipment.

Nitrogen Purge

A nitrogen purge rate of 0.2 scf/h per purge leg was initially used to measure liquid level and specific gravity in all storage tanks and leaching vessels. After Run 38 was completed, it was found that a restriction was forming in the purge legs of the mother liquor storage tank. This restriction was found to be water soluble and is assumed to be thorium nitrate.

During subsequent runs the purge rate to the mother liquor storage tank was increased to 1.0 scf/h per leg. This higher purge rate seems to have eliminated the problem.

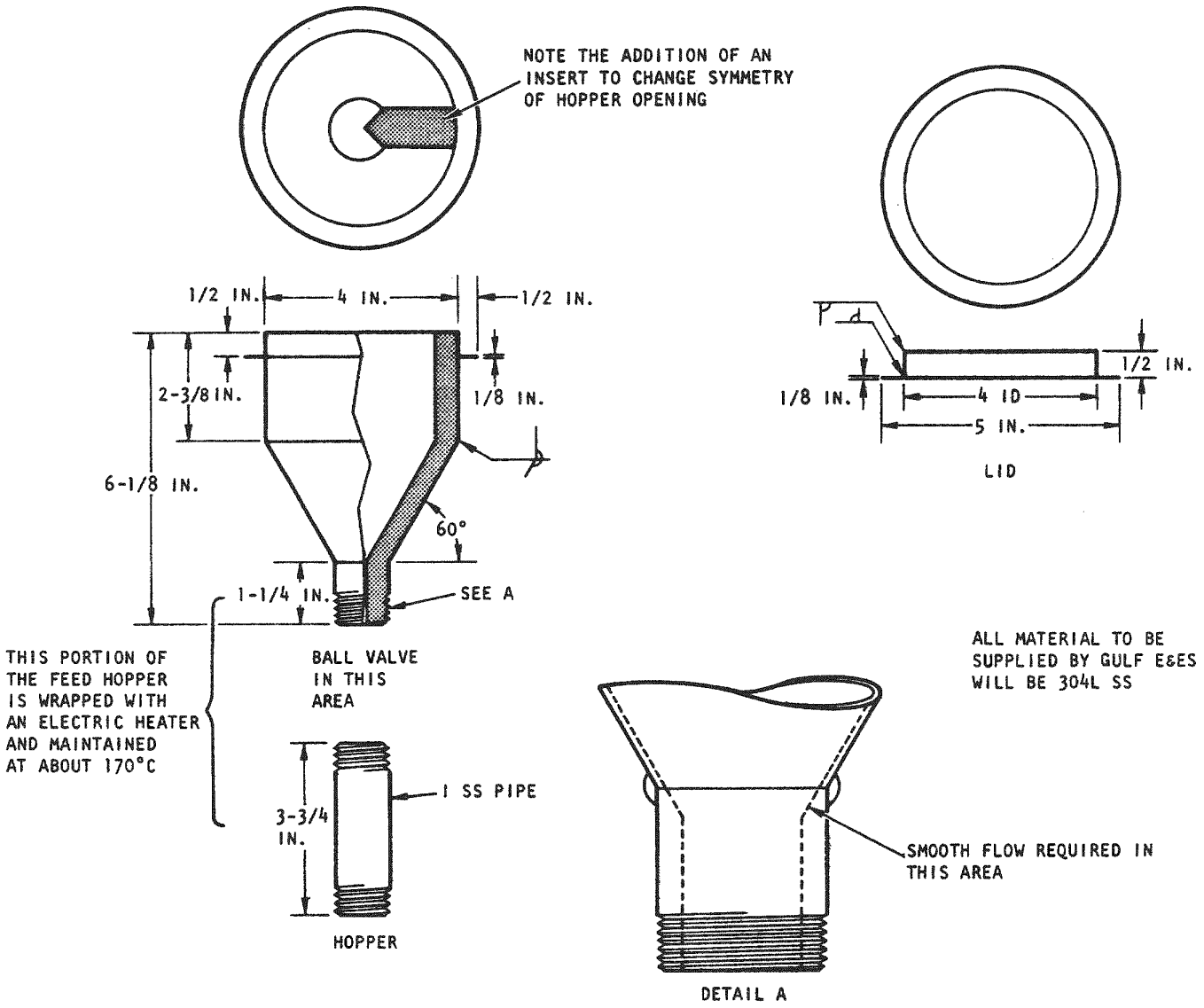

Fig. 5-17. Solids feed hopper change

Leaching Capacity

Leach runs 42 through 48 were conducted in a continuous 16-hour campaign in an attempt to establish the operating capability of the new leaching system. Overall operating efficiency for this test was less than expected. Problems were encountered with (1) bridging of burner ash in feed hoppers, (2) obtaining sufficient agitation of solids in the leachers, and (3) removing insolubles from the leachers. In addition, steam-jet transfer of solutions was not utilized because the existing steam supply is undersized. In spite of these difficulties, it was possible to obtain dissolution at an average rate of over 1.3 kg Th/hr.

TASK VIII
PHYSICS AND FUEL MANAGEMENT

NEUTRON NOISE ANALYSIS

A study of the potential usefulness of neutron noise analysis in HTGR reactors was begun with an extensive literature search. This survey led to the classification of noise experiments into three broad categories, namely, pulse counting techniques, input reactivity variations, and measurement of the power spectral density. The pulse counting techniques are useful in subcritical conditions only and their applicability is limited by the detector efficiency, expressed in counts per fission in the entire reactor. The counting efficiency in a large reactor system would be too low for the useful application of these methods. Therefore, no further effort was put in the study of pulse counting techniques, and attention was focused on the other two techniques. These techniques involve analysis in the frequency domain and, therefore, attention was given to the hardware and software of frequency analysis.

With regard to hardware, a survey was made of available equipment for correlation, Fourier transform, spectral density evaluation, and signal averaging. With regard to software, a package of computer codes for the frequency analysis of random and partially random signals was assembled. These codes have been used in producing simulated time records that are subsequently frequency analyzed. These time records contain a signal which might be intentionally introduced into a reactor to gain information (transfer function measurement) or which might be due to the onset of a malfunction. The use of these codes will permit the estimation of the experimental accuracy of a transfer function or power spectral density measurement as a function of the signal-to-noise ratio.

CROSS SECTION EVALUATION WORKING GROUP (CSEWG)

A recommendation as to the basis for choosing fine-group energy bounds for neutron cross sections in the fast (and epithermal) energy range was forwarded to the relevant CSEWG subcommittee chairman.

A report describing the GAND2/GFE2 neutron cross-section processing codes was completed. The GAND2 and GFE2 codes will be sent to the Argonne Code Center when copies of the report are available.

Titanium activation cross sections were reviewed and a Ti-46(n,p)Sc-46 data set was prepared.

CRITICAL EXPERIMENT ANALYSIS

Work on a re-analysis of the C/U = 5000 HTGR critical experiment was initiated.* Heterogeneity effects will be analyzed more rigorously using more refined analytical and computational methods.**

Some additional analysis of the HTLTR lattices containing U-233 was also initiated. It is planned to investigate the effect of the U-235 region (not enough U-233 was available to completely fill the experimental region), the effects of uncertainties in atom densities, and the effect (if any) caused by the use of more rigorous U-233 cross section values

---

*Bardes, R. G., et al., "Results of HTGR Critical Experiments Designed to Make Integral Checks on the Cross Sections in Use at Gulf General Atomic," Gulf General Atomic Report GA-8468, February 12, 1968.

**Wälti, P., and P. Koch, "MICROX - A Two-Region Flux Spectrum Code for Efficient Calculation of Group Cross Sections," Gulf General Atomic Report Gulf-GA-A10827, April 14, 1972.

computed via the Adler-Adler resonance formulae. The third HTLTR lattice, in which a very small reactivity change with temperature was observed, is particularly sensitive to small changes because a small temperature defect in such a dilute C/Th/U-233 lattice is due to a balance of competing effects.

TEST ELEMENT PROGRAM

The detail plans for the postirradiation examination of FTE-3 were completed during the reporting period, and the postirradiation examination was started on March 27, 1973. The major portion of the disassembly operations has been completed. Individual investigations, as listed below, are now being conducted, or will soon be started, on various samples.

1. Metallurgy on selected fuel rods.
2. Postirradiation fission gas release on selected fuel rods.
3. Disintegration-leach analysis on selected fuel rods.
4. Autoradiography on the fuel body graphite slices.
5. Graphite fuel body integrity and residual stress analysis.
6. Additional graphite dimensional change data.

All three FTE-3 graphite fuel bodies were removed from the Peach Bottom graphite sleeve without difficulty. The high-magnification examination revealed no cracks or other abnormalties in any of the fuel bodies. Photographs of the three fuel bodies are shown in Figs. 8-1 through 8-3. Analysis of the graphite dimensional change information has not yet been completed.

All of the fuel rods were pushed out of the fuel bodies without difficulty. The fuel rods appear to be in excellent condition based on photographs taken at low magnification. Photographs of representative fuel rods are shown in Fig. 8-4. Fuel rod dimensional change data are still undergoing analysis.

Fig. 8-1. Fuel body 1 from FTE-3

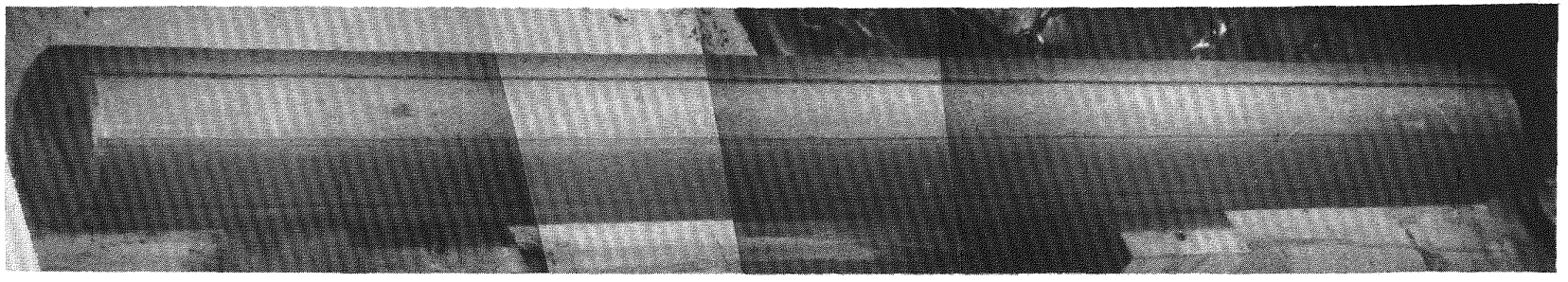

Fig. 8-2. Fuel body 2 from FTE-3

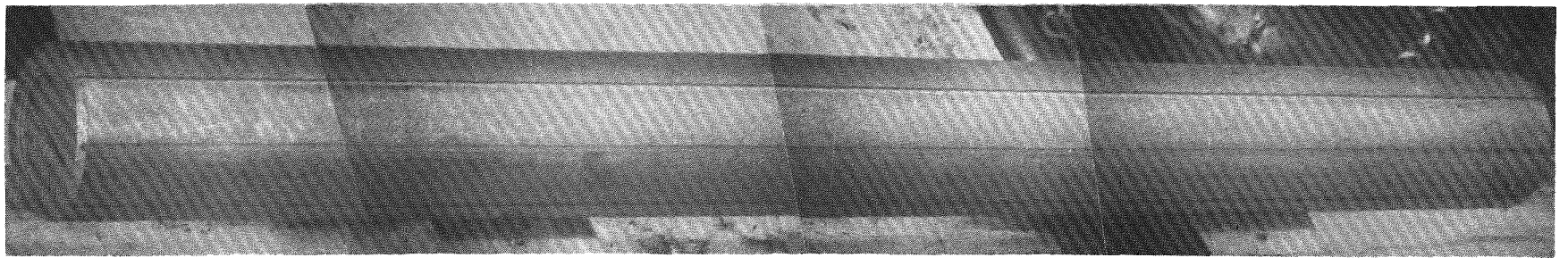

Fig. 8-3. Fuel body 3 from FTE-3

K7311-35

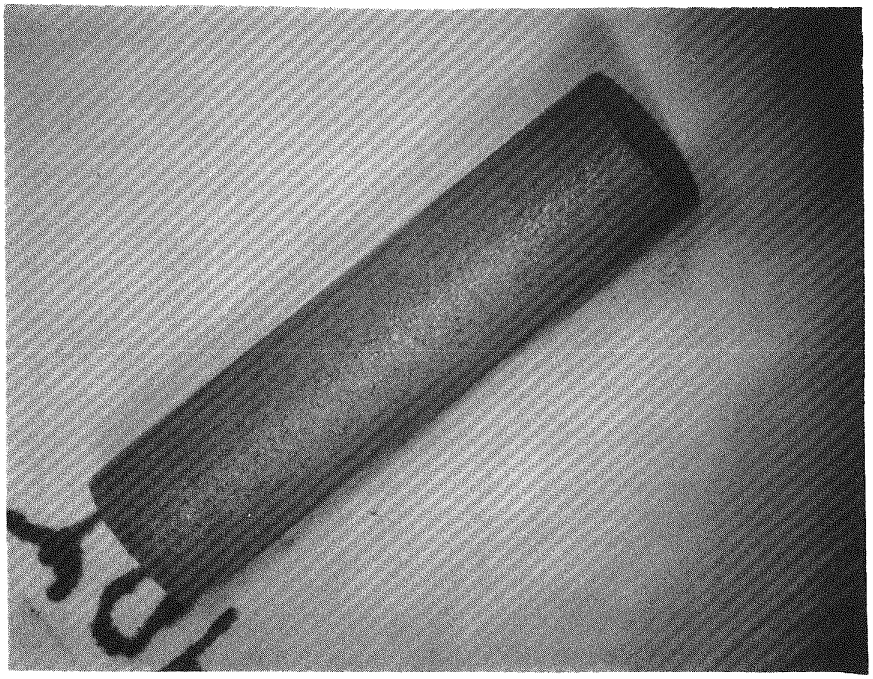

K7311-79

Fig. 8-4. Representative appearance of typical fuel rods from FTE-3

Fission gas release tests have been performed on several fuel rod samples containing typical HTGR fuel particles. The average R/B value for Kr-85m release from the rods tested to date is $\sim 3 \times 10^{-6}$, indicating very little change in the integrity of the particle coating during irradiation in the Peach Bottom HTGR. Fuel rods are also being annealed at relatively high temperatures (1600° to 2000°C) in an attempt to physically fail coatings. The fuel rods will then be exposed to reactor operating levels of H_2O to determine what effect hydrolysis has on fission gas release. One rod has been annealed at 1600°C for ~500 hours with little or no increase in Kr-85m R/B values. Additional fuel rods will be annealed at 1600°, 1800°, and 2000°C to determine the release of cesium from the total fuel rod.

The fuel rods irradiated in FTE-3 were:

UC_2 TRISO + ThC_2 BISO

$(Th,U)C_2$ TRISO + ThC_2 TRISO

UO_2 TRISO + ThO_2 BISO

$(Th,U)C_2$ TRISO + ThC_2 BISO

In addition, analysis is currently under way on various center spine samples, including:

1. Metallic fission product diffusion samples.

2. Fission product release samples on various small lots of fuel particles.

3. Thermal stability fuel particle samples.

Chemistry spine samples included in FTE-3 are of two types: (1) diffusion samples in which graphite matrix material was tagged with various metallic isotopes and contained in thick-walled H-327 graphite crucibles, and (2) fission product release samples containing various types of fuel particles inside graphite crucibles. The graphite crucibles from the metallic diffusion samples are being sectioned on a lathe and gamma counted to determine the concentration profile for Cs, Sr, Sm, and Ba in the wall of the crucible. Diffusion coefficients for the various isotopes can then be calculated.

Fission product release samples composed of loose fuel particles contained in a small inner graphite crucible surrounded by matrix material inside an outer graphite crucible are currently being separated into component parts for gamma counting. The fission product release behavior of the various particle batches used can then be determined at various irradiation temperatures.

In addition, the graphite crucibles will be sectioned and gamma counted to determine fission product concentration between the inner crucible - particle boundary and the outer crucible - matrix material boundary.

FTE-3 was irradiated in the Peach Bottom HTGR for 132 EFPD. Irradiation was started on 7/11/71 and ended 1/7/72. Calculations were made to determine the fuel temperature and the fast and thermal fluence conditions experienced by FTE-3. These results are shown in Fig. 8-5.

On February 5, 1973 Peach Bottom fuel element E06-01 was sent to ORNL per the GGA Task VIII Base Program agreement. The element will undergo postirradiation examination in the ORNL hot cells under an ORNL Base Program agreement. The overall purpose of the study is to determine the amount of metallic fission products leaving the Peach Bottom core.

It is now planned to operate the Peach Bottom HTGR through the summer of this year and to cancel the previously planned fuel handling shutdown

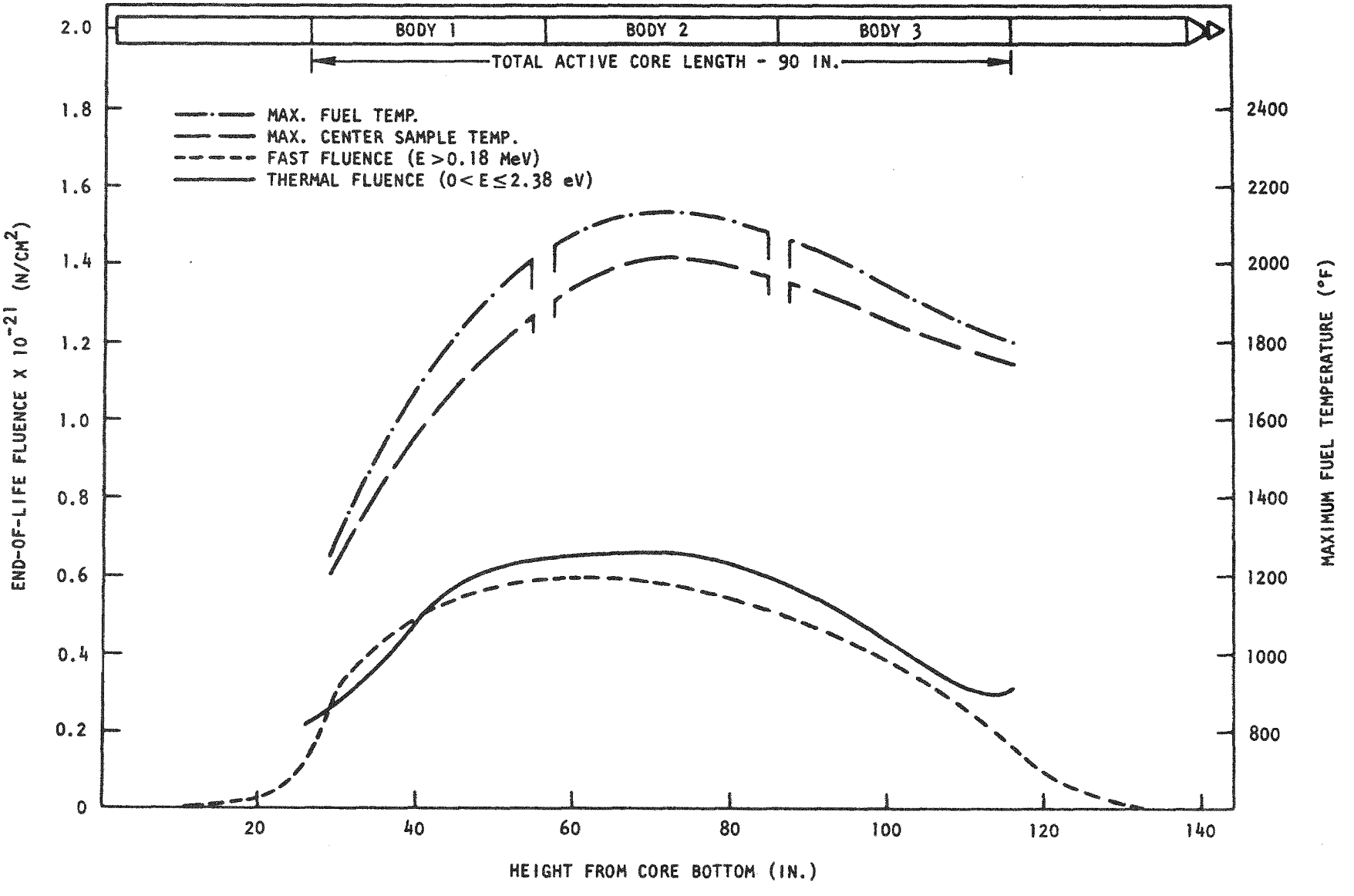

Fig. 8-5. FTE-3 end-of-life temperature and fluence

during the spring of this year. This will delay the planned removal of fuel test elements FTE-4 and FTE-14 and recycle test element RTE-2. A fall shutdown at approximately 700 EFPD is now planned, and these elements will be removed at that time.

During the reporting period, fuel test elements FTE-4, -6, -14, and -15 and recycle test elements RTE-1, -2, -5, -6, and -8 continued to operate well within the Peach Bottom HTGR.

TASK IX

FUEL MATERIALS DEVELOPMENT

MEASUREMENT OF GAS CONTENT OF IRRADIATED TRISO UC_2 AND UO_2 PARTICLES

Introduction

The measurement of gas content of irradiated fuel particles is continuing to further characterize HTGR fuel. This investigation will assist in predicting particle failure due to thermochemical reactions and coating stresses arising from gas pressure.

The present experimental work is concerned with the measurement of gas released in irradiated UC_2 and UO_2 TRISO coated particles. While both types of fuel kernels produce fission gases during irradiation, UO_2 fuel also releases oxygen to form CO/CO_2 gas.

Materials

A description of materials and the irradiation conditions of the UO_2 and UC_2 TRISO coated particles selected for this investigation are given in Table 9-1. Buffer coatings were obtained by the pyrolysis of acetylene mixed with a helium carrier gas at 1050°C. The inner and outer pyrolytic carbon coatings deposited at approximately 1420°C were formed from propane with helium as the carrier gas. The silicon carbide coatings were deposited from methyltrichorosilane in a hydrogen atmosphere at 1500°C. The coated fuel particles were irradiated in capsule P13L.

Experimental Procedures

The description of the apparatus and the analytical procedures used to determine the internal gas content were described in earlier Quarterly

TABLE 9-1
DESCRIPTION OF COATED FUEL PARTICLES AND IRRADIATION DATA

	Batch No.	
	4413-67	4413-5
Coating type	TRISO	TRISO
Fuel kernel		
Type	UO_2	UC_2
Nominal size, μm	124	106
Density, g/cm^3	9.32	10.2
Buffer layer		
Thickness, μm	46	53
Density, g/cm^3	1.26	1.30
Inner isotropic layer		
Thickness, μm	22	24
Density, g/cm^3	1.85	1.83
SiC layer		
Thickness, μm	20	20
Density, g/cm^3	3.16	3.20
Outer isotropic layer		
Thickness, μm	22	23
Density, g/cm^3	1.75	1.80
Irradiation conditions		
Burnup, % FIMA	68	74
Temperature, °F	870	1400
Fast neutron fluence (E > 0.18 MeV), x 10^{21} n/cm^2	5.8	7.8

Progress Reports (Gulf-GA-A12422, Gulf-GA-A12515). Each particle was crushed at room temperature or a selected higher temperature in order to measure the total internal fission gas content released.

The activity of Ru-106 in each particle was determined from the gamma spectrum counted with a lithium-drifted germanium detector interfaced to a 4096 SDS Sigma II computer analyzer. The theoretical amounts of Kr and Xe gas produced during irradiation and the initial U-235 content of each particle were then calculated with a computer program using Ru-106 as the reference isotope. The assumption was made that Ru-106 is retained in the kernel. Fractional release of fission gas in this report refers to the ratio of the measured fission gas release to the theoretical Kr and Xe content.

After irradiation, the kernel was no longer spherical and the kernel boundary was indistinct due to heavy metal diffusion into the surrounding coatings. Due to the difficulty in calculating the kernel volume from a two-dimensional radiograph plate, a preirradiated kernel volume of each particle was calculated using the theoretical amount of U-235 and the preirradiated density of the kernel. This theoretical kernel volume has an accuracy of approximately ±15% and is used in presenting results of this investigation.

Results and Discussion

The results of the particle crushing investigation of the irradiated TRISO coated UC_2 and UO_2 particles are given in Tables 9-2 and 9-3, respectively. Some of the data for UO_2 particles were reported in an earlier Quarterly Progress Report (Gulf-GA-A12422).

The total gas pressure of each irradiated UC_2 and UO_2 particle versus the temperature at which the particle has crushed is plotted in Figs. 9-1 and 9-2, respectively. The gas pressures do not include the gas contributed from condensable fission products or fission products which are only gases

TABLE 9-2
RESULTS OF GAS RELEASE MEASUREMENTS IN UC_2 TRISO PARTICLES IRRADIATED IN CAPSULE P13L
(BATCH 4413-5, 1400°C, 74% FIMA)

Experiment No.	Particle No.	Measured Kernel Volume (10^{-6} cm^3)	Initial Theoretical Kernel Volume[a] (10^{-6} cm^3)	Particle Void Volume (10^{-6} cm^3)		Cs-137/Zr-95 Atom Ratio[b] (Theoretical Ratio = 16.7)	Crushing Temp. (°C)	Theoretical Kr + Xe Content[a] (10^{-9} moles)	Total Gas Release[c] (10^{-9} moles)	Total Gas Pressure At Crushing Temp. (atm)		Fission Gas Fractional Release[d]
				Min.	Max.					Min.	Max.	
5847-146	1	1.18	1.54	1.57	1.85	13.4	1035	11.6	8.80	510	605	0.76
5847-148	2	0.41	1.18	2.57	2.60	12.6	25	8.90	5.35	50	51	0.60
5847-150	3	0.56	1.35	2.32	2.40	13.2	1110	10.2	8.40	406	420	0.83
6046-6	4	0.46	0.97	1.75	1.80	11.8	25	7.30	3.82	52	53	0.52
6046-8	5	1.35	1.65	2.45	2.79	13.1	950	12.4	9.55	344	391	0.77
6046-24	6	0.93	1.68	2.89	3.09	11.9	1160	12.7	7.10	272	290	0.56
6046-48	7	1.12	1.36	3.49	3.76	12.6	980	10.2	5.15	142	152	0.50
6046-60	8	1.12	1.44	3.58	3.84	12.8	1120	10.8	8.03	240	256	0.74
6046-62	9	1.35	1.42	2.84	3.17	12.9	25	10.6	5.30	41	46	0.50
6046-64	10	1.29	1.34	3.43	3.76	13.0	1310	10.1	7.30	252	276	0.72
6046-66	11	0.80	1.74	3.00	3.17	11.7	25	13.2	5.30	42	44	0.40
6046-68	12	0.76	1.88	2.47	2.61	12.3	1085	14.2	7.85	337	356	0.55
6046-72	13	0.84	1.63	3.41	3.58	12.2	820	12.3	6.75	169	178	0.55
6046-76	14	1.23	1.94	1.94	2.24	12.1	820	14.8	8.21	328	379	0.56
6046-78	15	0.97	1.34	1.73	1.94	13.2	25	10.1	5.11	64	73	0.51
6046-80	16	1.18	1.72	1.87	2.04	12.1	800	13.0	7.30	315	344	0.56

[a] Determined from Ru-106 activity of each particle.

[b] Cs-137/Ru-106 ratio was actually measured; then Cs-137/Zr-95 ratio was estimated using theoretical calculations.

[c] Calculated from measured pressure rise in crushing system at pressures $<10^{-3}$ Torr assuming ideal gas law and a correction factor (α) = 0.5 (Quarterly Progress Report Gulf-GA-A12422).

[d] $\frac{\text{Total gas released}}{\text{Theoretical Kr + Xe content}}$.

TABLE 9-3
RESULTS OF GAS RELEASE MEASUREMENTS IN UO_2 TRISO PARTICLES IRRADIATED IN CAPSULE P13L
(BATCH 4413-67, 870°C, 68% FIMA)

Experiment No.	Particle No.	Measured Kernel Volume (10^{-6} cm^3)	Initial Theoretical Kernel Volume[a] (10^{-6} cm^3)	Particle Void Volume (10^{-6} cm^3)		Cs-137/Zr-95 Atom Ratio[b] (Theoretical Ratio = 11.5)	Crushing Temp (°C)	Theoretical Kr + Xe Content[a] (10^{-9} moles)	Total Gas Release[c] (10^{-9} moles)	Total Gas Pressure At Crushing Temp (atm)		Normalized Total Gas Release[d] (10^{-3} moles/cm^3)
				Min.	Max.					Min.	Max.	
5368-146	4	1.07	1.40	2.40	2.50	9.58	25	8.95	5.08	50	52	3.6
5368-148	5	1.28	1.44	2.05	2.22	9.29	1180	9.33	11.5	612	663	8.0
5847-6	7	1.18	1.41	1.80	1.94	9.50	1355	9.15	8.55	584	629	6.1
5847-8	8	1.18	1.38	2.16	2.30	9.62	1350	8.96	12.7	737	788	9.2
5847-10	9	1.18	1.15	3.07	3.21	9.41	1085	7.45	9.45	326	341	8.2
5847-34	11	0.98	1.25	1.60	1.67	8.30	1050	8.13	4.80	312	326	3.8
5847-36	12	1.07	1.62	1.49	1.60	9.03	1150	10.5	5.23	376	404	3.2
5847-38	13	1.32	1.71	1.20	1.38	8.51	1080	11.8	8.25	656	758	4.8
5847-42	15	1.32	1.32	3.03	3.21	9.66	25	8.57	4.86	37	39	3.7
5847-20	16	1.12	1.15	3.91	4.03	8.95	1015	7.48	6.88	179	185	6.0
5847-22	17	0.93	1.12	2.01	2.09	9.70	1015	5.27	4.44	224	233	4.0
5847-30	19	0.97	1.11	2.37	2.68	8.73	1125	7.20	4.58	196	221	4.1
5847-44	20	1.35	1.48	3.14	3.29	9.62	1195	9.62	10.6	386	404	7.2
5847-54	25	1.35	1.56	2.00	2.19	9.41	920	10.1	9.30	414	454	6.0
5847-78	26	0.97	1.02	2.39	2.47	10.6	935	6.54	12.6	505	521	12.4
5847-130	27	0.93	0.98	3.23	3.30	9.75	1020	6.40	11.5	368	371	11.7
6046-12	28	1.29	1.22	1.52	1.70	10.6	810	7.96	9.75	509	569	8.0
6046-14	29	1.40	1.51	2.23	2.43	8.70	940	9.80	7.16	296	320	4.7
6046-16	30	1.18	1.38	2.15	2.47	9.54	795	8.95	6.02	214	246	4.4
6046-18	31	1.44	1.66	2.08	2.29	8.95	800	10.8	6.75	259	285	4.0
6046-22	32	1.08	1.14	2.65	2.77	9.36	1320	7.40	7.43	353	369	6.5
6046-42	33	1.07	1.46	1.42	1.53	9.62	1115	9.49	11.2	833	908	7.3
6046-44	34	1.66	1.52	1.38	1.64	10.1	1305	9.90	13.0	1033	1238	8.6
6046-46	35	1.02	1.20	1.33	1.42	9.10	1300	7.80	6.60	608	649	5.5

[a] Determined from Ru-106 activity of each particle.

[b] Cs-137/Ru-106 ratio was actually measured; then Cs-137/Zr-95 ratio was estimated using theoretical calculations.

[c] Calculated from measured pressurerise in crushing system at pressures $<10^{-3}$ Torr assuming ideal gas law and a correction factor (α) = 0.75 (Quarterly Progress Report Gulf-GA-A12422).

[d] $\frac{\text{Total gas released}}{\text{Initial theoretical void volume}}$.

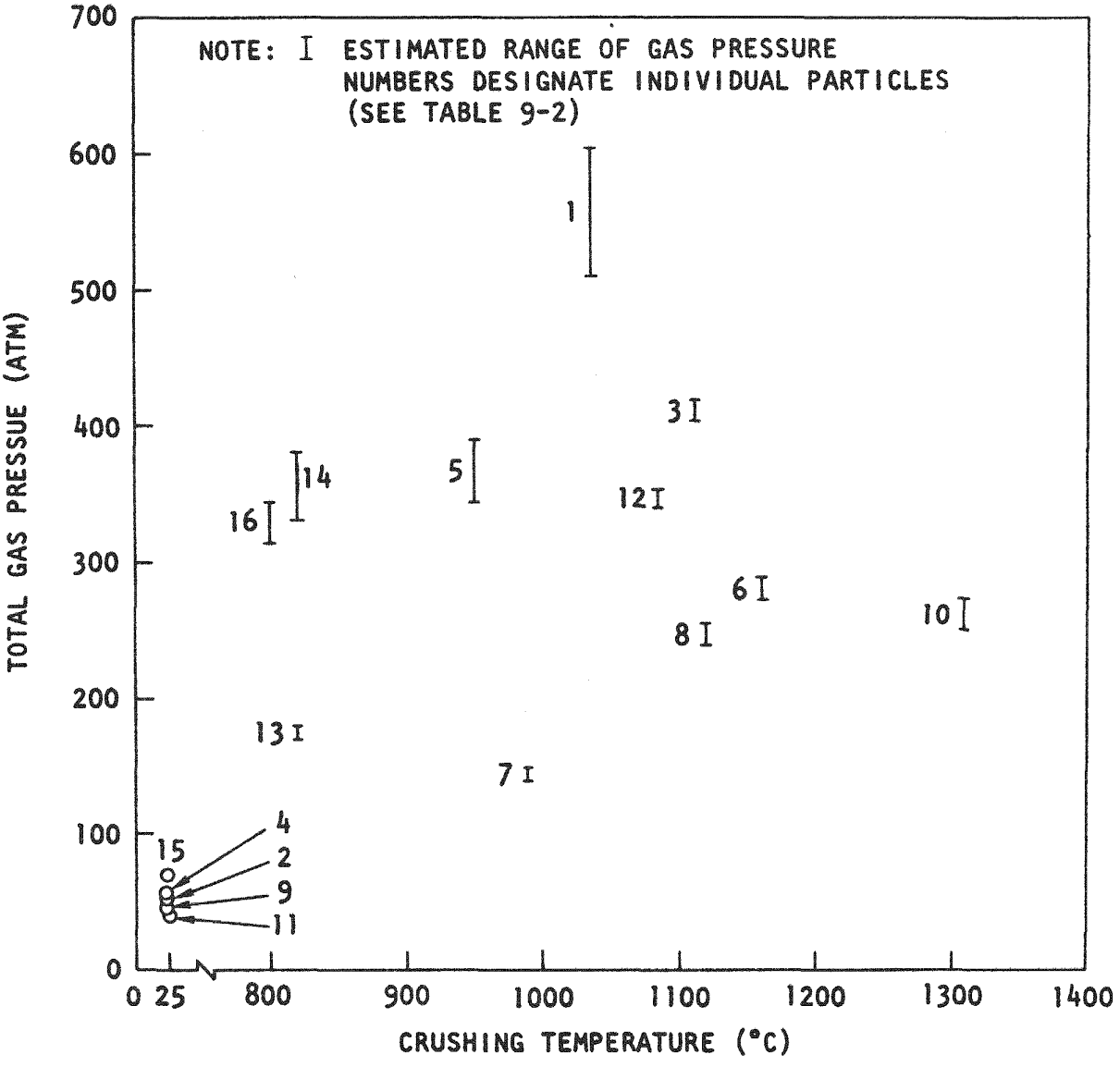

Fig. 9-1. Total gas pressure of irradiated UC_2 TRISO particles versus crushing temperature

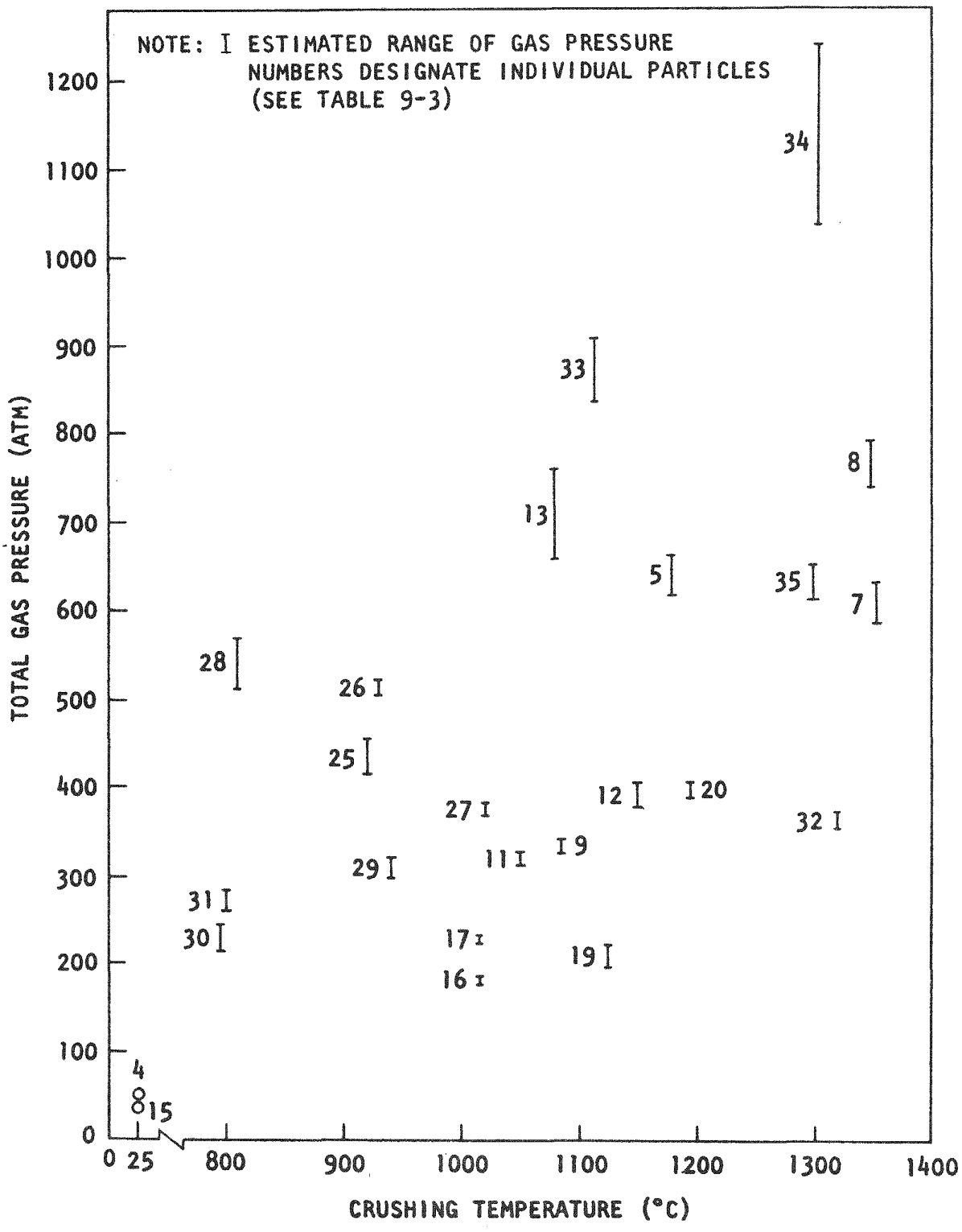

Fig. 9-2. Total gas pressure of irradiated UO_2 TRISO particles versus crushing temperature

above room temperature. The large differences in void volumes and kernel volumes in individual particles contributed to the variability in total gas pressure. No method has been devised to directly measure the void volume in an irradiated fuel particle. The range of void volumes given in the tables is estimated from the preirradiated porosity in the kernel and the buffer coating.

When an irradiated UC_2 fuel particle was crushed, the gases released were assumed to be Xe and Kr isotopes. A plot of the fractional release of fission gas in UC_2 particles versus the crushing temperature is shown in Fig. 9-3. The fractional release numbers have an accuracy of approximately ±20%. There is no conclusive dependence of temperature on the fractional release of fission gas. It is noted that the Cs/Zr atom ratios are slightly lower for particles that had lower fractional release numbers. These particles may have released some of their fission gas during irradiation, which would indicate the individual silicon carbide coatings had failed. This batch of particles was exposed to severe irradiation temperatures, as high as 1675°C, which could have caused SiC coating failure. There appears to be a linear relationship between the amount of fission gas released and the kernel volume, as shown in Fig. 9-4. Assuming no fission gas was lost during irradiation, a linear function would indicate that the fractional release of gas is constant for this range of kernel sizes and independent of crushing temperature.

Irradiated UO_2 TRISO particle test data are more difficult to analyze due to the uncertainties in CO/CO_2 gas formation during irradiation. In earlier Quarter Progress Reports, the assumption was made that 100% of the theoretical Kr and Xe gases was released from the crushed particle. The CO/CO_2 gas content was then estimated to be the difference between the measured total gas content and the theoretical calculation. The less than complete release of fission gas in UC_2 TRISO particles indicates that this assumption cannot be made and, therefore, the absolute amount of CO/CO_2 gas cannot be determined. However, the theoretical Kr + Xe content in

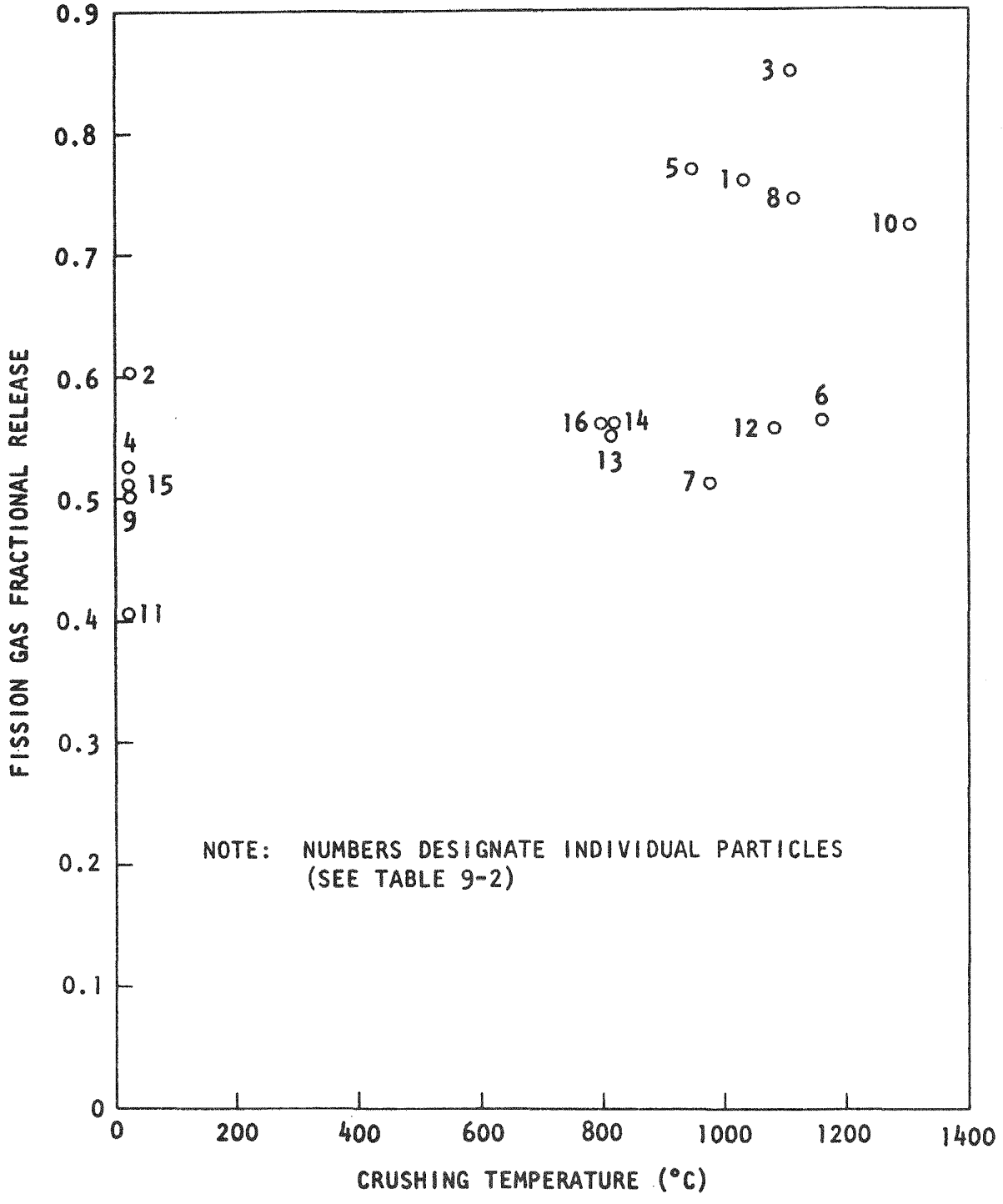

Fig. 9-3. Fission gas fractional release of UC_2 TRISO particles versus crushing temperature

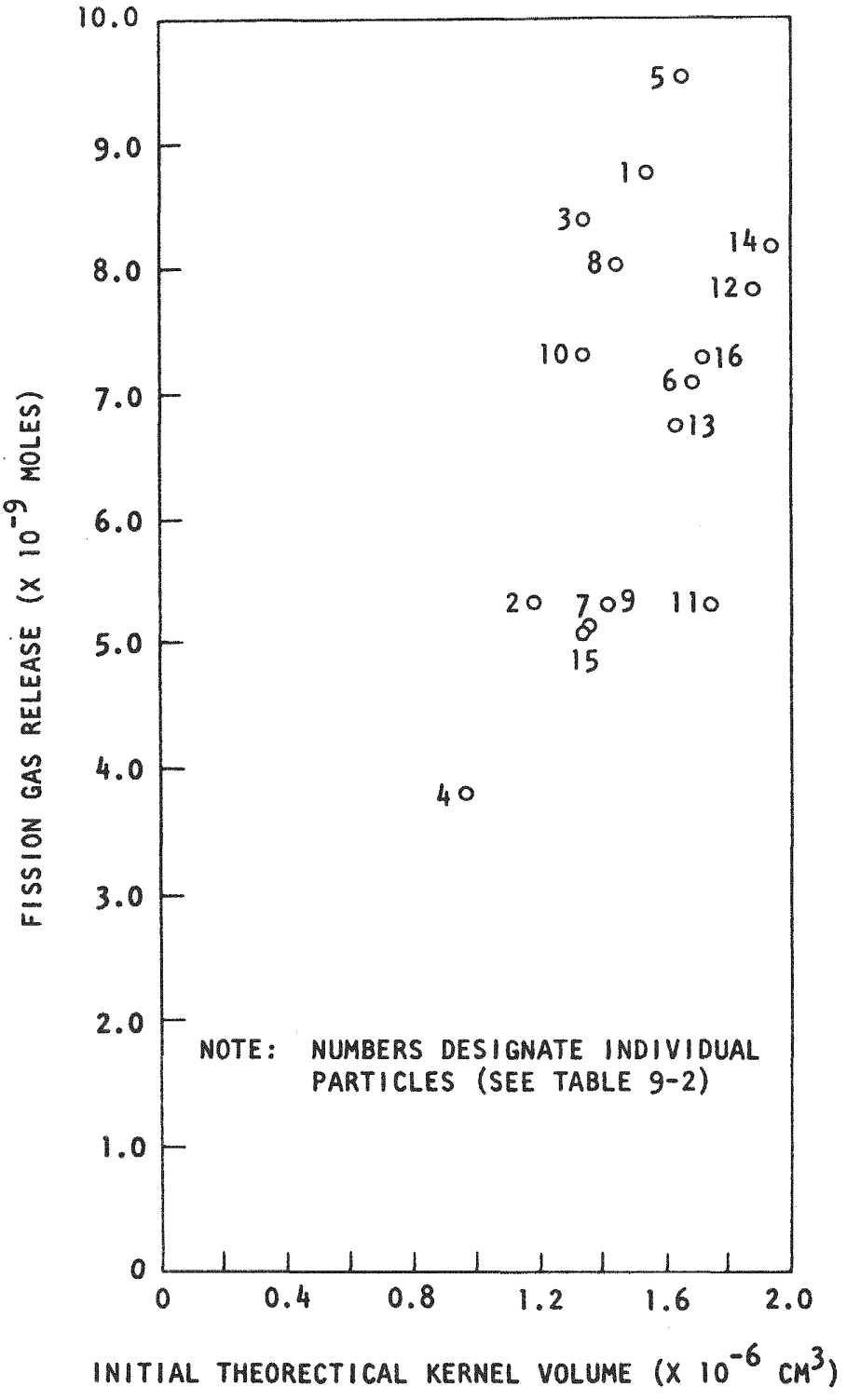

Fig. 9-4. Fission gas release of UC_2 TRISO particles versus initial theoretical kernel volume[2]

some UO_2 particles was much larger than the total amount of gas released, which would indicate very little CO/CO_2 gas is in these particles. The total gas released from each particle is plotted as a function of crushing temperature in Fig. 9-5. In order to take into account the variability in kernel size, the total gas released was normalized by dividing it by the initial theoretical kernel volume. The scatter of the data points makes it difficult to determine how CO/CO_2 formation varies with temperature.

Gas release measurements of irradiated fuel particles are continuing. As more data are accumulated, attempts will be made to estimate expected average, maximum, and minimum gas release as a function of kernel volume, temperature, burnup, and particle type.

FUEL IRRADIATIONS

A series of capsule irradiations is being conducted to evaluate recyclable fuel systems for a large HTGR under the irradiation environments expected in a large HTGR.

Capsule P13M

The Hot-Cell portion of the postirradiation examination of capsule P13M has been completed. These results were reported in an earlier Quarterly Progress Report (Gulf-GA-A12422).

The majority of UC_2 TRISO particles irradiated in fuel rods and as unbonded particle samples showed signs of fission product and/or fuel diffusion into the IPyC coating on one side of the particle. From metallographic examination of fuel rod samples it was observed that diffusion of the heavy metals was toward the cooler side of the particles. Similar diffusion of metallic fission products down a temperature gradient was also observed in UC_2 TRISO particles irradiated in capsule P13L and annealed out-of-pile in a thermal gradient.*

*Scott, C. B., "Thermochemical Stability of Irradiated HTGR Fuel Particles," USAEC Report Gulf-GA-B12409, Gulf General Atomic, May 1, 1973.

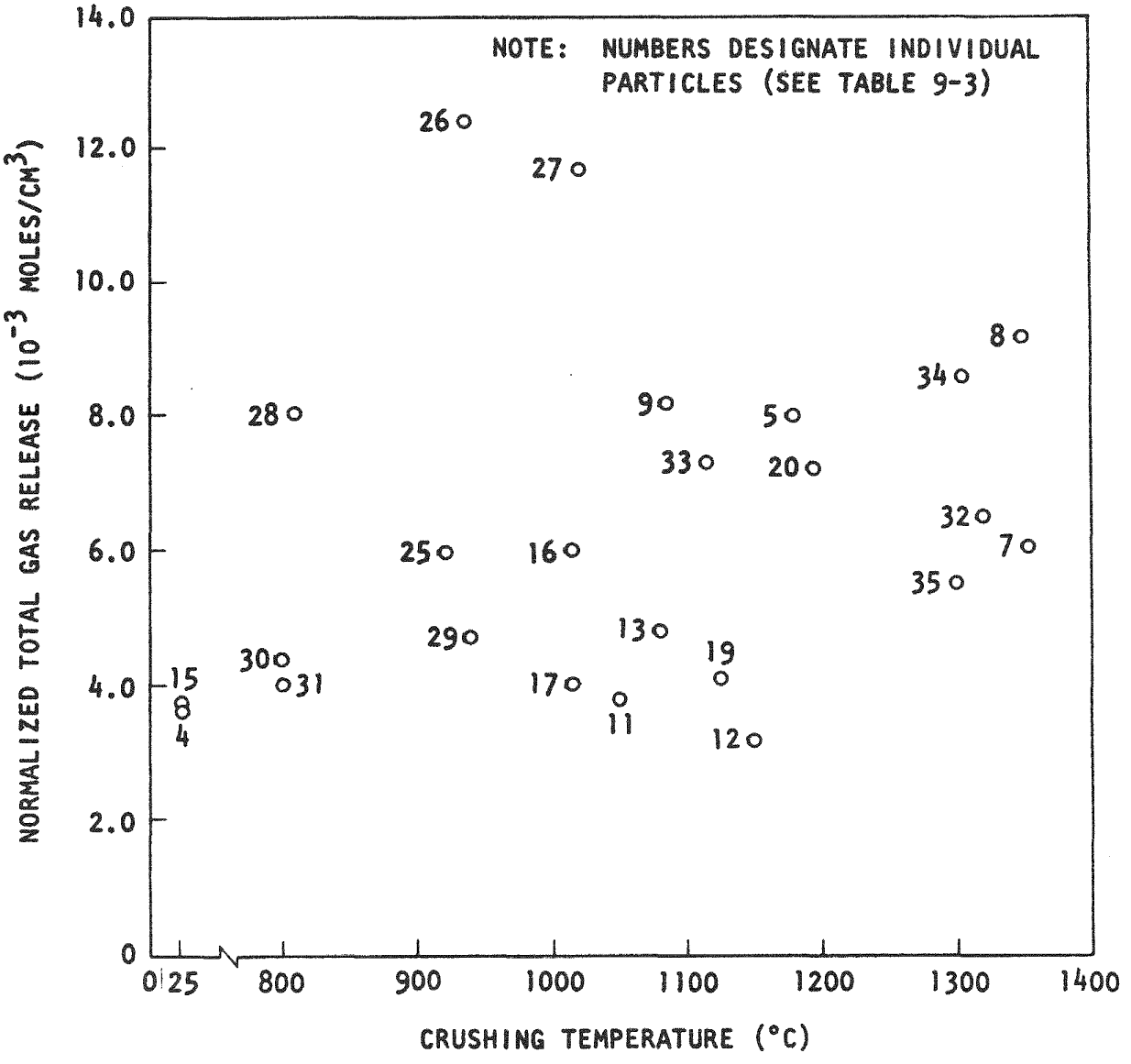

Fig. 9-5. Temperature dependence of normalized total gas release of UO_2 TRISO particles

A noticeable change in the IPyC coating structure occurred where high concentrations of heavy metal were observed, and a metallic-appearing deposit was often observed at the IPyC/SiC coating interface. In a few instances a reaction had occurred between the metallic phase and the SiC coating.

Radiograph and electron microprobe studies were initiated to identify the composition and extent of the heavy metal diffusion. Thirty-five UC_2 TRISO particles from batch 4000-325 were radiographed and then mounted for metallography. Radiographs and photomicrographs of UC_2 particles from this sample showing heavy metal concentrations on one side of the particle are shown in Fig. 9-6.

Five particles in the metallographic mount were examined with an electron microprobe. The only heavy metals observed to be preferentially diffusing out of the fuel kernel to the SiC coating were the rare earth fission products Ce, Nd, La, Sm, Pr, and Eu. Figures 9-7 and 9-8 show electron microprobe scanning photographs of the particle shown in Fig. 9-6. The rare earth fission products (Fig. 9-7) have diffused to the side of the particle exhibiting the reaction zone at the SiC/IPyC coating interface. Cerium was present in concentrations up to 35 wt % in the reaction zone. The concentrations of other rare earth fission products were present in relative amounts corresponding to the ratio of the fission product yields of these isotopes during thermal fissioning of U-235. As shown in Fig. 9-8, the stable oxide formers Mo, Zr, and Ru remained in the fuel kernel and were not positively correlated with any of the fission products in the reaction zone. Chlorine, however, did appear to be correlated with the fission products in the reaction zone (see Fig. 9-8), indicating the possibility of the formation and transport of rare earth fission product chlorides to the reaction zone. Barium, strontium, cesium, and xenon were also found in the particles, indicating the SiC coating in the particles had not failed during irradiation.

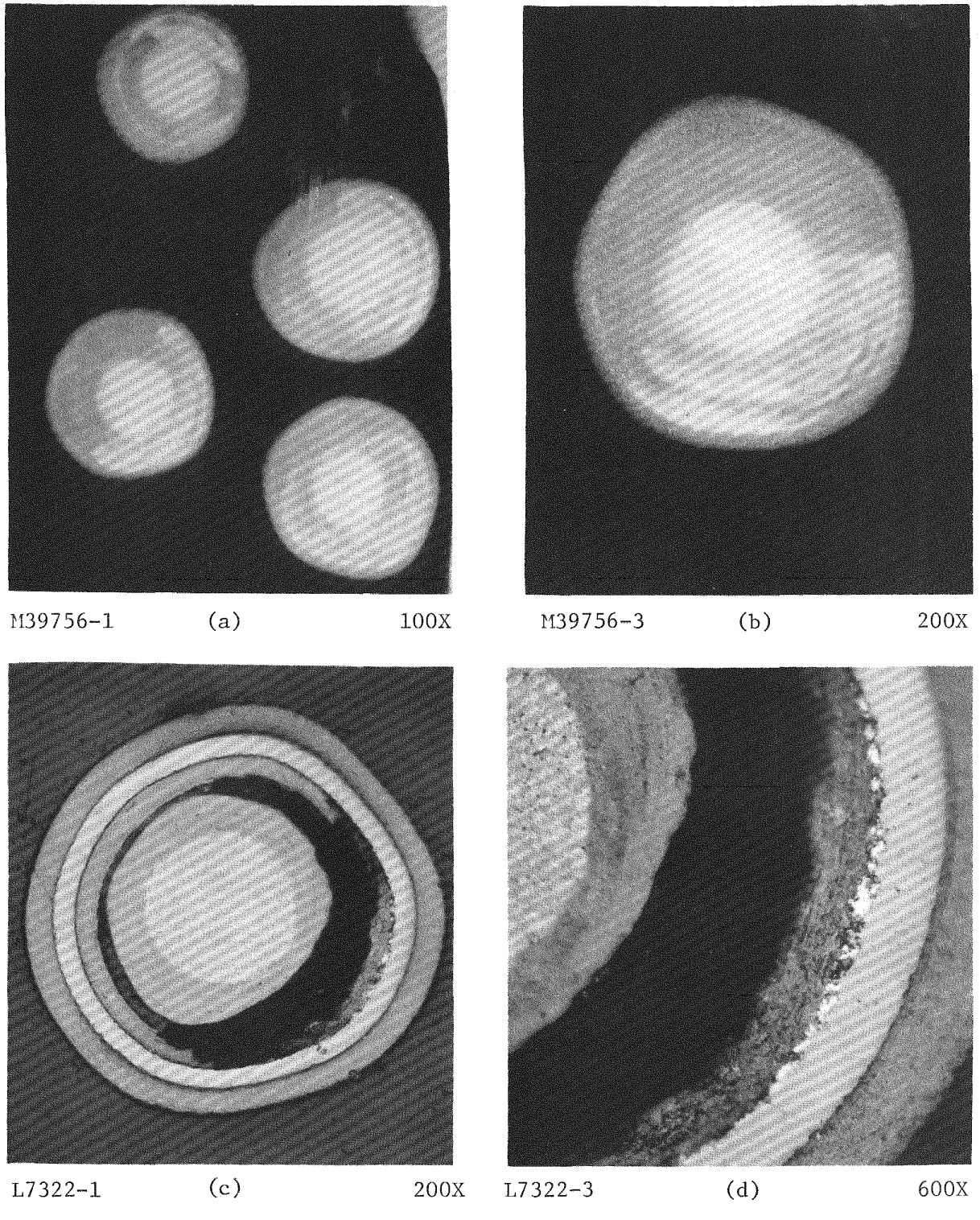

Fig. 9-6. Contact micrographs (a,b) and photomicrographs (c,d) showing diffusion of metallic fission products out to the SiC coating in UC_2 TRISO particles irradiated in capsule P13M (C4T5) to 6.6×10^{21} n/cm^2 and 70% FIMA at 1300°C.

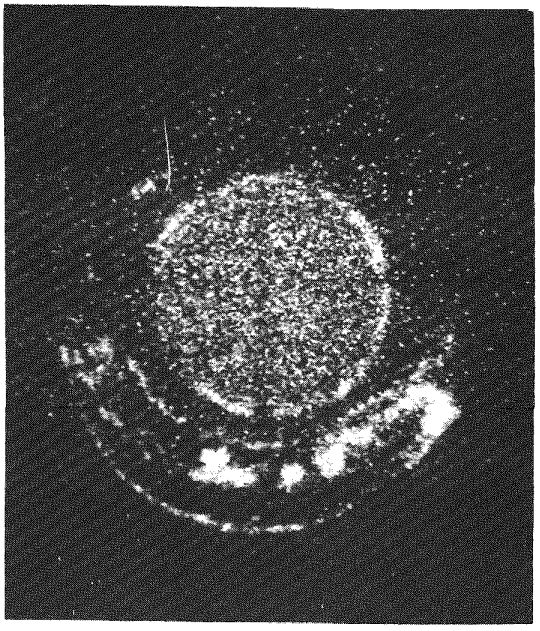

Ce ($L\alpha$)

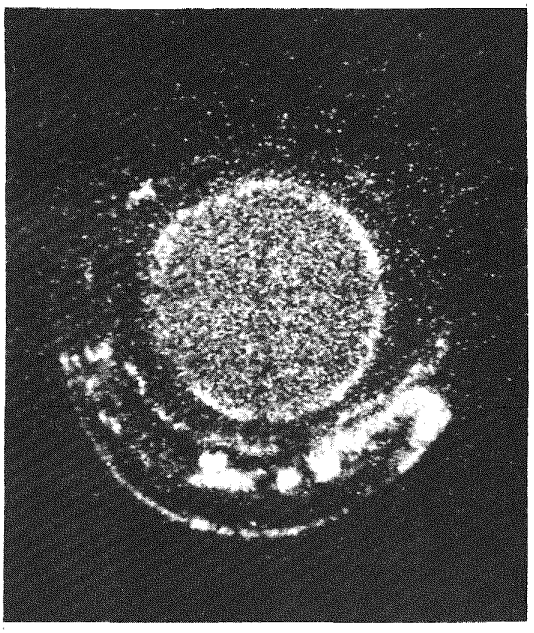

Nd ($L\alpha$)

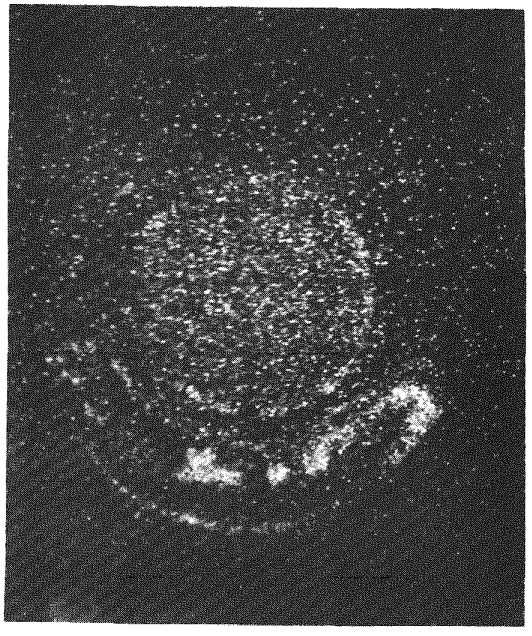

La ($L\alpha$)

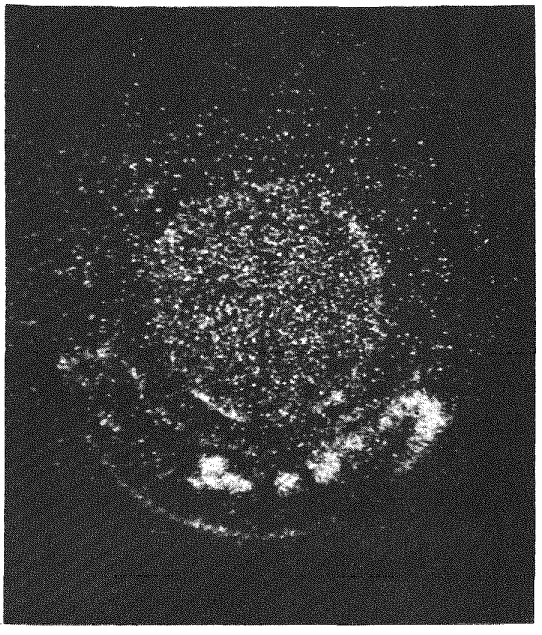

Pr ($L\alpha$)

Fig. 9-7. Electron microprobe scanning photographs of the UC_2 TRISO particle shown in Fig.9-6c. The bright regions indicate relative abundance of the indicated element (Ce, Nd, La, Pr). These photographs are a mirror image of the bright-field photomicrograph.

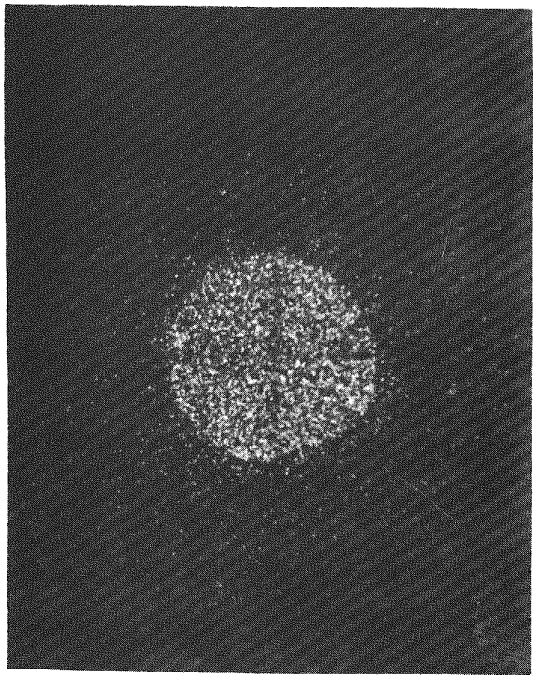

Mo (L_α)

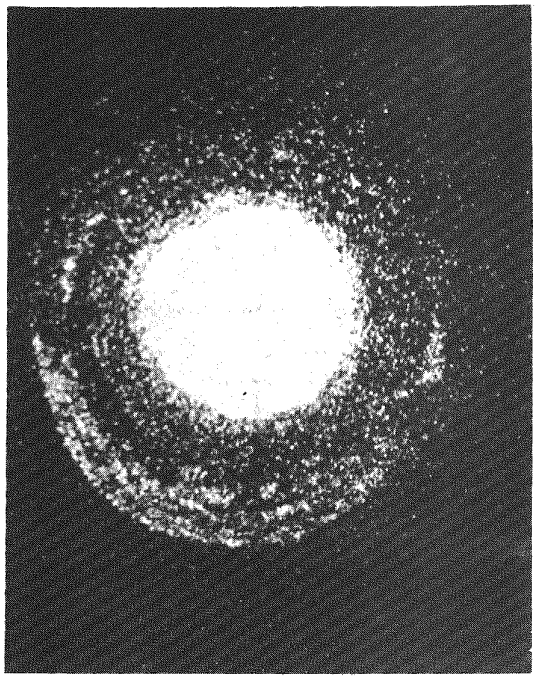

Zr (L_α)

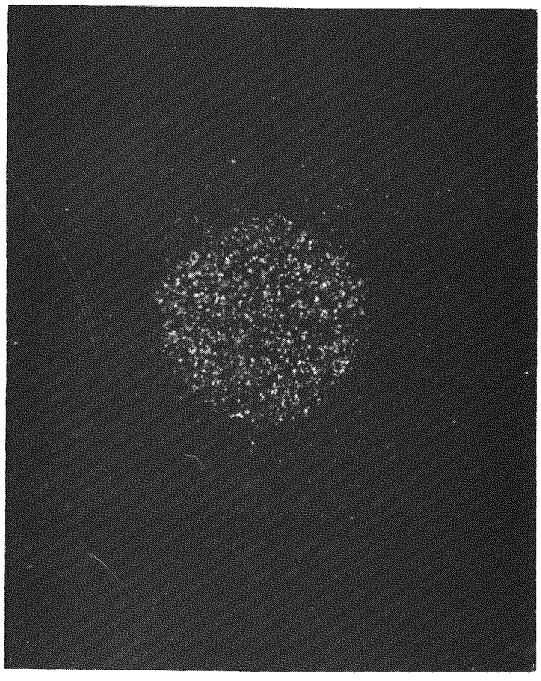

Ru (L_α)

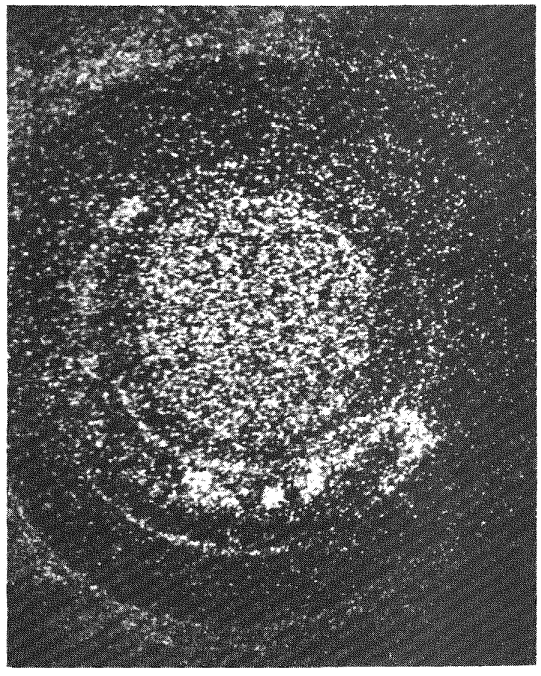

Cl (K_α)

Fig. 9-8. Electron microprobe scanning photographs of the UC_2 TRISO particle shown in Fig. 9-6c. The bright regions indicate the relative abundance of the indicated element (Mo, Zr, Ru, Cl). These photographs are a mirror image of the bright-field photomicrographs.

Additional electron microprobe studies of UC_2 TRISO particles exhibiting fission product attack of the SiC coating are in progress; the results will be reported in future quarterly reports.

Capsule P13N

Capsule P13N is the fourth in a series of irradiation tests of typical HTGR recyclable-type fuels, and is the first P-capsule to be monitored for in-pile fission gas release during the irradiation. The capsule contains five cells in which oxide and carbide particles, in fuel rods and as unbonded particle samples, are being tested.

Capsule P13N contained 22 fuel rods, 24 loose particle samples, and 175 piggyback samples. Descriptions of the fuel particles and fuel rod samples were given in an earlier Quarterly Progress Report (Gulf-GA-A12150).

Capsule P13N was inserted in the ETR (I-135W core position) in cycle 114E on January 19, 1972, and completed its scheduled irradiation on January 5, 1973 after 3732 hr of full-power operation. It was then shipped to the GGA Hot Cell, where it is currently undergoing postirradiation examination.

The results of Kr-85m release based on periodic fission gas release samples taken during irradiation are plotted in Fig. 9-9. The R/B values were obtained by averaging all R/B Kr-85m values for fluences within an interval of $\pm 0.25 \times 10^{21}$ n/cm^2. The gas release from cells 1 and 3, which contained predominately carbide fuel, remained higher than the release from cells 2, 4, and 5 during the entire irradiation period.

Disassembly of the capsule was completed and all fuel samples from the five cells were removed. All but one of the fuel rod samples in cells 2, 4, and 5 were intact and in relatively good condition. These cells contained 11 fuel rods comprised of oxide particles and 2 fuel rods containing carbide fuel particles. Fuel rod 4A-13 was broken and failed fertile

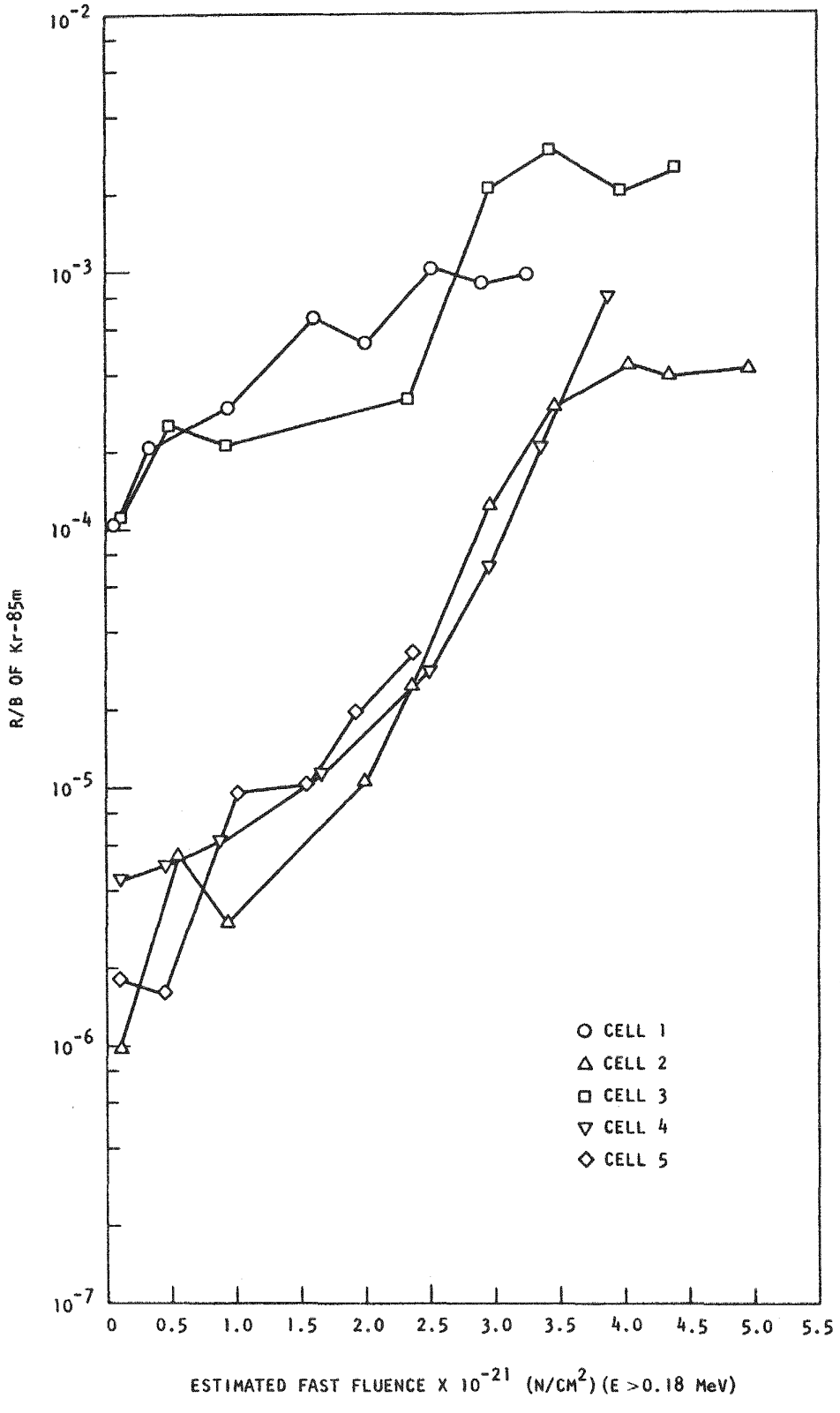

Fig. 9-9. In-pile fission gas release data for capsule P13N

particles were observed at the fracture interfaces during stereo examination. Four of the six rods in cells 1 and 3 containing carbide fuel particles were broken. Stereo examination of the fracture interfaces of these rods also revealed a large fraction of failed particles. The two ORNL fuel rods (1D-1 and 3A-1) containing resin U(C,S) TRISO fissile and ThO_2 BISO fertile particles were observed to be in good condition. Photographs of the fuel rods taken during the visual examination are shown in Figs. 9-10 through 9-31. Dimensional change measurements and postirradiation fission gas release measurements (TRIGA activation) were made on all intact fuel rods. These data are reported in Table 9-4, which also includes a description of the fuel rods and irradiation conditions. Metallography and disintegration-leach studies are being performed on selected fuel rods. These results will be reported in the next quarterly report.

Twenty-four samples were also irradiated as unbonded particle samples. Fission gas release measurements, metallography, radiography, electron microprobe analysis, density gradient column separations, and acid leach studies are being utilized to evaluate these samples. The results will be reported in future quarterly reports.

Capsule P13P

Capsule P13P is a companion test to Capsule P13N and is the fifth in a series of irradiation tests of candidate HTGR recyclable-type fuels. These capsules are the first P-capsules being monitored for in-pile fission gas release during irradiation. Capsule P13P contains five cells in which both fuel rod and unbonded particle samples are being tested; oxide and carbide fuels are included. Capsule P13P was designed for irradiation at 1050° and 1350°C to peak exposures of $\geq 8 \times 10^{21}$ n/cm^2.

The ETR completed its normal operation on April 30, 1973. Capsule P13P was discharged from the reactor on May 3 and sent to the GGA Hot Cell. The capsule is being stored in a specially fabricated purge (N_2) tube until July when the postirradiation of this capsule will commence.

PREIRRADIATION

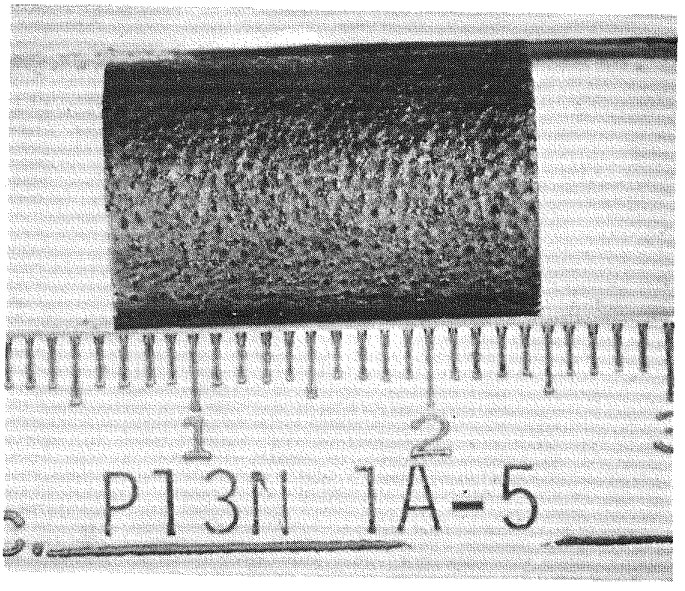

M36604-3 3X

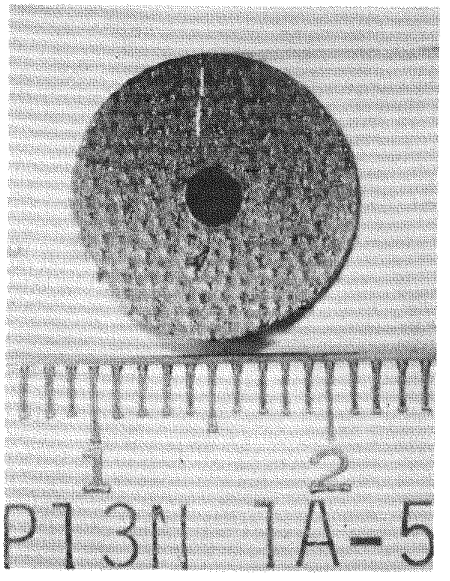

M36604-2 3X

POSTIRRADIATION

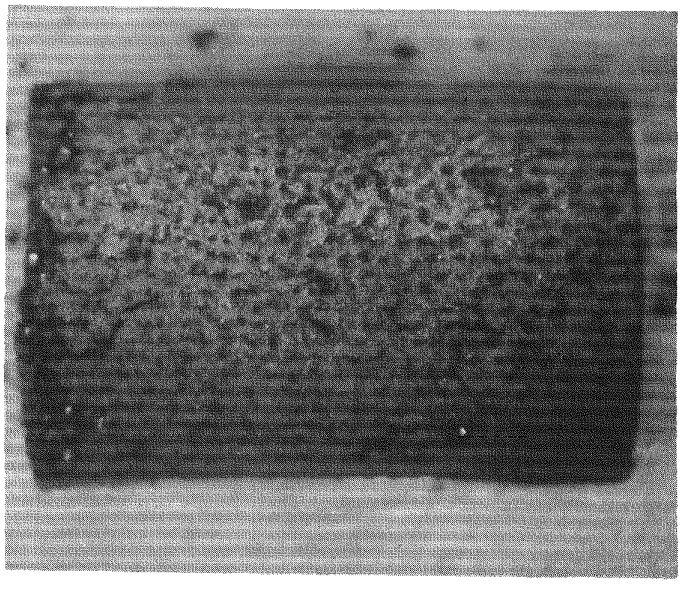

S7306-32 4X

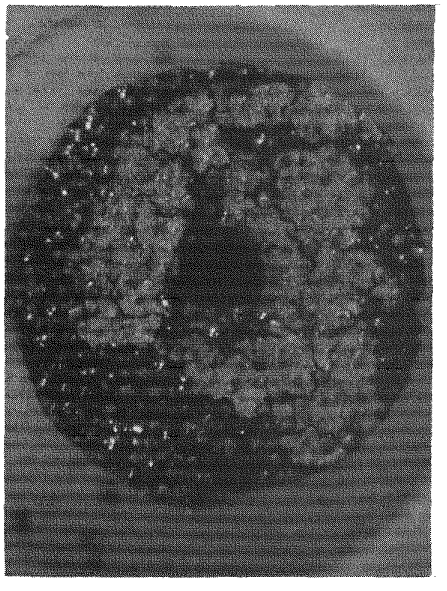

S7306-34 4X

Fig. 9-10. Fuel rod 1A-5 before and after irradiation in capsule P13N to 4.2 x 10^{21} n/cm^2 at 1415°C. Rod 1A-5 was fabricated by the hot-injection process using pitch binder and natural-flake graphite filler, followed by a heat treatment at 1800°C. This rod contained UC_2 TRISO fissile, ThC_2 TRISO fertile, and TRISO coated carbon inert particles.

PREIRRADIATION

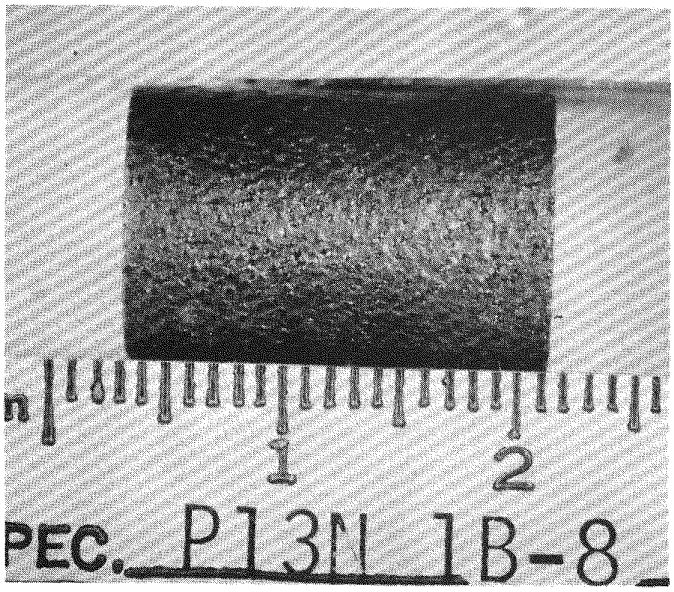

M36605-3 3X

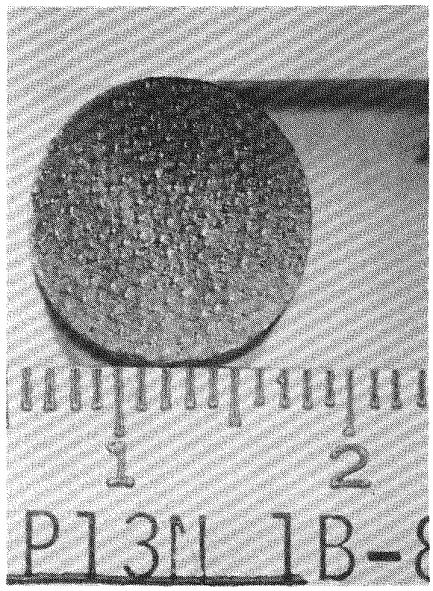

M36605-1 3X

POSTIRRADIATION

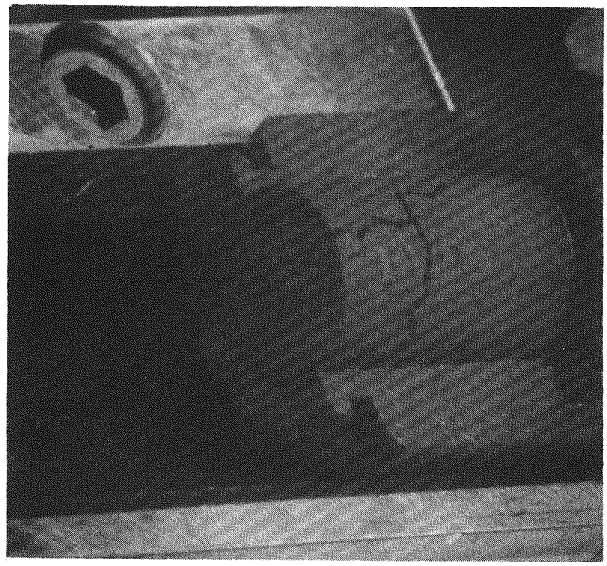

K7306-53 2X

Fig. 9-11. Fuel rod 1B-8 before and after irradiation in capsule P13N to 4.3 x 10^{21} n/cm^2 at 1490°C. Rod 1B-8 was fabricated by the hot-injection process using pitch binder and natural-flake graphite filler, followed by a heat treatment at 1800°C. This rod contained UC_2 TRISO fissile, ThC_2 BISO fertile, and TRISO coated carbon inert particles. The rod was cracked and broke into several fragments during removal from the graphite crucible.

PREIRRADIATION

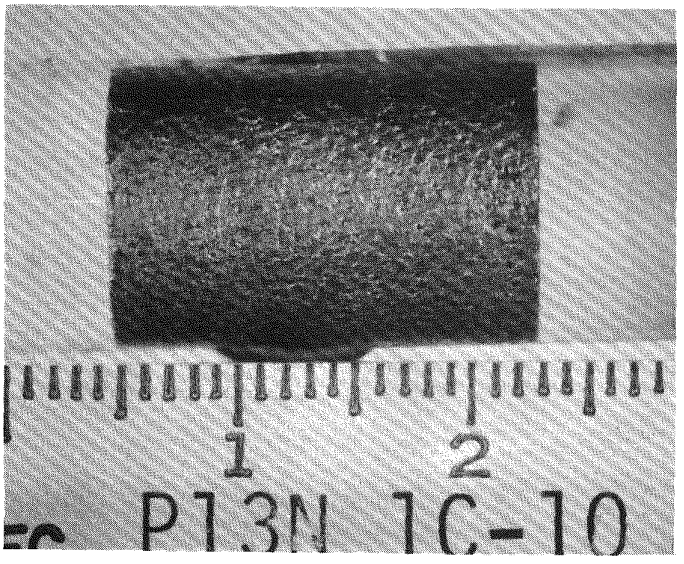

M36606-3 3X

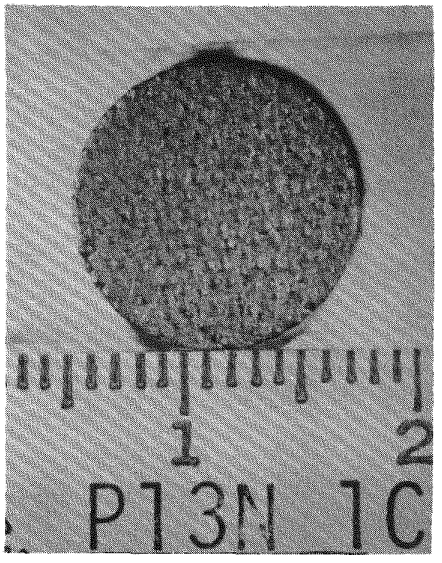

M36606-1 3X

POSTIRRADIATION

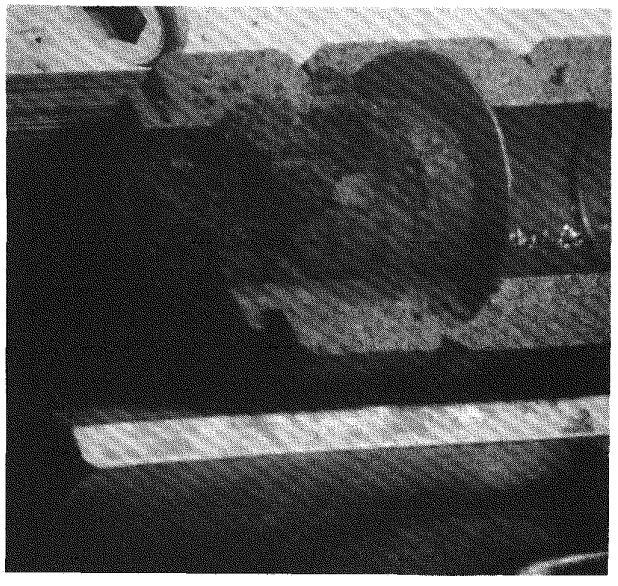

K7306-56 2X

Fig. 9-12. Fuel rod 1C-10 before and after irradiation in capsule P13N to 4.4 x 10^{21} n/cm^2 at 1475°C. Rod 1C-10 was fabricated by the hot-injection process using pitch binder and natural-flake graphite filler, followed by a heat treatment at 1800°C. This rod contained UC_2 TRISO fissile, ThC_2 BISO fertile, and TRISO coated carbon inert particles. Rod debonded due to particle failure.

PREIRRADIATION

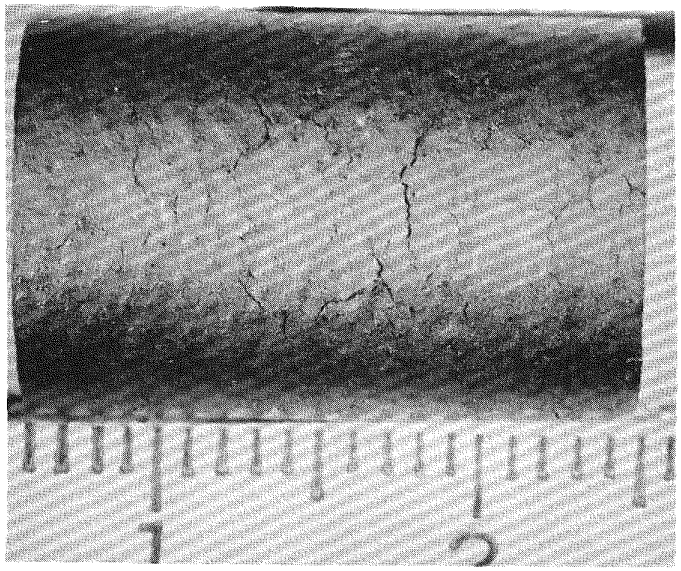

M36499-3 4X

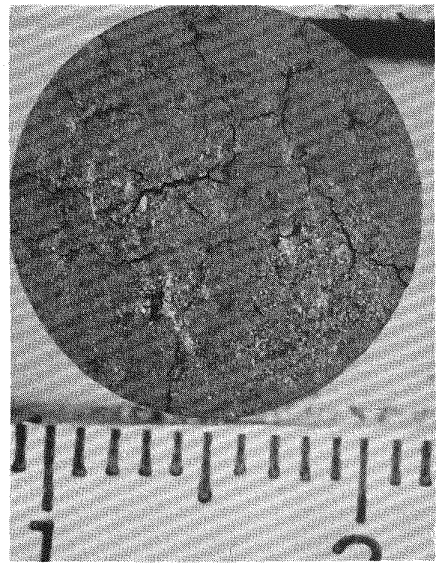

M36499-1 4X

POSTIRRADIATION

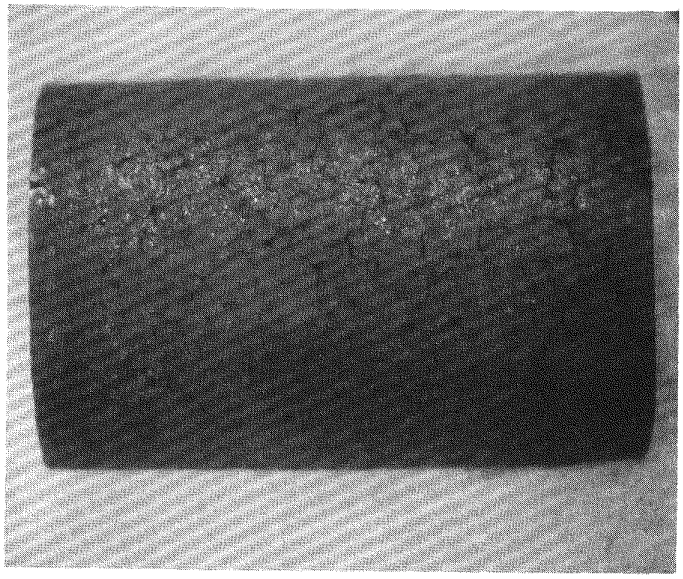

S7306-27 4X

S7306-30 4X

Fig. 9-13. Fuel rod 1D-1 before and after irradiation in capsule P13N to 4.6 x 10^{21} n/cm^2 at 1415°C. Rod 1D-1 was fabricated by a slurry blended, warm molded process at ORNL. This rod contained TRISO U(C,S) fissile and BISO ThO_2 fertile particles.

PREIRRADIATION

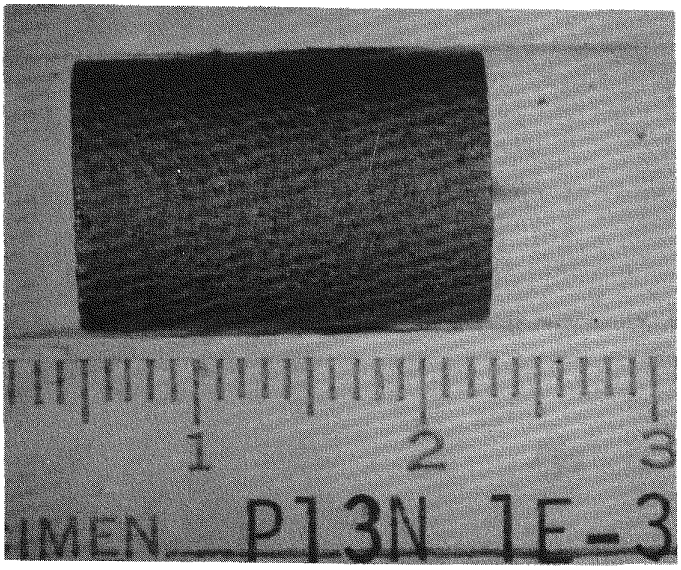

M36778-3 3X

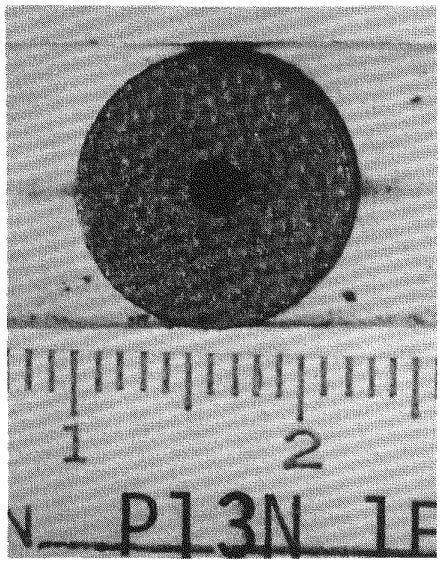

M36778-1 3X

POSTIRRADIATION

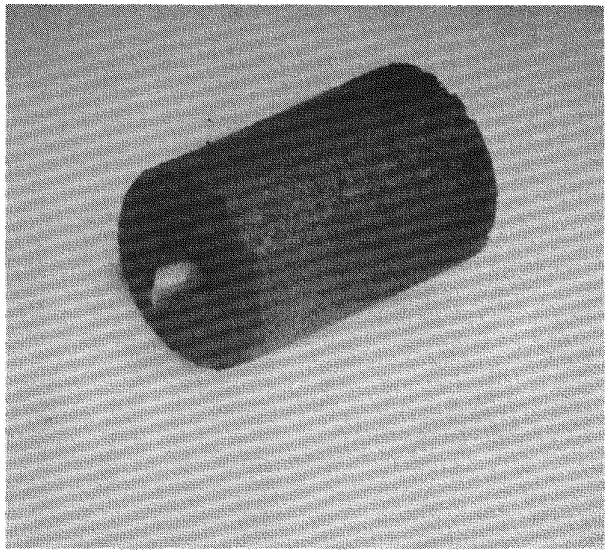

K7306-4 2X

Fig. 9-14. Fuel rod IE-3 before and after irradiation in capsule P13N to 4.7 x 10^{21} n/cm^2 at 1445°C. Rod IE-3 was fabricated by the hot-injection process using pitch binder and natural-flake graphite filler, followed by a heat treatment at 1800°C. This rod contained (Th,U)O_2 TRISO fissile, ThO_2 BISO fertile, and TRISO coated carbon inert particles. Rod was accidentally broken during dimensioning prior to the stereo examination.

PREIRRADIATION

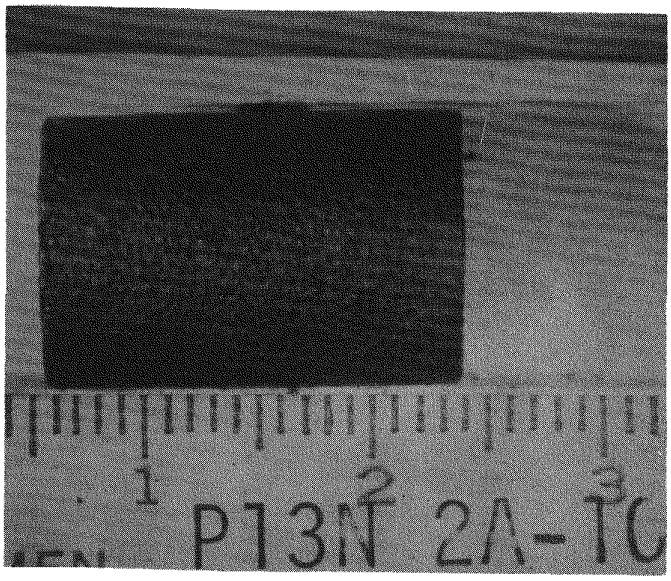

M36763-3 3X

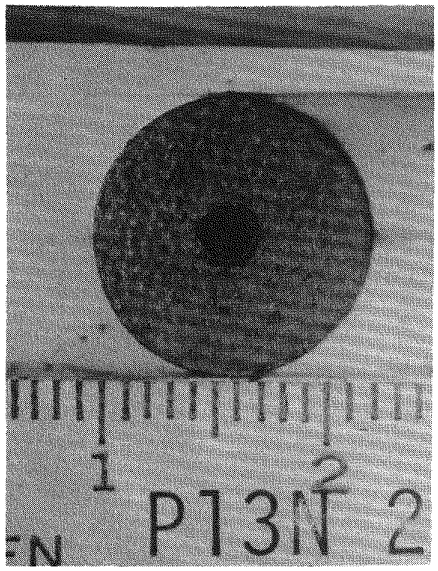

M36763-1 3X

POSTIRRADIATION

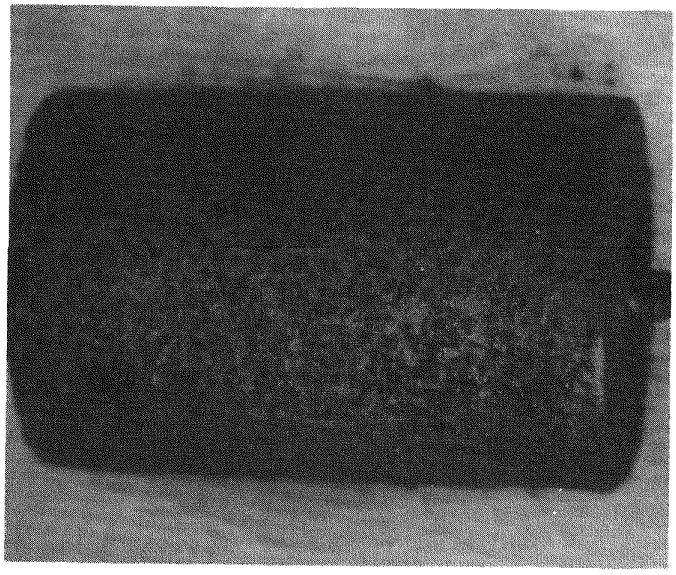

S7306-43 4X

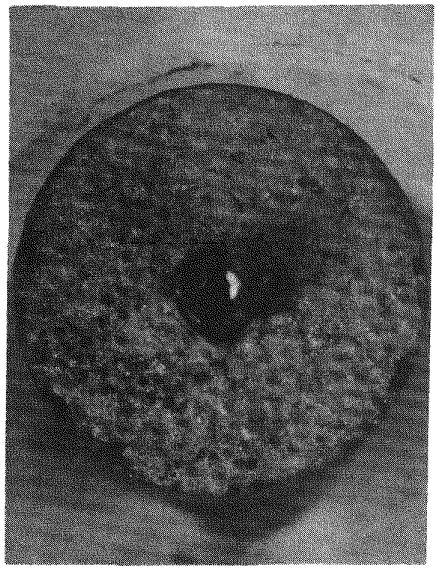

S7306-45 4X

Fig. 9-15. Fuel rod 2A-10 before and after irradiation in capsule P13N to 5.2 x 10^{21} n/cm^2 at 1220°C. Rod 2A-10 was fabricated by the hot-injection process using pitch binder and natural-flake graphite filler followed by a heat treatment at 1800°C. This rod contained UO_2 TRISO fissile, ThO_2 TRISO fertile, and TRISO coated carbon inert particles.

PREIRRADIATION

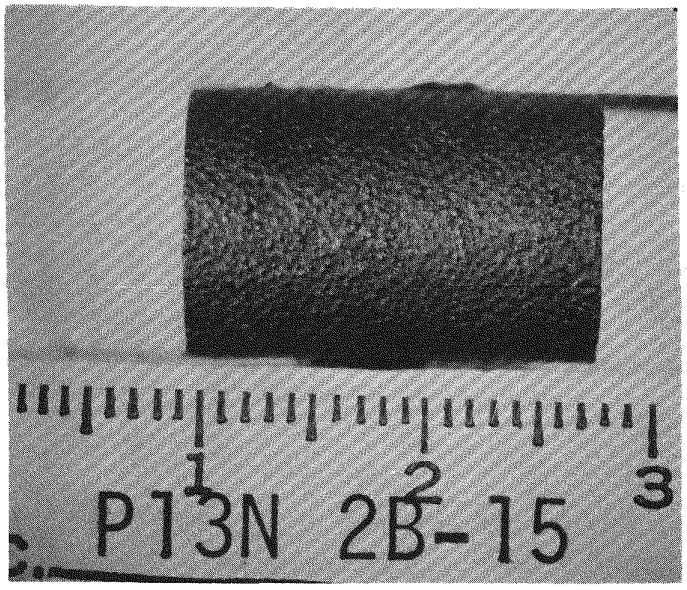

M36736-3 3X

M36736-1 3X

POSTIRRADIATION

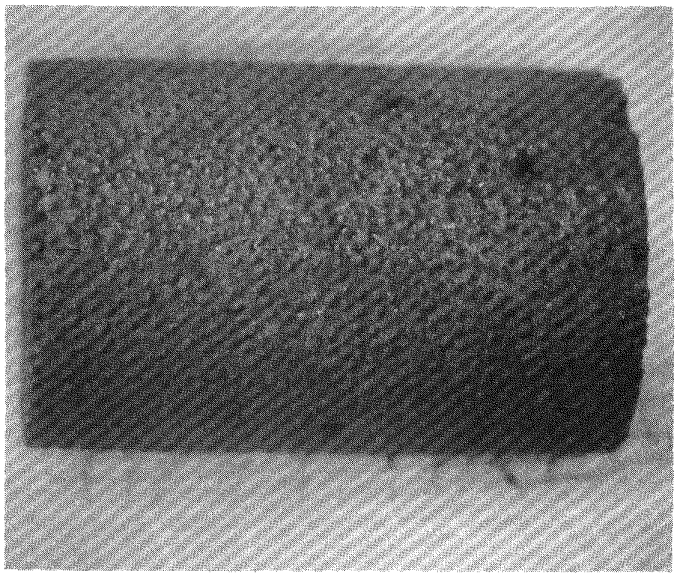

S7306-47 4X

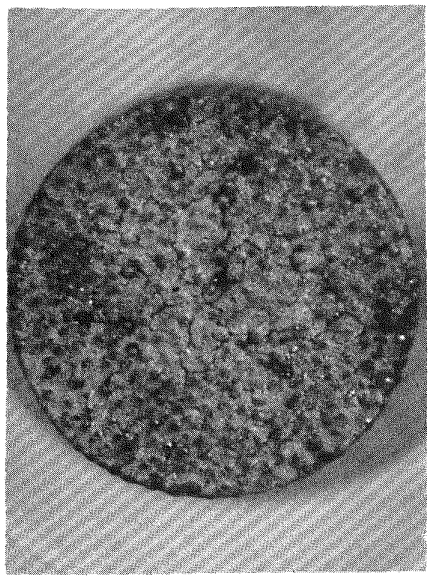

S7306-48 4X

Fig. 9-16. Fuel rod 2B-15 before and after irradiation in capsule P13N to 5.3 x 10^{21} n/cm^2 at 1230°C. Rod 2B-15 was fabricated by the hot-injection process using pitch binder and natural-flake graphite filler, followed by a heat treatment at 1800°C. This rod contained UO_2 TRISO fissile, ThO_2 BISO fertile, and TRISO coated carbon inert particles.

PREIRRADIATION

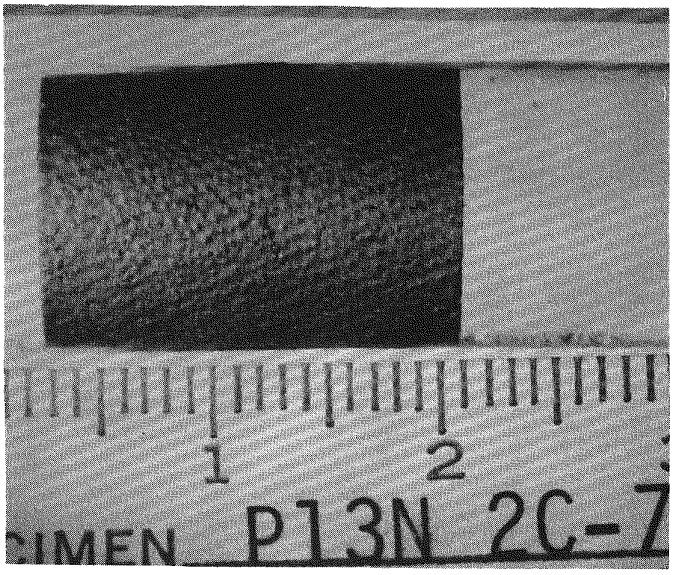

M36756-3 3X

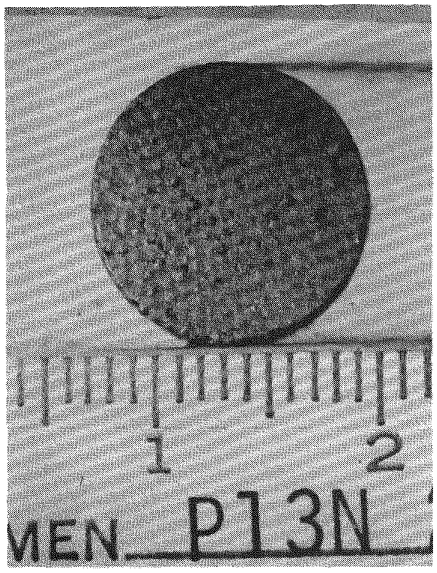

M36756-2 3X

POSTIRRADIATION

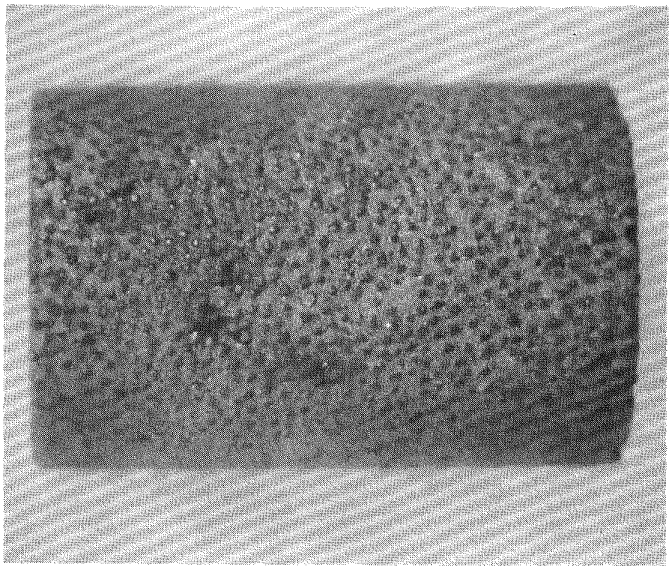

S7306-55 4X

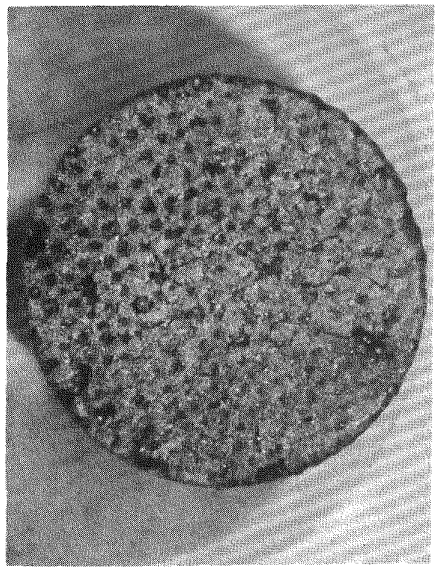

S7306-56 4X

Fig. 9-17. Fuel rod 2C-7 before and after irradiation in capsule P13N to 5.4×10^{21} n/cm^2 at 1360°C. Rod 2C-7 was fabricated by the hot-injection process using pitch binder and natural-flake graphite filler, followed by a heat treatment at 1800°C. This rod contained UO_2 TRISO fissile, ThO_2 TRISO fertile, and TRISO coated carbon inert particles.

PREIRRADIATION

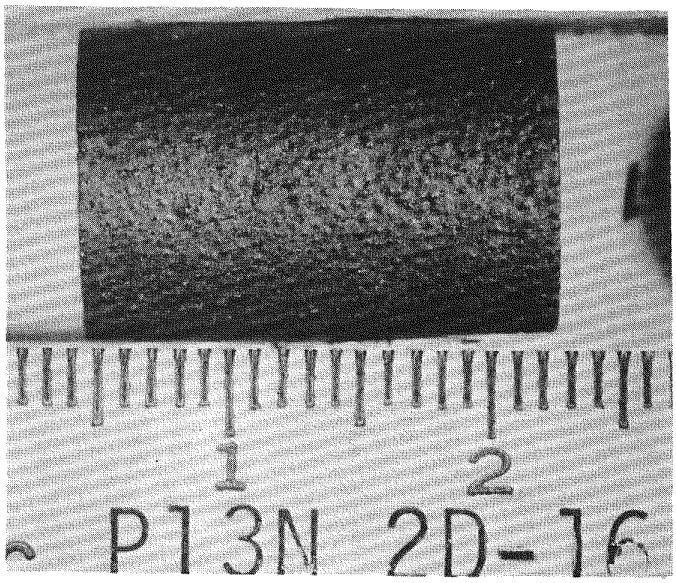

M36567-3 3X

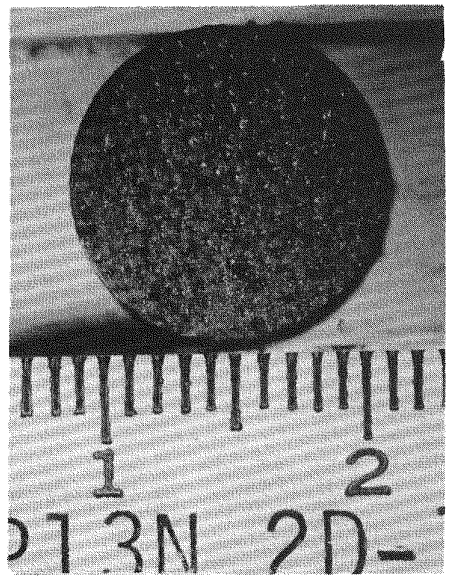

M36567-1 3X

POSTIRRADIATION

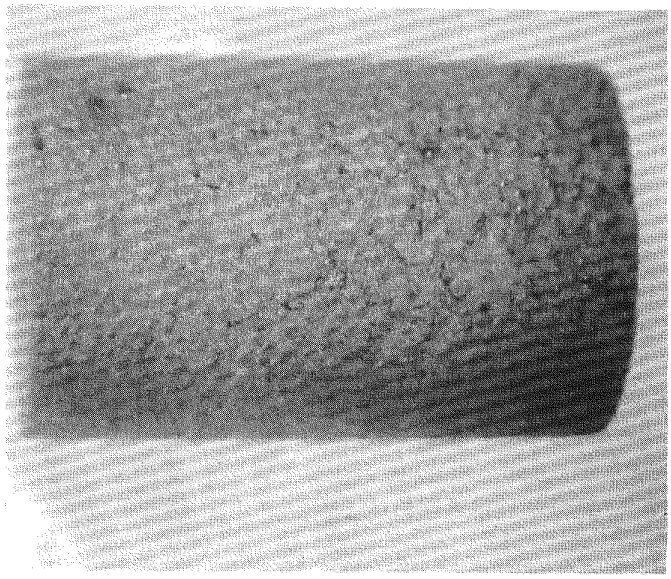

S7306-50 4X

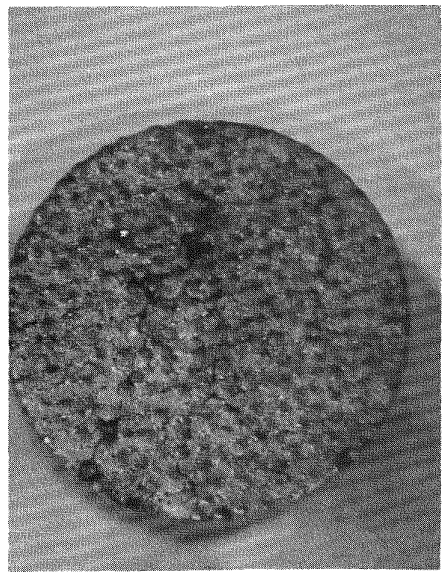

S7306-52 4X

Fig. 9-18. Fuel rod 2D-16 before and after irradiation in capsule P13N to 5.4 x 10^{21} n/cm^2 at 1350°C. Rod 2D-16 was fabricated by the hot-injection process using pitch binder and natural-flake graphite filler, followed by a heat treatment at 1800°C. This rod contained UO_2 TRISO fissile, ThO_2 BISO fertile, and TRISO coated carbon inert particles.

PREIRRADIATION

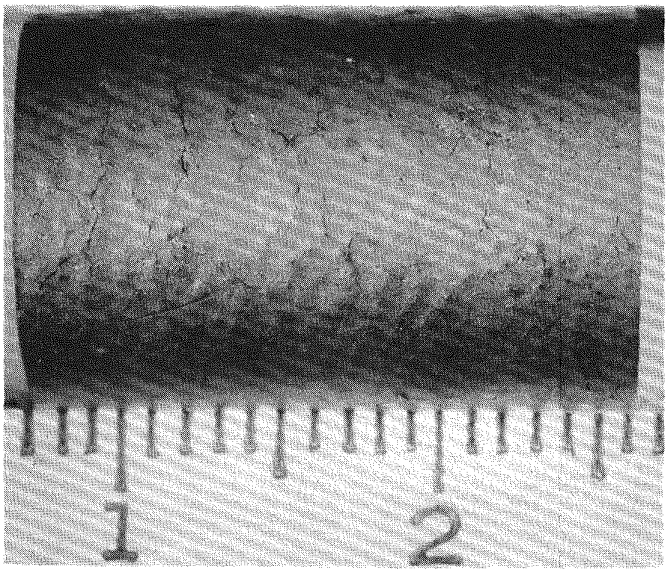

M36496-3 4X

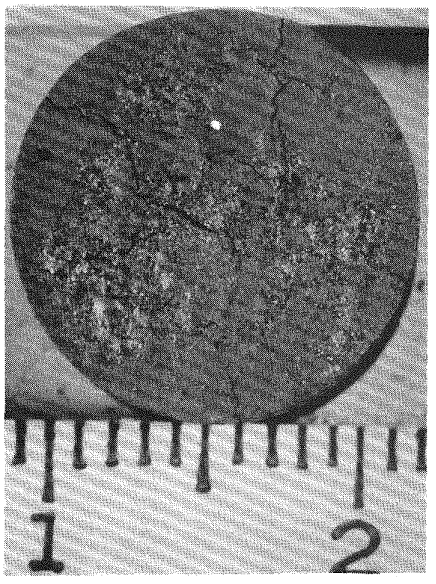

M36496-2 4X

POSTIRRADIATION

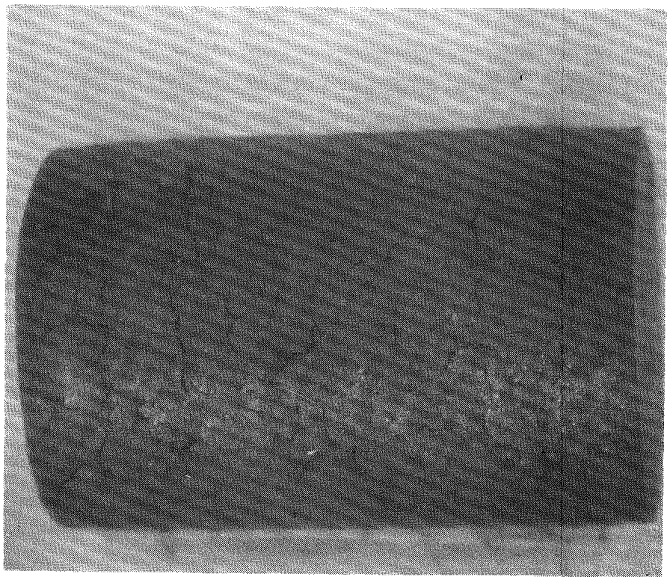

S7306-163 4X

S7306-165 4X

Fig. 9-19. Fuel rod 3A-1 before and after irradiation in capsule P13N to 5.1 x 10^{21} n/cm^2 at 1450°C. Rod 3A-1 was fabricated by a slurry-blended, warm molded process at ORNL. This rod contained TRISO U(C,S) fissile and BISO ThO_2 fertile particles.

PREIRRADIATION

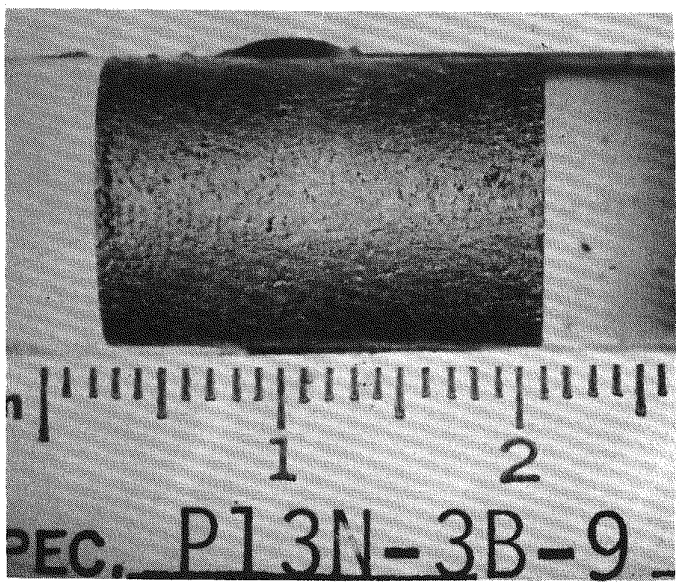

M36546-2 3X

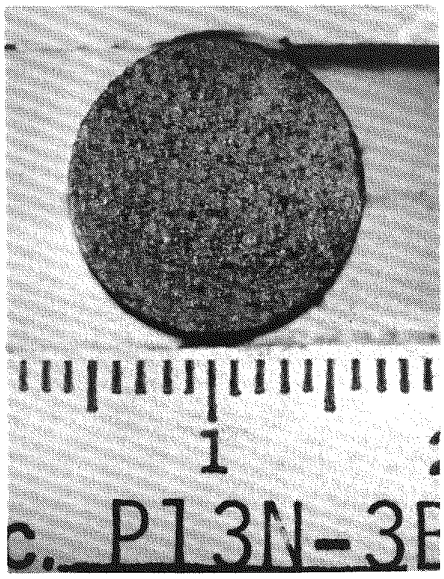

M36546-3 3X

POSTIRRADIATION

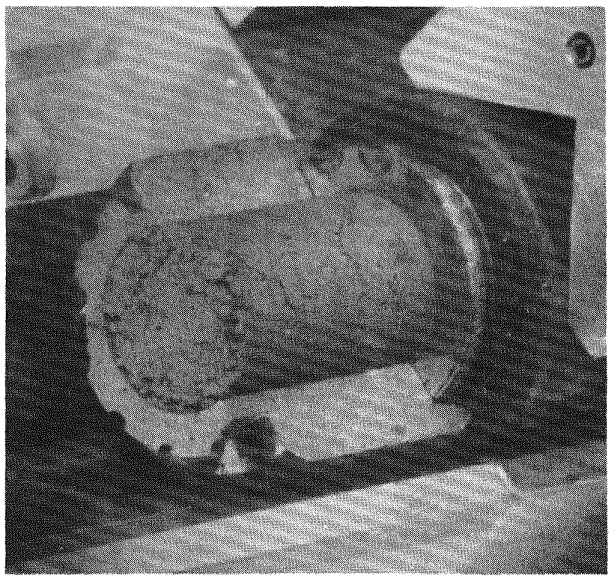

K7306-100 2X

Fig. 9-20. Fuel rod 3B-9 before and after irradiation in capsule P13N to 5.0 x 10^{21} n/cm^2 at 1365°C. Rod 3B-9 was fabricated by the hot-injection process using pitch binder and natural-flake graphite filler, followed by a heat treatment at 1800°C. This rod contained UC_2 TRISO fissile, ThC_2 BISO fertile, and TRISO coated carbon inert particles. The rod debonded during subsequent unloading from the graphite crucible.

PREIRRADIATION

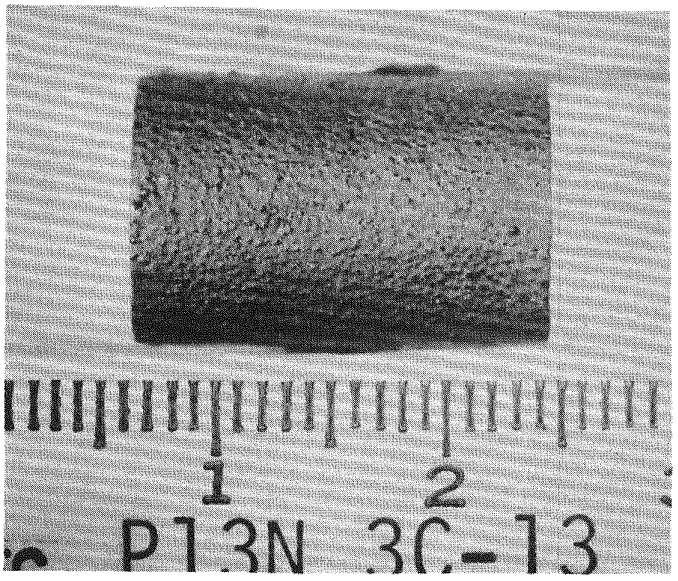

M36734-3 3X

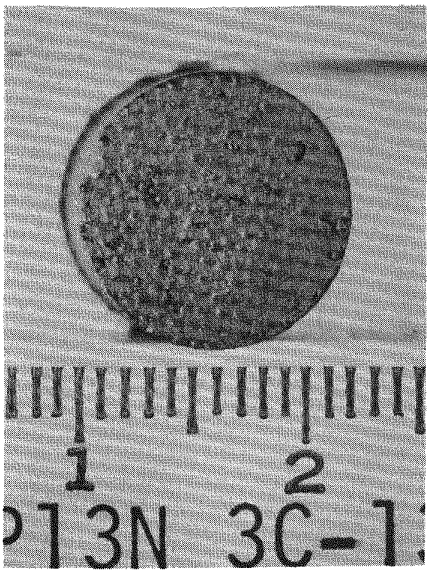

M36734-2 3X

POSTIRRADIATION

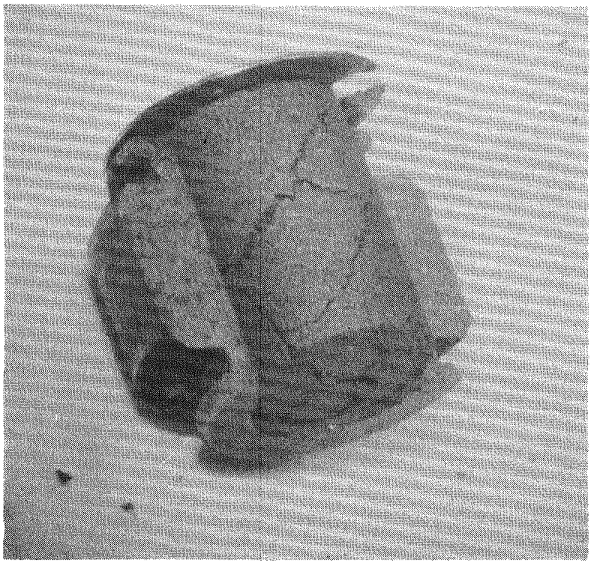

K7306-102 2X

Fig. 9-21. Fuel rod 3C-13 before and after irradiation in capsule P13N to 4.9 x 10^{21} n/cm^2 at 1350°C. Rod 3C-13 was fabricated by the hot-injection process using pitch binder and natural-flake graphite filler, followed by a heat treatment of 1800°C. This rod contained UC_2 TRISO fissile, ThC_2 BISO fertile, and TRISO coated carbon inert particles. Rod was cracked and it debonded during removal from graphite crucible.

PREIRRADIATION

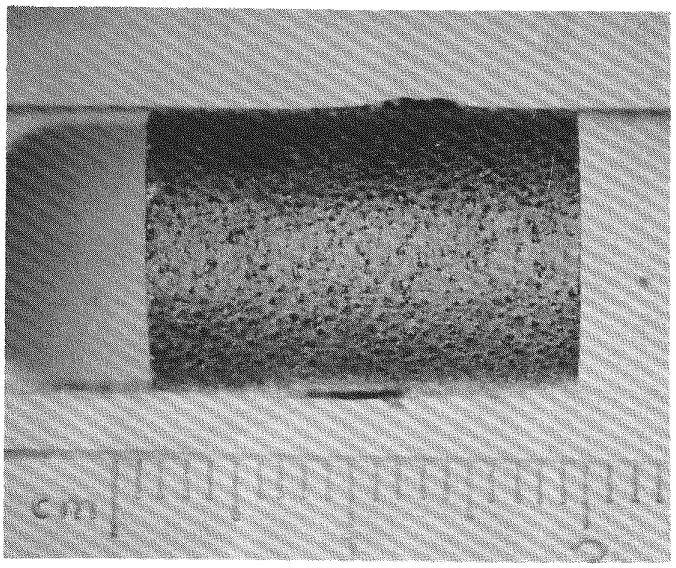

M36633-1 3X

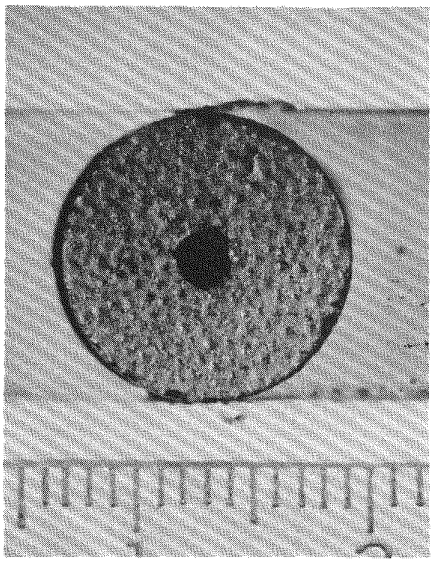

M36633-4 3X

POSTIRRADIATION

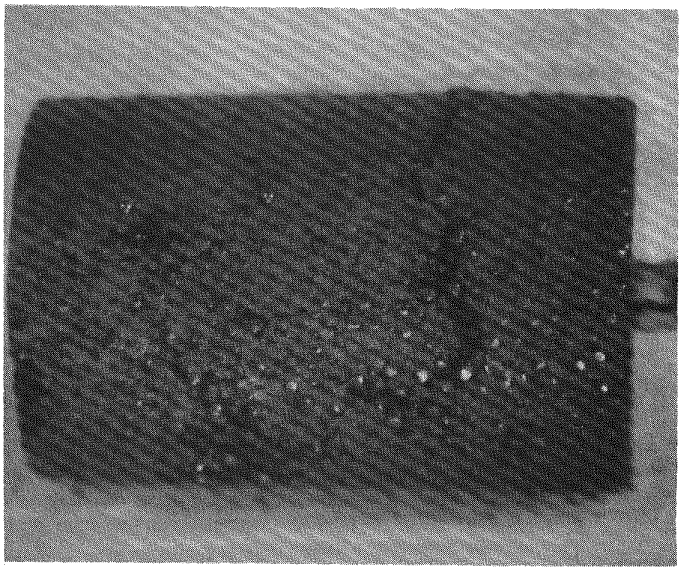

S7306-158 4X

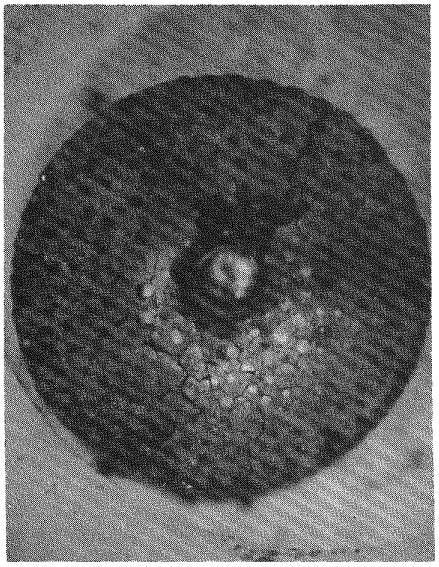

S7306-161 4X

Fig. 9-22. Fuel rod 3D-7 before and after irradiation in capsule P13N to 4.7 x 10^{21} n/cm^2 at 1375°C. Rod 3D-7 was fabricated by the hot-injection process using pitch binder and natural-flake graphite filler, followed by a heat treatment at 1800°C. This rod contained UC_2 TRISO fissile, ThC_2 TRISO fertile, and TRISO coated carbon inert particles. Although badly cracked, the rod remained intact during examination.

PREIRRADIATION

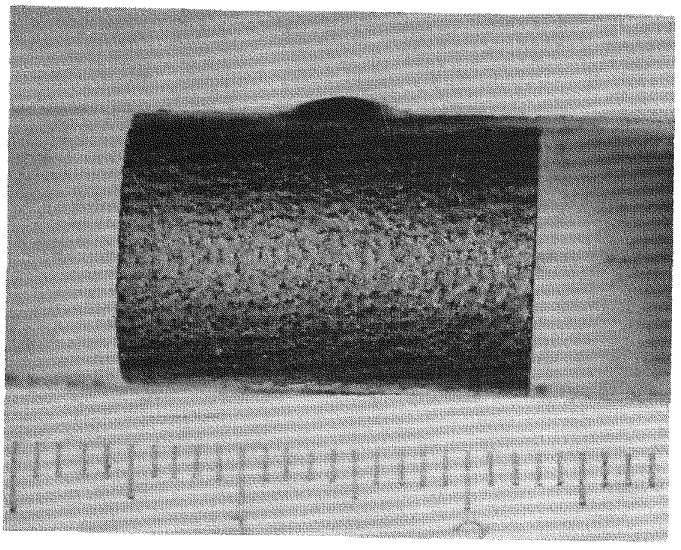

M36682-4 3X

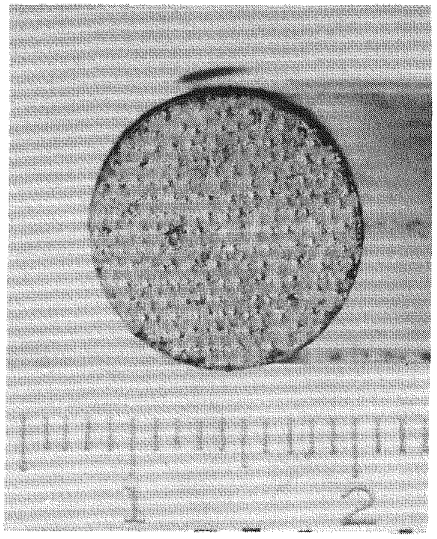

M36682-2 3X

POSTIRRADIATION

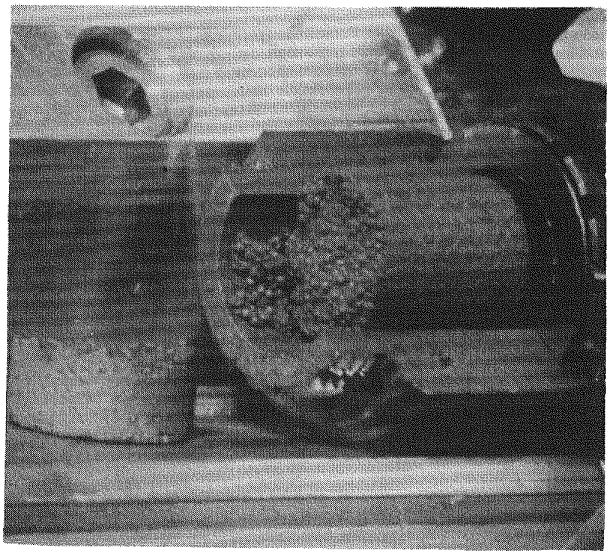

K7306-78 2X

Fig. 9-23. Fuel rod 4A-13 before and after irradiation in capsule P13N to 3.9 x 10^{21} n/cm^2 at 1335°C. Rod 4A-13 was fabricated by the hot-injection process using pitch binder and natural-flake graphite filler, followed by a heat treatment at 1800°C. This rod contained UO_2 TRISO fissile and ThO_2 BISO fertile particles. Rod broke into two pieces during unloading.

PREIRRADIATION

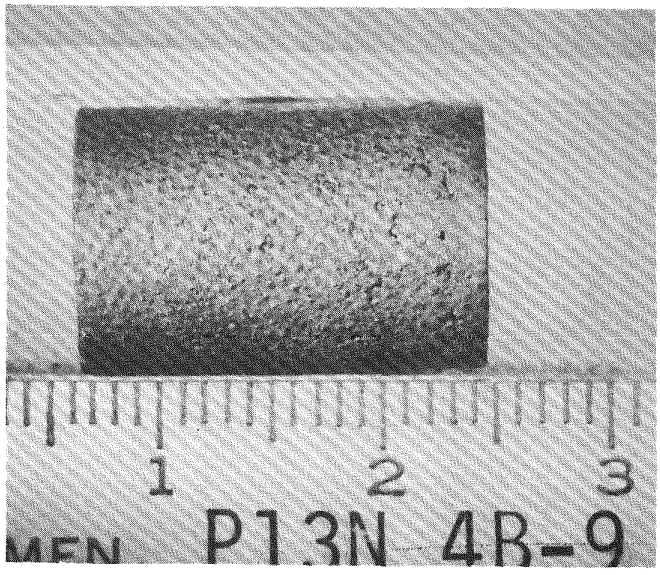

M36757-4 3X

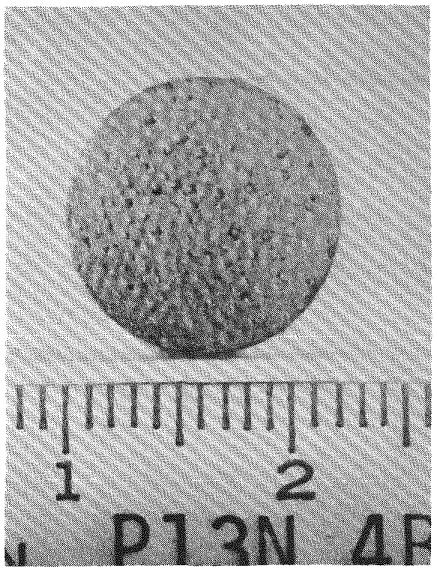

M36757-3 3X

POSTIRRADIATION

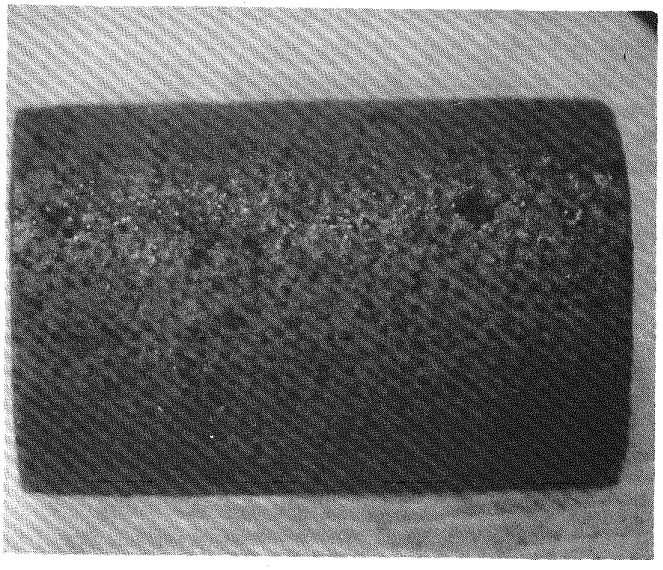

S7306-118 4X

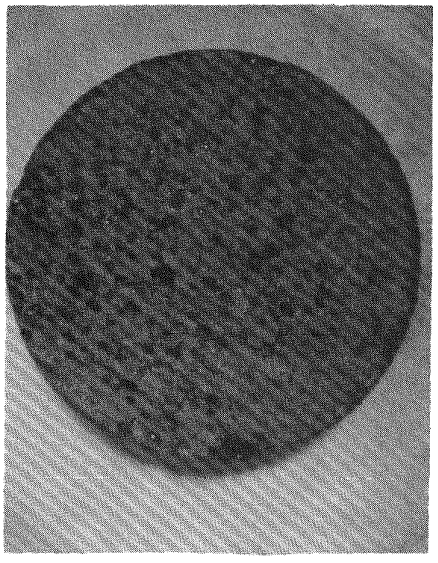

S7306-121 4X

Fig. 9-24. Fuel rod 4B-9 before and after irradiation in capsule P13N to 3.7×10^{21} n/cm^2 at 1300°C. Rod 4B-9 was fabricated by the hot-injection process using pitch binder and natural-flake graphite filler, followed by a heat treatment at 1800°C. This rod contained UO_2 TRISO fissile, ThO_2 TRISO fertile, and TRISO coated carbon inert particles.

PREIRRADIATION

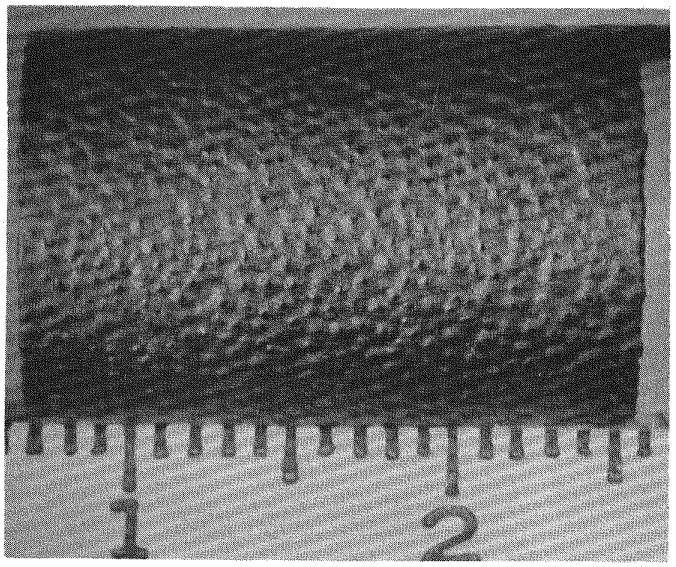

M36500-4 4X

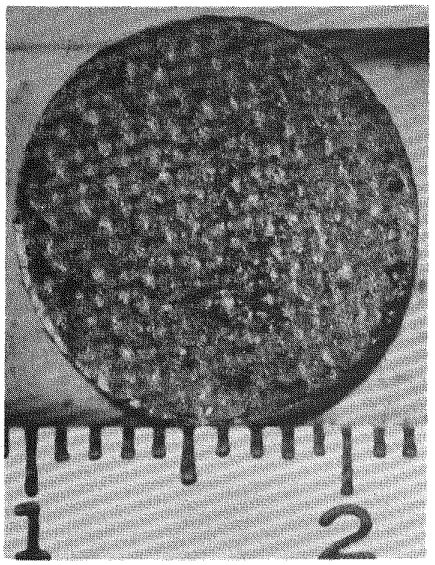

M36500-2 4X

POSTIRRADIATION

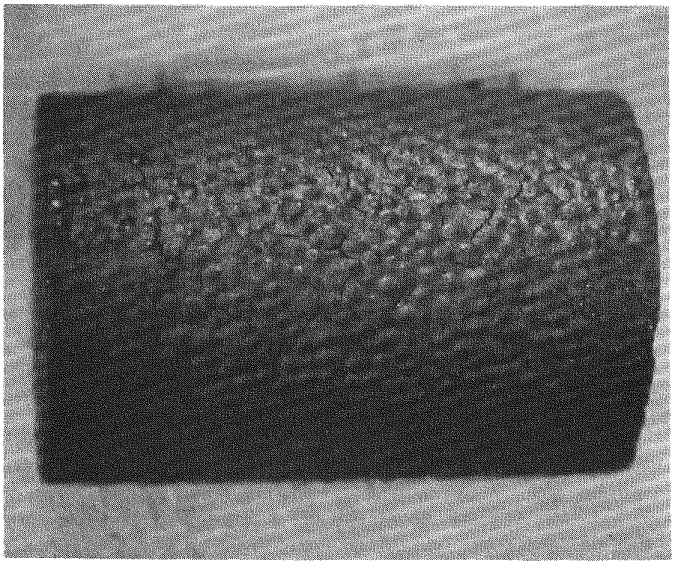

S7306-128 4X

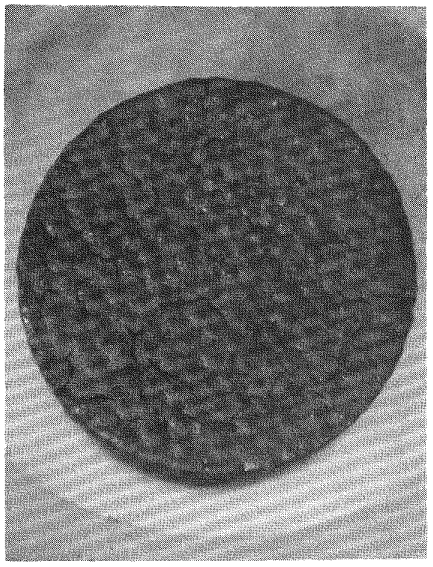

S7306-129 4X

Fig. 9-25. Fuel rod 4C-9 before and after irradiation in capsule P13N to 3.6 x 10^{21} n/cm^2 at 1260°C. Rod 4C-9 was fabricated by the hot-injection process using pitch binder and natural-flake graphite filler, followed by a heat treatment at 1800°C. This rod contained UO_2 TRISO fissile, ThO_2 BISO fertile, and TRISO coated carbon inert particles.

PREIRRADIATION

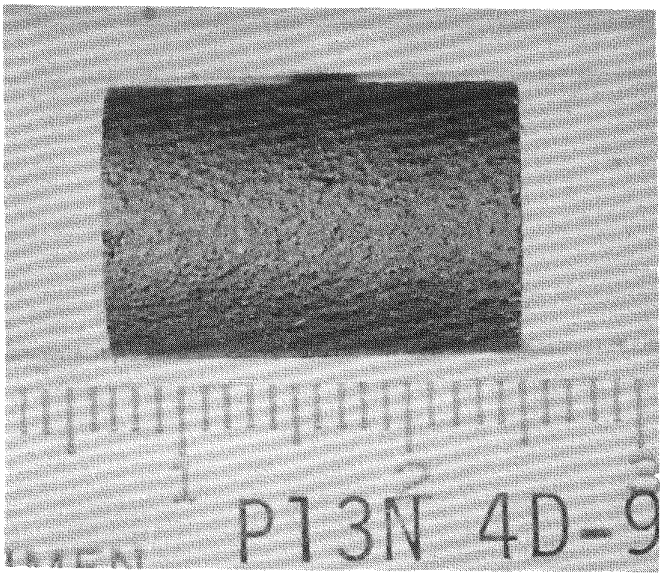

M36777-4 3X

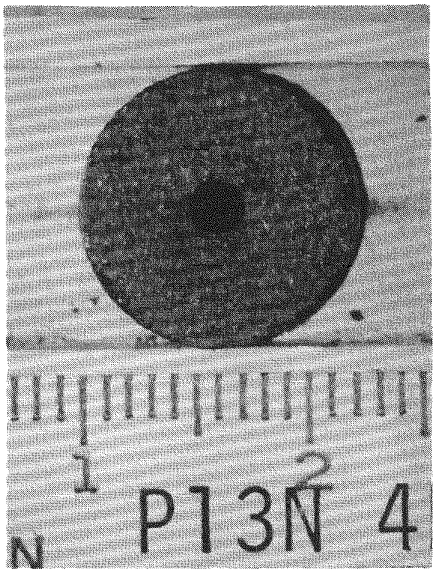

M36777-2 3X

POSTIRRADIATION

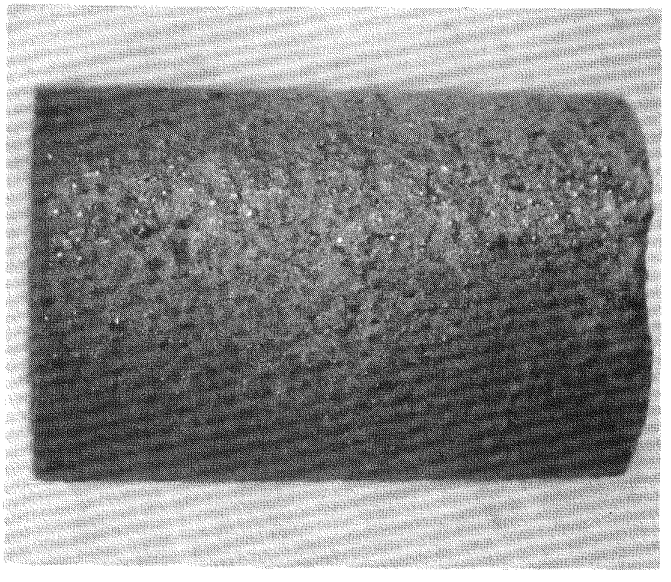

S7306-122 4X

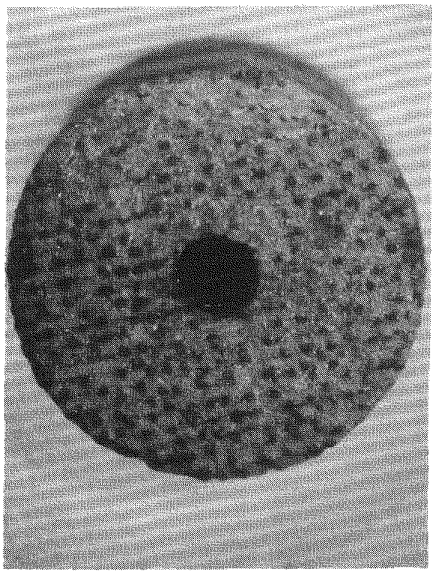

S7306-125 4X

Fig. 9-26. Fuel rod 4D-9 before and after irradiation in capsule P13N to 3.4 x 10^{21} n/cm^2 at 1255°C. Rod 4D-9 was fabricated by the hot-injection process using pitch binder and natural-flake graphite filler, followed by a heat treatment at 1800°C. This rod contained UO_2 TRISO fissile, ThO_2 TRISO fertile, and TRISO coated carbon inert particles.

PREIRRADIATION

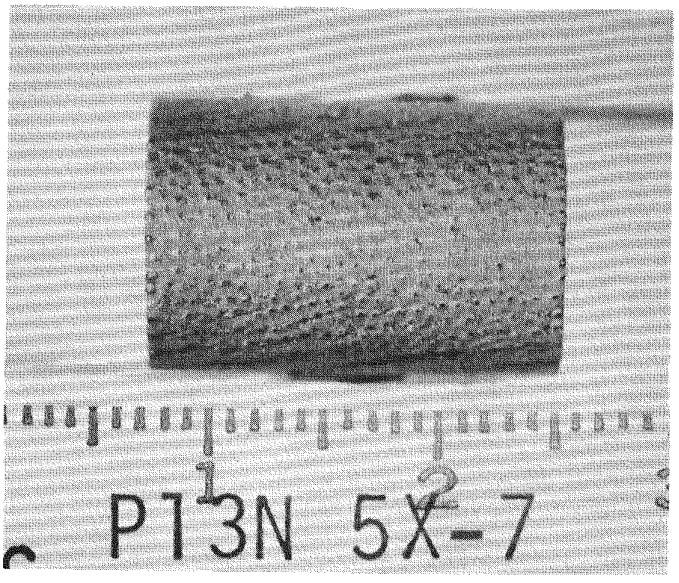

M36735-4 3X

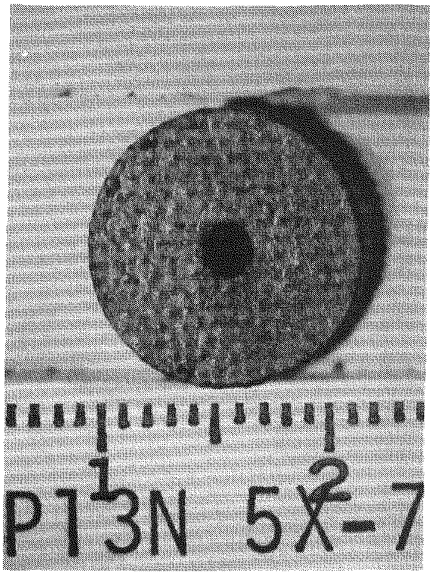

M36735-1 3X

POSTIRRADIATION

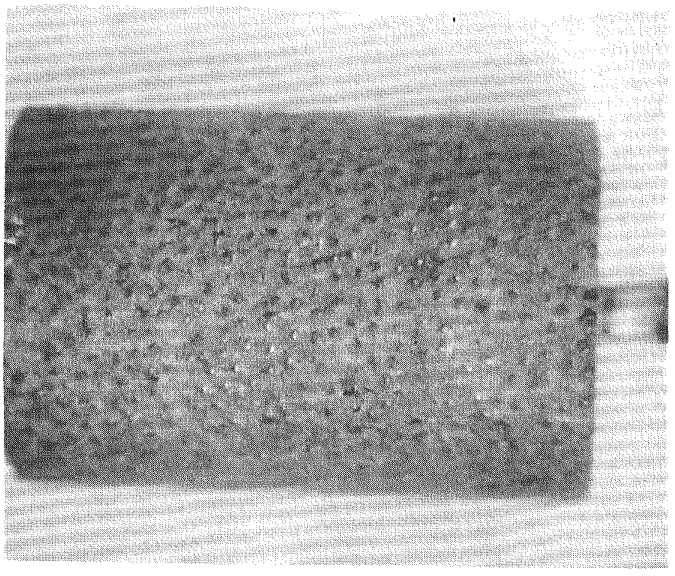

S7306-2 4X

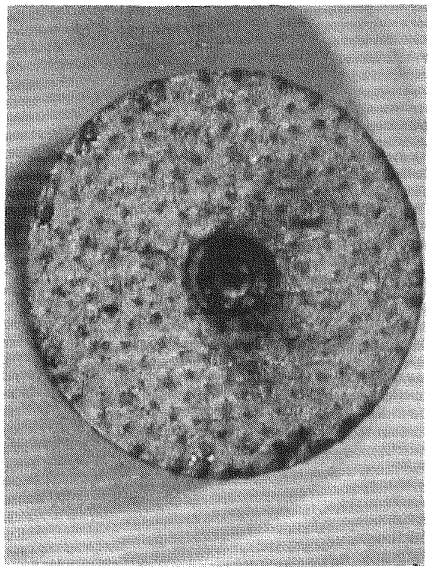

S7306-5 4X

Fig. 9-27. Fuel rod 5X-7 before and after irradiation in capsule P13N to 2.4 x 10^{21} n/cm^2 at 1290°C. Rod 5X-7 was fabricated by the hot-injection process using pitch binder and natural-flake graphite filler, followed by a heat treatment at 1800°C. This rod contained $(Th,U)O_2$ TRISO fissile, ThO_2 BISO fertile, and TRISO coated carbon inert particles.

PREIRRADIATION

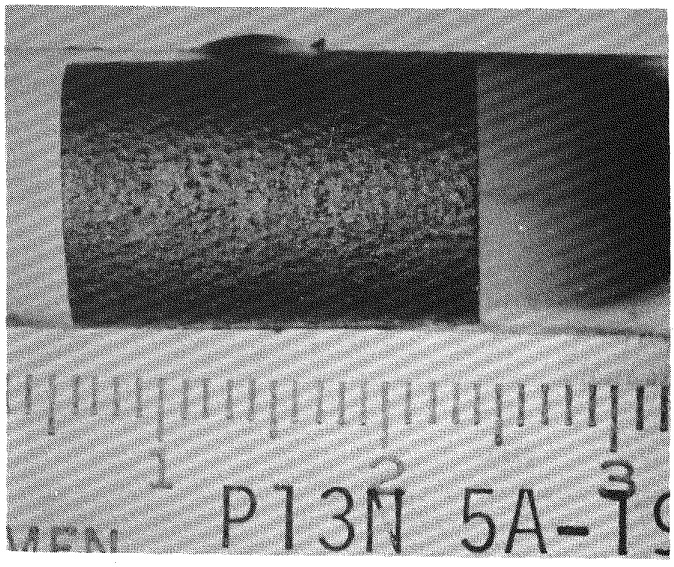

M36683-1 3X

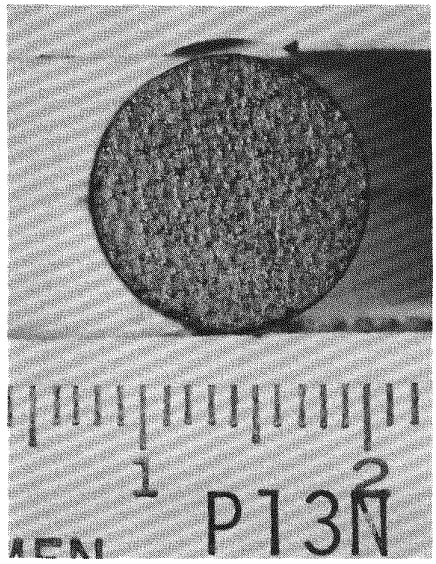

M36683-3 3X

POSTIRRADIATION

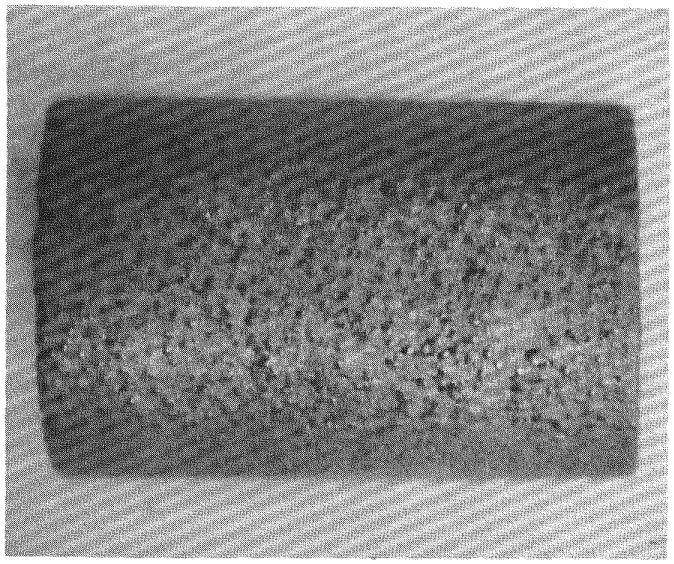

S7306-8 4X

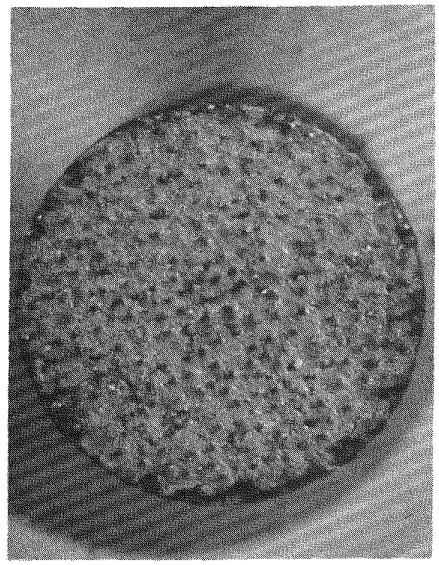

S7306-9 4X

Fig. 9-28. Fuel rod 5A-19 before and after irradiation in capsule P13N to 2.2 x 10^{21} n/cm^2 at 1335°C. Rod 5A-19 was fabricated by the hot-injection process using pitch binder and natural-flake graphite filler, followed by a heat treatment at 1800°C. This rod contained UO_2 TRISO fissile and ThO_2 BISO fertile particles.

PREIRRADIATION

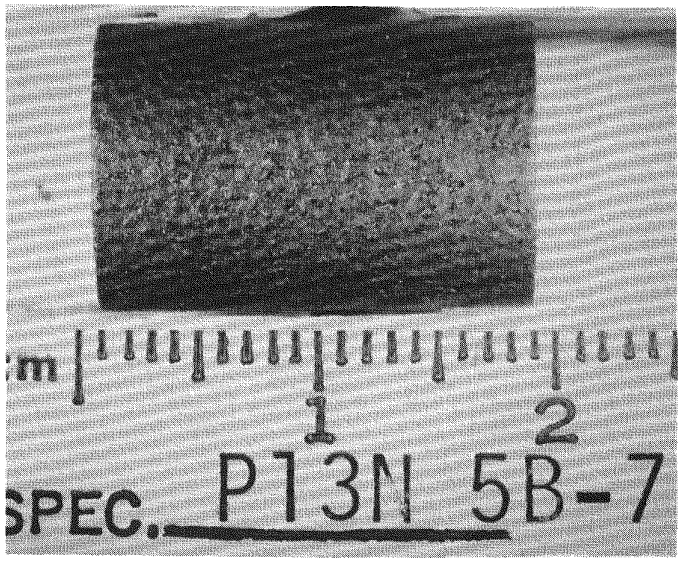

M36569-3 3X

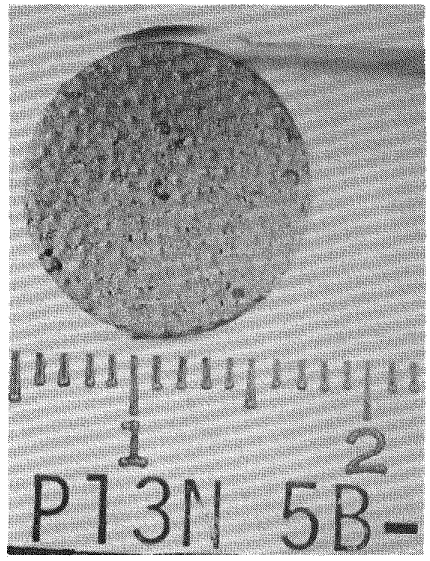

M36569-1 3X

POSTIRRADIATION

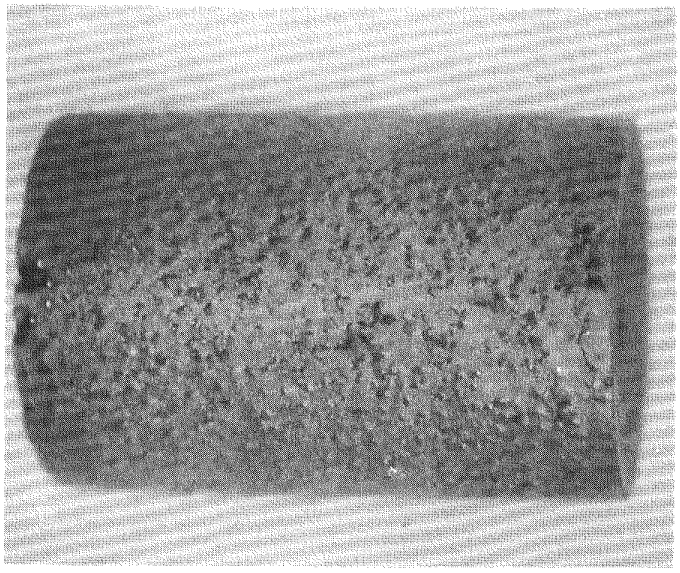

S7306-20 4X

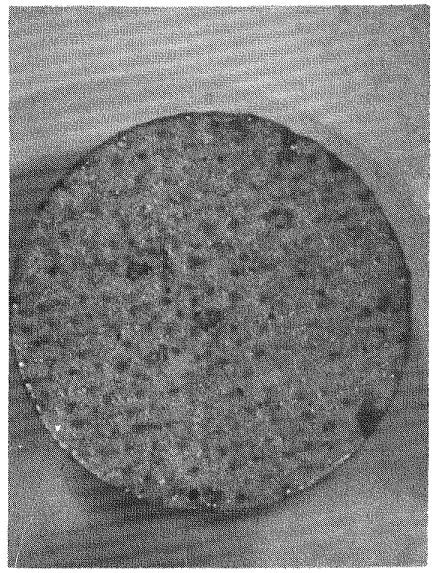

S7306-22 4X

Fig. 9-29. Fuel rod 5B-7 before and after irradiation in capsule P13N to 2.0 x 10^{21} n/cm^2 at 1325°C. Rod 5B-7 was fabricated by the hot-injection process using pitch binder and natural-flake graphite filler, followed by a heat treatment of 1800°C. This rod contained UO_2 TRISO fissile and ThO_2 BISO fertile particles.

PREIRRADIATION

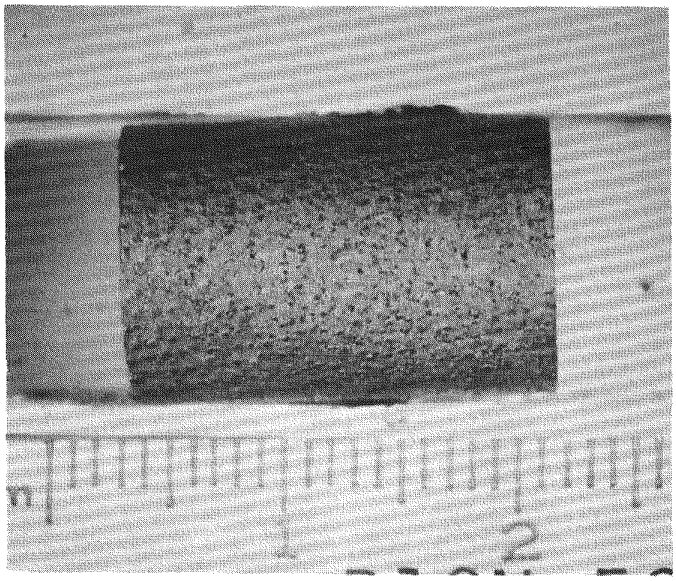

M36634-3 3X

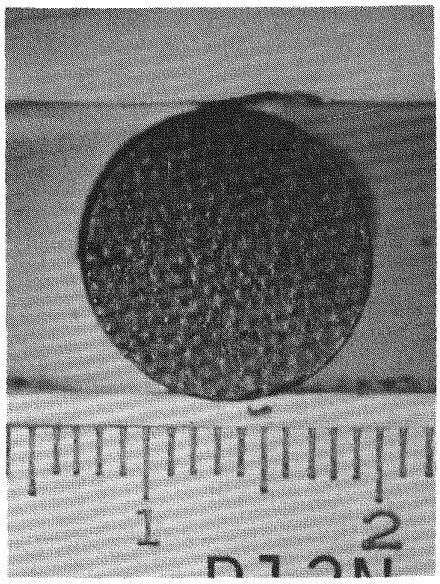

M36634-1 3X

POSTIRRADIATION

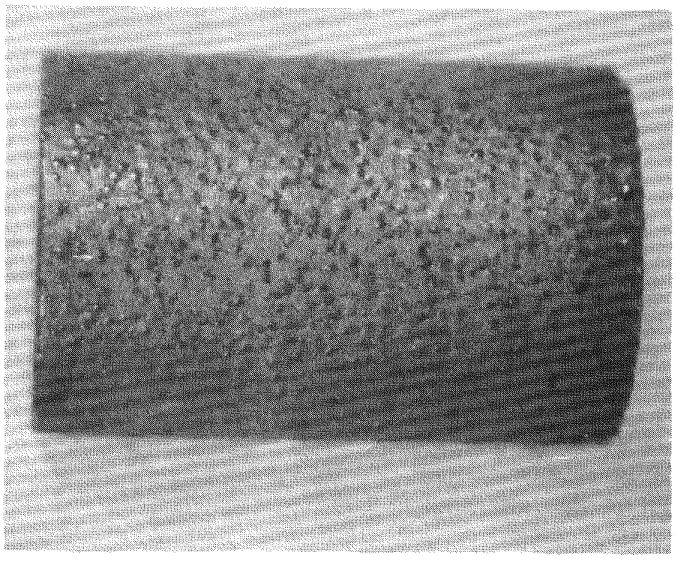

S7306-15 4X

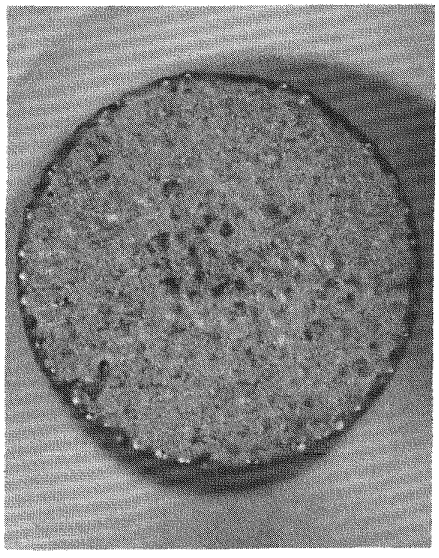

S7306-18 4X

Fig. 9-30. Fuel rod 5C-9 before and after irradiation in capsule P13N to 1.8 x 10^{21} n/cm^2 at 1275°C. Rod 5C-9 was fabricated by the hot-injection process using pitch binder and natural-flake graphite filler, followed by a heat treatment at 1800°C. This rod contained UC_2 TRISO fissile, ThC_2 BISO fertile, and TRISO coated carbon inert particles.

PREIRRADIATION

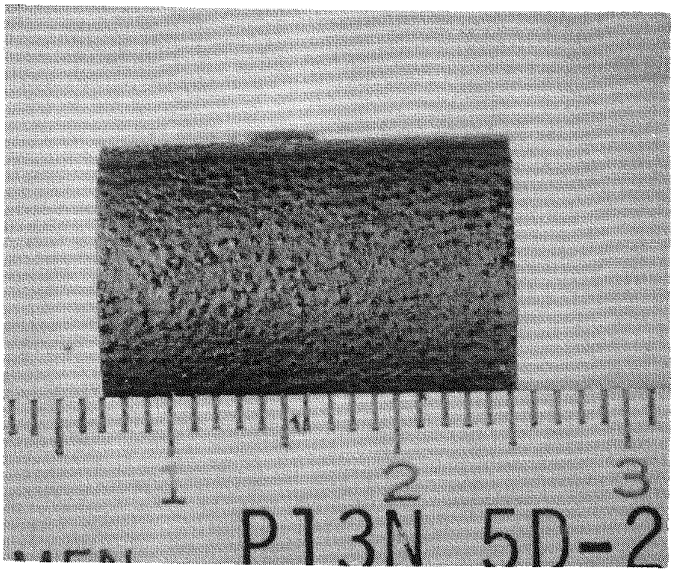

M36759-3 3X

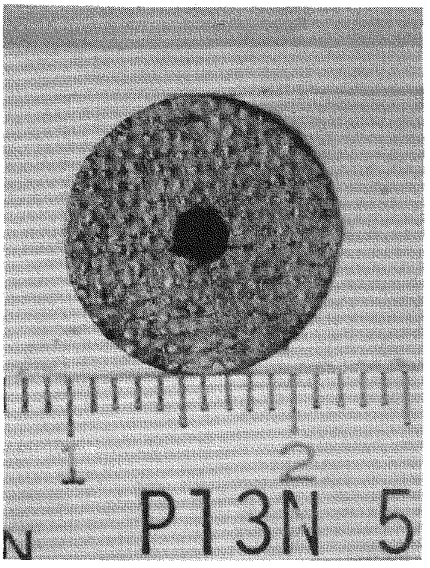

M36759-1 3X

POSTIRRADIATION

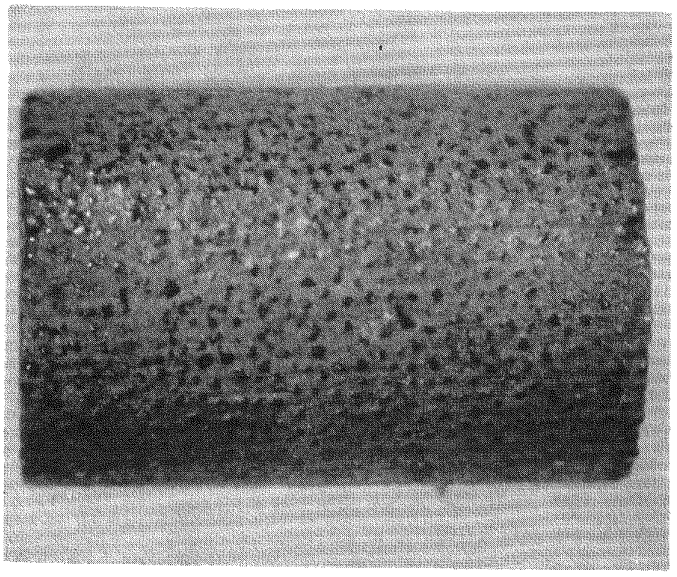

S7306-12 4X

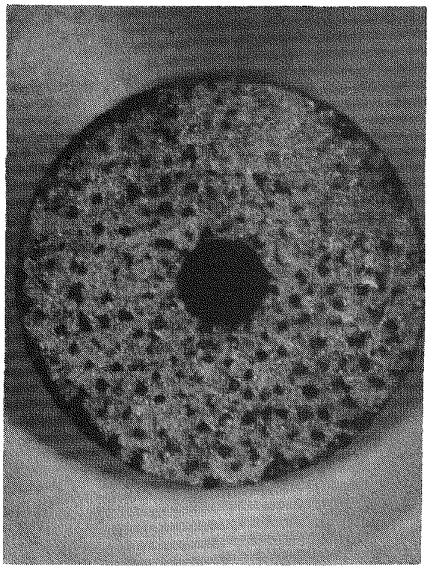

S7306-13 4X

Fig. 9-31. Fuel rod 5D-25 before and after irradiation in capsule P13N to 1.6 x 10^{21} n/cm^2 at 1120°C. Rod 5D-25 was fabricated by the hot-injection progress using pitch binder and natural-flake graphite filler, followed by a heat treatment at 1800°C. This rod contained UC_2 TRISO fissile, ThC_2 TRISO fertile, and TRISO coated carbon inert particles.

It appears from current fluence projections that P13P came very close to achieving the desired peak fast fluence of 8 to 9 x 10^{21} n/cm^2.

Capsules P13R and P13S

Thermal design studies for capsules P13R and P13S are essentially complete. Bids for fabricating the graphite components have been submitted and the parts are expected to be delivered in August 1973. Delivery of the metallic components for the capsules is expected during the latter part of July. All coated particle samples have been fabricated for testing in these capsules and fuel rod fabrication is scheduled to commence at the beginning of FY-74.

Two additional tests will be incorporated in these capsules. Cell 5 of P13S will be designed to operate at 1500°C to obtain further high-temperature data on reference fuel, and cell 1 of P13S will be thermal cycled from its normal operation temperature of 1050°C to 1400° to 1600°C periodically throughout the irradiation.

GGA-ORNL Cooperative Irradiation Capsules

A series of cooperative irradiation tests is being carried out with ORNL in their irradiation facilities. These irradiations include tests in the HFIR target position (HT-capsules), the HFIR beryllium-reflector position (HRB-capsules), and the ORR facility.

Capsule P13Q

Fuel rod fabrication for capsule P13Q was completed. A summary description of the fuel rod types fabricated is given in Table 9-5. Fuel rods to be irradiated were also loaded in P13Q capsule bodies, sealed in the GGA portion of the capsule, and sent to ORNL where the experiment awaits fabrication and assembly of the required ORNL components. The completed experiment is scheduled for insertion in ORR on July 15, 1973.

TABLE 9-4
DESCRIPTION OF FUEL RODS IRRADIATED IN CAPSULE P13N

Sample No.[a]	Coated Particles[b]						Matrix[c]			Particle Packing Fraction[d] (%)	Loading Uniformity[f] (± %)	Pre-irradiation Fission Gas Release[g]	Pre-irradiation Thorium Contamination[h]	Irradiation Conditions		Postirradiation Examination			
	Fissile		Fertile		Inert		Filler (wt %)	Apparent Density[d] (g/cm^3)	Macro-porosity[e] (%)					Temp.[i] (°C)	Fast Fluence x 10^{-21} (n/cm^2) (E > 0.18 MeV)	Fission Gas Release[j]	Dimensional Change (%)		Visual Appearance of Fuel Rod
	Type	Batch No.	Type	Batch No.	Type	Batch No.											Diam.	Length	
Cell 1																			
1A-5	UC_2 TRISO	4161-00-020	ThC_2 TRISO	4261-00-010	C-TRISO	3516-147	31.8	0.54	20.0	64.0	4.6	1.3×10^{-6}	3.5×10^{-5}	1415	4.2	8.4×10^{-4}	N.D.	N.D.	Cracked, slight particle debonding
1B-8	UC_2 TRISO	4161-00-020	ThC_2 BISO	4251-00-030	C-TRISO	3516-147	29.7	0.57	17.3	62.1	5.4	6.7×10^{-7}	$<6.7 \times 10^{-6}$	1490	4.3	N.D.[m]	N.D.	N.D.	Broken
1C-10	UC_2 TRISO	4161-00-020	ThC_2 BISO	4251-00-030	C-TRISO	3516-147	29.8	0.57	23.5	61.9	11.3	1.9×10^{-6}	$<4.2 \times 10^{-6}$	1475	4.4	N.D.	N.D.	N.D.	Broken
1D-1[k]	U(C,S) TRISO	OR1602[1]	ThO_2 BISO	OR1652[1]	--	--	N.A.	1.45	3.0	42.9	0.5	3.2×10^{-6}	7.0×10^{-6}	1415	4.6	1.4×10^{-4}[n]	-2.4	-1.8	Excellent condition
1E-3	$(Th,U)O_2$ TRISO	5466-37	ThO_2 BISO	4252-00-010	C-TRISO	3516-147	26.2	0.58	32.2	60.5	14.5	6.9×10^{-7}	$<6.0 \times 10^{-6}$	1445	4.7	1.2×10^{-3}	-1.8	N.D.	Good condition
Cell 2																			
2A-10	UO_2 TRISO	4162-01-020	ThO_2 TRISO	4262-00-050	C-TRISO	3516-149	30.6	0.64	30.4	58.6	13.0	9.7×10^{-6}	4.3×10^{-4}	1220	5.2	5.1×10^{-3}[n]	-0.8	-0.5	Excellent condition
2B-15	UO_2 TRISO	4162-01-020	ThO_2 BISO	4252-00-010	C-TRISO	3516-149	24.8	0.58	24.9	58.3	4.3	5.7×10^{-7}	$<9.1 \times 10^{-6}$	1230	5.3	7.8×10^{-4}	-2.1	-1.6	Excellent condition
2C-7	UO_2 TRISO	4162-01-020	ThO_2 TRISO	4262-00-050	C-TRISO	3516-149	30.3	0.62	31.0	59.4	13.9	4.9×10^{-6}	9.0×10^{-4}	1360	5.4	3.9×10^{-5}[n]	-1.2	-0.9	Excellent condition
2D-16	UO_2 TRISO	4162-01-020	ThO_2 BISO	4252-00-010	C-TRISO	3516-149	29.6	0.59	17.7	60.1	2.1	1.2×10^{-5}	9.8×10^{-6}	1350	5.4	9.1×10^{-4}[n]	-1.9	-1.3	Good condition
Cell 3																			
3A-1[k]	U(C,S) TRISO	OR1602[1]	ThO_2 BISO	OR1652[1]	--	--	N.A.	1.43	5.0	42.7	12.3	4.0×10^{-6}	6.6×10^{-6}	1450	5.1	2.6×10^{-5}[n]	-2.5	-1.8	Excellent condition
3B-9	UC_2 TRISO	4161-00-020	ThC_2 BISO	4251-00-030	C-TRISO	3516-147	33.6	0.66	4.3	60.5	3.7	2.0×10^{-6}	1.3×10^{-5}	1365	5.0	N.D.	N.D.	N.D.	Broken
3C-13	UC_2 TRISO	4161-00-020	ThC_2 BISO	4251-00-030	C-TRISO	3516-147	25.8	0.56	30.7	61.2	2.0	3.1×10^{-6}	$<8.2 \times 10^{-6}$	1350	4.9	2.9×10^{-3}	N.D.	N.D.	Broken
3D-7	UC_2 TRISO	4161-00-020	ThC_2 TRISO	4261-00-010	C-TRISO	3516-147	27.5	0.62	25.2	62.8	0.3	2.7×10^{-6}	6.6×10^{-5}	1375	4.7	9.1×10^{-4}	-0.9	N.D.	Slightly cracked
Cell 4																			
4A-13	UO_2 TRISO	4162-01-020	ThO_2 BISO	4252-00-010	--	--	28.0	0.57	28.7	62.8	5.2	2.7×10^{-7}	$<4.7 \times 10^{-6}$	1335	3.9	5.1×10^{-5}[n]	-3.0	N.D.	Broken
4B-9	UO_2 TRISO	4162-01-020	ThO_2 TRISO	4260-00-050	C-TRISO	3516-149	31.2	0.61	29.3	60.3	7.0	1.2×10^{-5}	1.4×10^{-4}	1300	3.7	3.0×10^{-4}	-0.8	-0.6	Excellent condition
4C-9	UO_2 TRISO	4162-01-020	ThO_2 BISO	4252-00-010	C-TRISO	3516-147	32.7	0.61	30.5	62.1	1.8	1.4×10^{-6}	N.A.	1260	3.6	2.8×10^{-4}	-2.4	-2.4	Excellent condition
4D-9	UO_2 TRISO	4162-01-020	ThO_2 TRISO	4252-00-050	C-TRISO	3516-147	30.5	0.59	28.7	58.7	8.3	1.5×10^{-5}	3.8×10^{-4}	1255	3.4	1.6×10^{-4}[n]	-0.8	-0.8	Excellent condition
Cell 5																			
5X-7	$(Th,U)O_2$ TRISO	5466-37[1]	ThO_2 BISO	4252-00-010	C-TRISO	3516-149	22.8	0.58	28.7	60.0	2.4	1.5×10^{-6}	$<6.0 \times 10^{-6}$	1290	2.4	1.5×10^{-5}[n]	-2.4	-2.2	Excellent condition
5A-19	UO_2 TRISO	4162-01-020	ThO_2 BISO	4252-00-010	--	--	27.2	0.58	31.0	59.9	3.1	5.8×10^{-7}	$<4.9 \times 10^{-6}$	1335	2.2	3.8×10^{-5}	-2.6	-2.8	Excellent condition
5B-7	UO_2 TRISO	4162-01-020	ThO_2 BISO	4252-00-010	--	--	29.5	0.62	25.6	59.4	1.1	8.8×10^{-7}	5.0×10^{-6}	1325	2.0	4.8×10^{-6}	-2.4	-2.3	Excellent condition
5C-9	UC_2 TRISO	4161-00-020	ThC_2 BISO	4251-00-030	C-TRISO	3516-149	29.2	0.56	25.9	61.7	3.5	2.4×10^{-6}	6.6×10^{-6}	1275	1.8	1.8×10^{-5}	-2.6	-2.5	Excellent condition
5D-25	UC_2 TRISO	4161-00-020	ThC_2 TRISO	4261-00-010	C-TRISO	3516-149	31.1	0.61	20.0	62.2	0.4	1.5×10^{-5}	5.8×10^{-6}	1120	1.6	1.6×10^{-5}[n]	-0.8	-0.8	Excellent condition

(a) All fuel rods were nominally 0.49 in. in diameter by 0.73 in. long.

(b) Particles coated in production-scale equipment, except where noted.

(c) Except where noted, fuel rod matrices have 15V pitch for the binder and 6353 natural-flake graphite for the filler. Rods were fabricated by the hot-injection process and were given on 1800°C preirradiation heat-treatment.

(d) Calculated from fired fuel rod dimensions and nominal particle parameters.

(e) Determined from metallographic cross section of a fuel rod from same batch.

(f) Percent variation from the mean uranium loading from end-to-end of the rod.

(g) R/B for Kr-85m at 1400°C.

(h) Determined by hydrolysis test (G Th/G Th). Value indicates amount of exposed thorium.

(i) Corrected to P13M thermocouple decalibration data.

(j) R/B for Kr-85m at 1100°C. Not corrected for steady state.

(k) Rods prepared by slurry-blended, warm-molded process at ORNL. Matrix composition is 31.5 wt % 240 pitch, 53.5 wt % 1074 graphite, and 15.0 wt % Thermax.

(l) Particles coated in laboratory equipment.

(m) N.D. - not determined.

(n) R/B measured at irradiation temperature and extrapolated to 1100°C based on temperature correlation.

TABLE 9-5
FUEL ROD VARIABLES TO BE TESTED IN CAPSULE P13Q

Fuel Rod Position	Expected Fast Neutron Exposure x 10^{-21} $(n/cm^2)(E > 0.18\ MeV)$	Fertile Particle OPyC Density (g/cm^3)	Shim Particle Type	Firing Temp (°C)	Firing Medium	Fuel Rod Fabrication Process
3-1A[a]	4.6	1.80[b]	1099[c]	1800	H451[d]	Hot injection
3-2A[a]	4.6	1.80	1099	1500	H451	Hot injection
3-3A[a]	4.6	1.90[e]	1099	1800	H451	Hot injection
3-1B	5.7	1.80	1099	1800	H451	Admix compaction
3-2B	5.7	1.80	1099	1500	H451	Admix compaction
3-3B	5.7	1.90	1099	1800	H451	Admix compaction
2-1A	7.0	1.80	1099	1800	H451	Admix compaction
2-2A	7.0	1.80	1099	1800	H451	Admix compaction
2-3A[f]	7.0	1.80	1099	1800	H451	Admix compaction
2-1B	7.8	1.80	1099	1800	H451	Hot injection
2-2B	7.8	1.80	1099	1800	H451	Hot injection
2-3B[f]	7.8	1.80	1099	1800	H451	Hot injection
1-1A	8.5	1.80	1099	1800	H451	Admix compaction
1-2A	8.5	1.80	1099	1800	Packed Bed	Admix compaction
1-3A	8.5	1.90	1099	1800	H451	Admix compaction
1-1B	8.9	1.80	1099	1800	H451	Hot injection
1-2B	8.9	1.80	1099	1800	Packed Bed	Hot injection
1-3B	8.9	1.90	1099	1800	H451	Hot injection

[a] Rods 3-1A, 3-2A, and 3-3A will have a central thermocouple hole.

[b] Fertile particle batch No. 6542-01-010; fissile particle batch No. 6151-00-010.

[c] GLCC type 1099 isotropic powder.

[d] Type H451 isotropic graphite tube.

[e] Fertile particle batch No. 6542-02-010; fissile particle batch No. 6151-00-010.

[f] Fuel rod matrix contains 30% type 6353 natural-flake graphite filler. All other matrices contain 40% tvpe 1089 isotropic graphite filler.

Capsules HRB-4 and HRB-5

Capsules HRB-4 and HRB-5 represent a cooperative GGA-ORNL irradiation effort designed to evaluate the irradiation performance of fuel rods fabricated using candidate processes and materials for large HTGR startup and recycle fuel systems. Capsule HRB-4 is a companion capsule to HRB-5, and both capsules were inserted in the beryllium-reflector position of the HFIR on October 8, 1972. Both capsules are designed to operate isothermally with a 1250°C axial (centerline) temperature and are monitored for in-pile fission gas release during irradiation. Capsule HRB-4 is scheduled to be irradiated to a peak fluence of $\sim 8 \times 10^{21}$ n/cm^2 (11 cycles). Capsule HRB-5 was discharged from the beryllium-reflector region of the HFIR in February 1973, after completing its scheduled irradiation (5 cycles) to a peak fast neutron fluence of $\sim 3.6 \times 10^{21}$ n/cm^2.

The GGA samples consisted of six fuel rods (two each of three different types) having nominal dimensions of 0.50 x 1.00 in. These samples include rods fabricated with three different graphite fillers, one binder, and two types of graphite shim material. All rods were fabricated by the admix-compaction process and were carbonized and high-fired in H-327 graphite tubes to simulate in-block curing. The rather low fuel particle loadings specified by ORNL ($\sim$19% of fuel volume) required the use of coated inert particles to simulate higher particle loadings in the rods. The fissile particles (TRISO coated weak acid resins) and inert particles (BISO coated carbon) used in the fuel rods were supplied by ORNL, while the fertile particles (BISO coated ThO_2) were fabricated at GGA. A description of the fuel rods tested in capsules HRB-4 and HRB-5 was given in an earlier Quarterly Progress Report (Gulf-GA-A12422).

After irradiation the fuel rod samples were removed from the capsule at ORNL, visually examined, and then shipped to GGA for further postirradiation examination.

Photographs of the fuel rods taken during the visual examination are shown in Figs. 9-32 through 9-37. All rods were intact and judged to be

PREIRRADIATION

POSTIRRADIATION

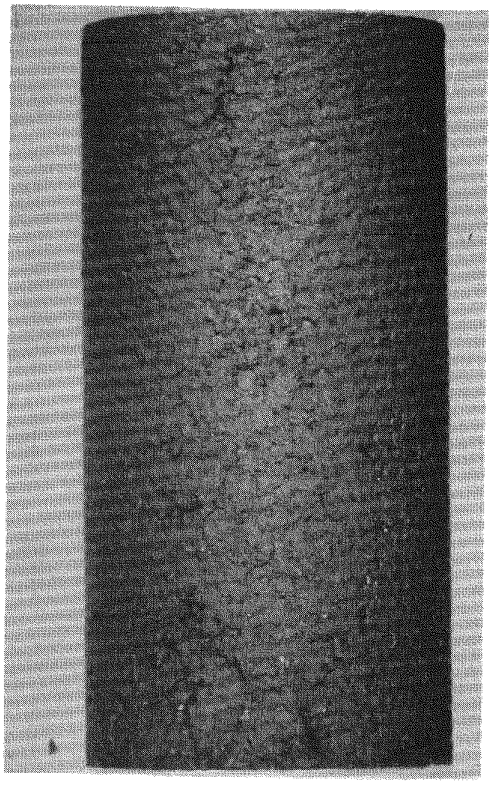

M38305-1 4X

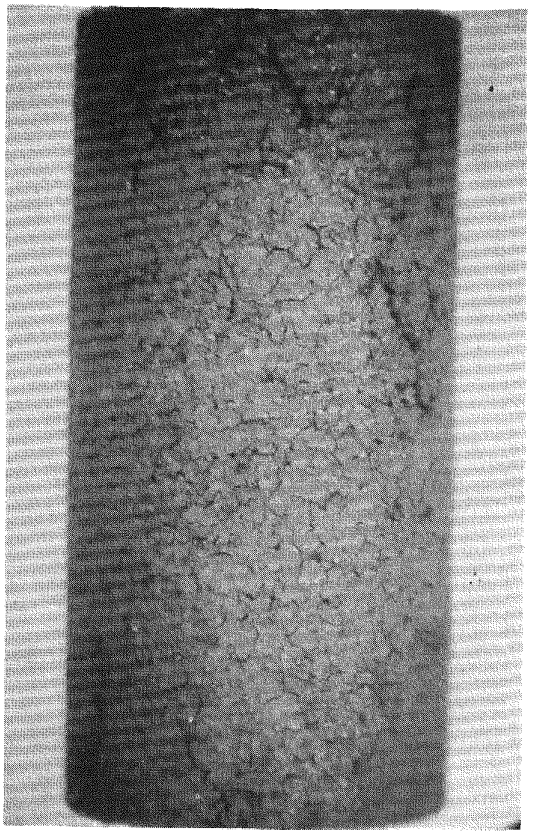

S7328-1 5X

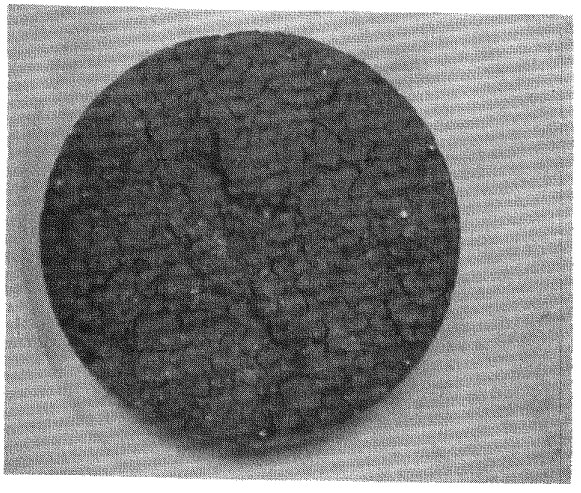

M38305-4 4X

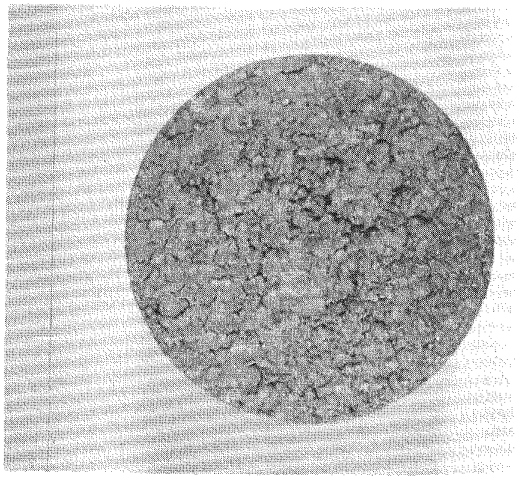

S7328-4 5X

Fig. 9-32. Fuel rod 2A-123 before and after irradiation in capsule HRB-5 to 3.3 x 10^{21} n/cm^2 at 1250°C (design). Rod 2A-123 was fabricated by the admix-compaction process using uncoated GLCC 1099 shim and GLCC 1089 isotropic graphite filler and was high-fired in H-327 graphite tubes to simulate in-block curing. This rod contained TRISO UC_2 (resin) fissile, BISO ThO_2 fertile, and BISO carbon inert particles.

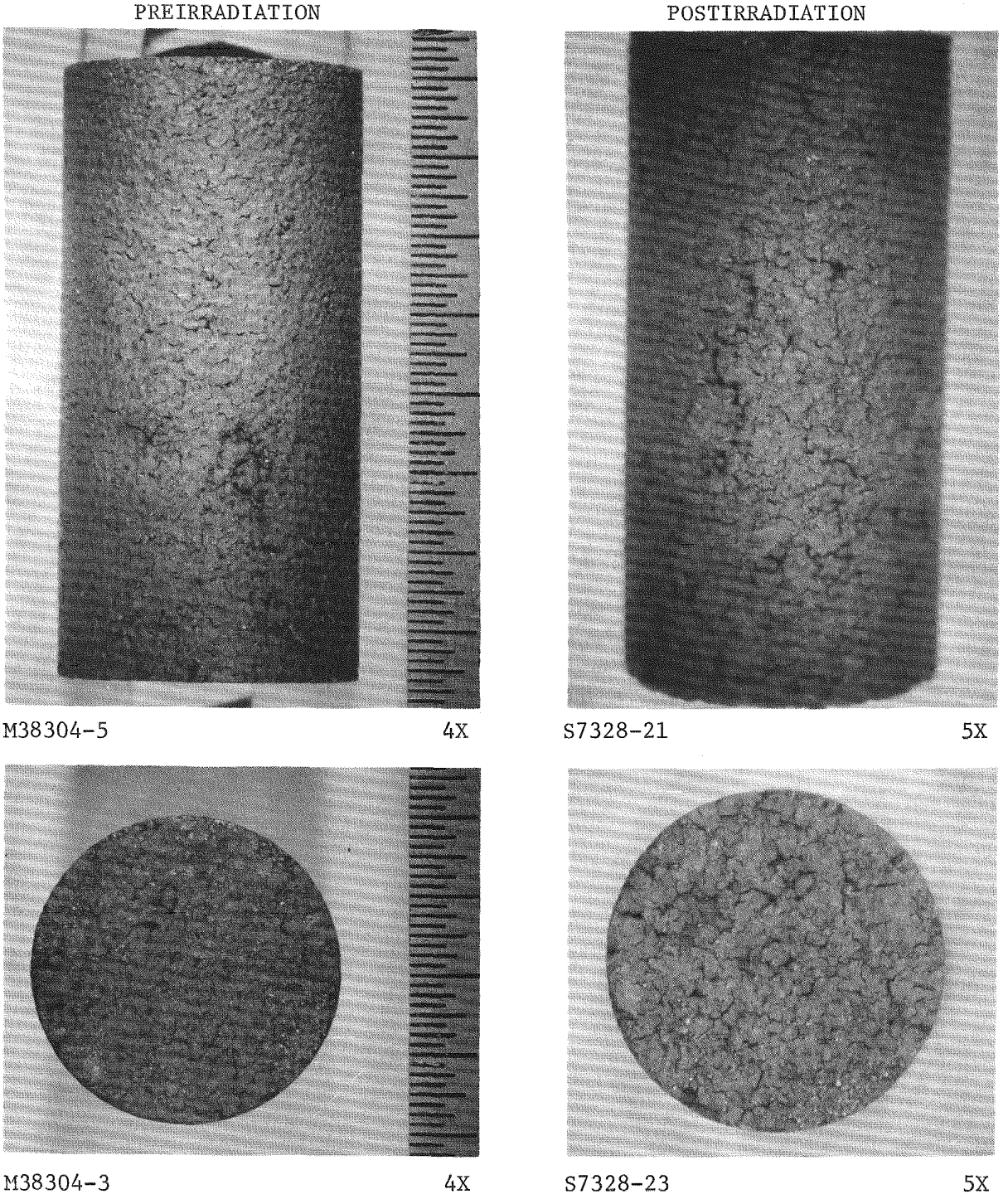

Fig. 9-33. Fuel rod 4A-115 before and after irradiation in capsule HRB-5 to 1.9 x 10^{21} n/cm^2 at 1250°C (design). Rod 4A-115 was fabricated by the admix-compaction process using uncoated GLCC 1099 shim and GLCC 1089 isotropic graphite filler and was high-fired in H-327 graphite tubes to simulate in-block curing. This rod contained TRISO UC_2 (resin) fissile, BISO ThO_2 fertile, and BISO carbon inert particles.

PREIRRADIATION

POSTIRRADIATION

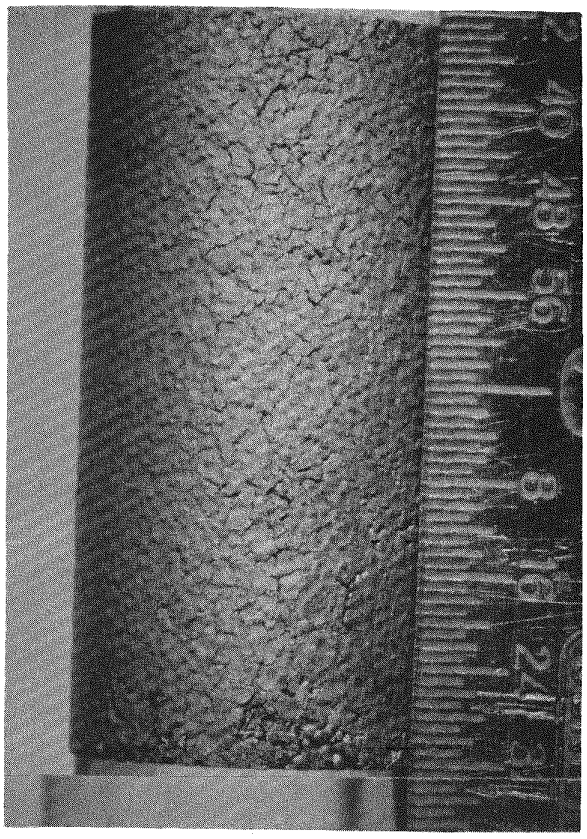

M38356-1 4X

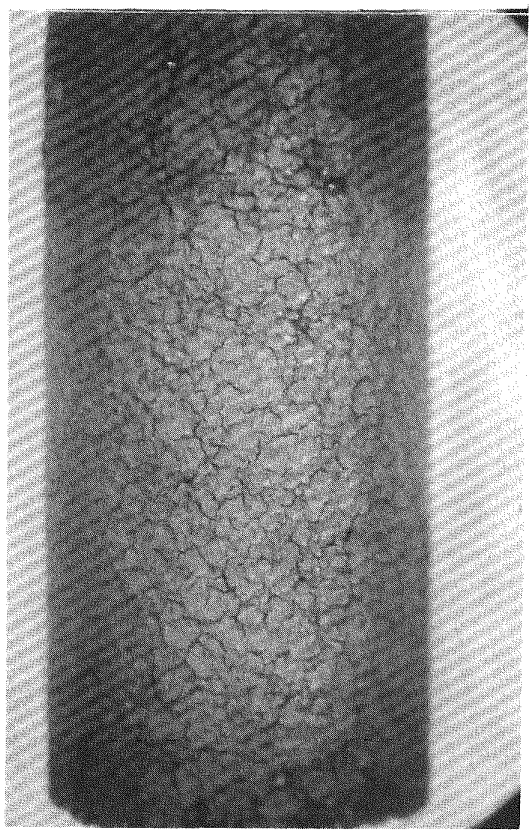

S7328-6 5X

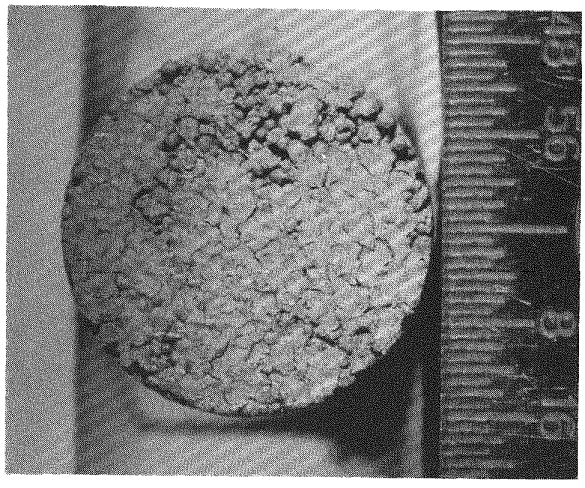

M38356-4 4X

S7328-8 5X

Fig. 9-34. Fuel rod 2B-184 before and after irradiation in capsule HRB-5 to 3.3 x 10^{21} n/cm^2 at 1250°C (design). Rod 2B-184 was fabricated by the admix-compaction process using uncoated GLCC 1099 shim, GLCC 1089 isotropic graphite filler, and Thermax powder and was high-fired in H-327 graphite tubes to simulate in-block curing. This rod contained TRISO UC_2 (resin) fissile, BISO ThO_2 fertile, and BISO carbon inert particles.

PREIRRADIATION

POSTIRRADIATION

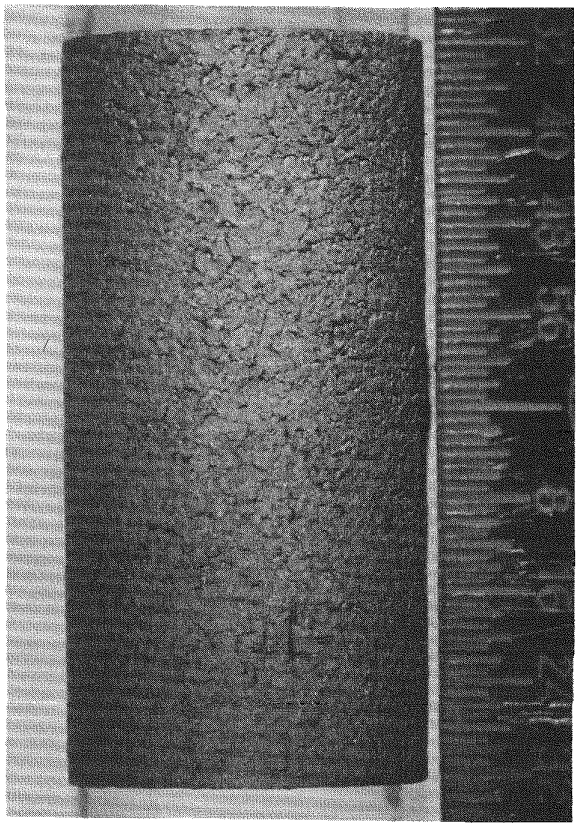

M38342-1 4X

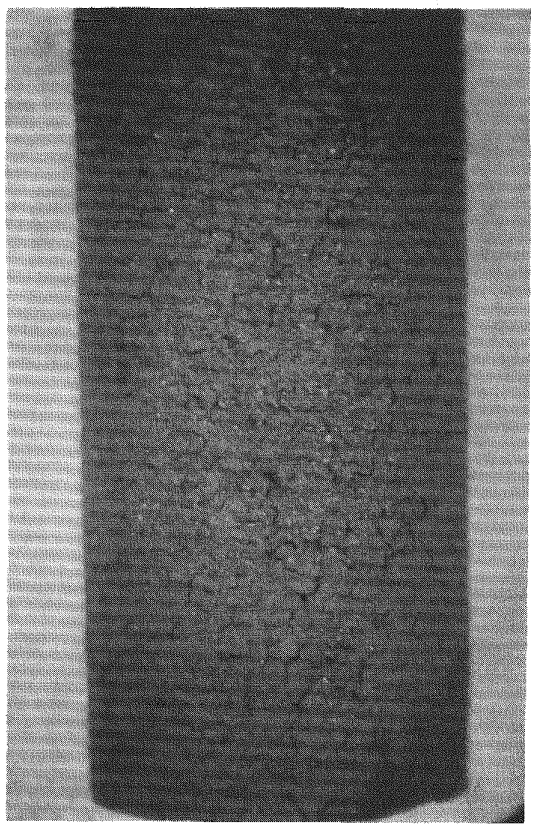

S7328-13 5X

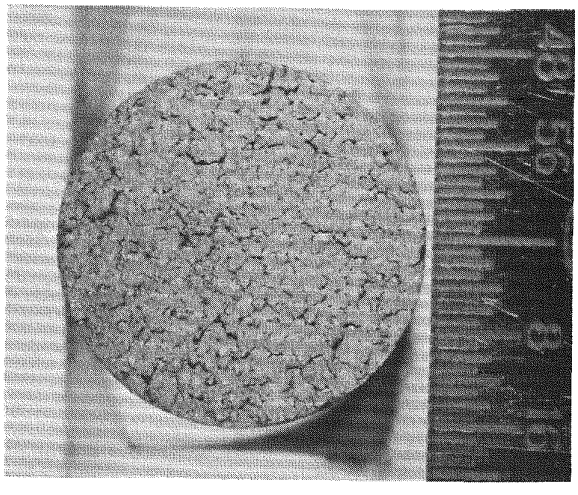

M38342-1 4X

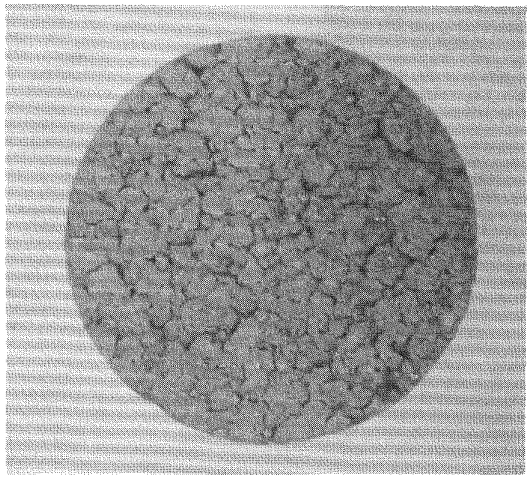

S7328-16 5X

Fig. 9-35. Fuel rod 2C-149 before and after irradiation in capsule HRB-5 to 3.2 x 10^{21} n/cm^2 at 1250°C (design). Rod 2C-149 was fabricated by the admix-compaction process using uncoated RC4 shim and isotropic graphite filler and was high-fired in H-327 graphite tubes to simulate in-block curing. This rod contained TRISO UC_2 (resin) fissile, BISO ThO_2 fertile, and BISO carbon inert particles.

PREIRRADIATION

POSTIRRADIATION

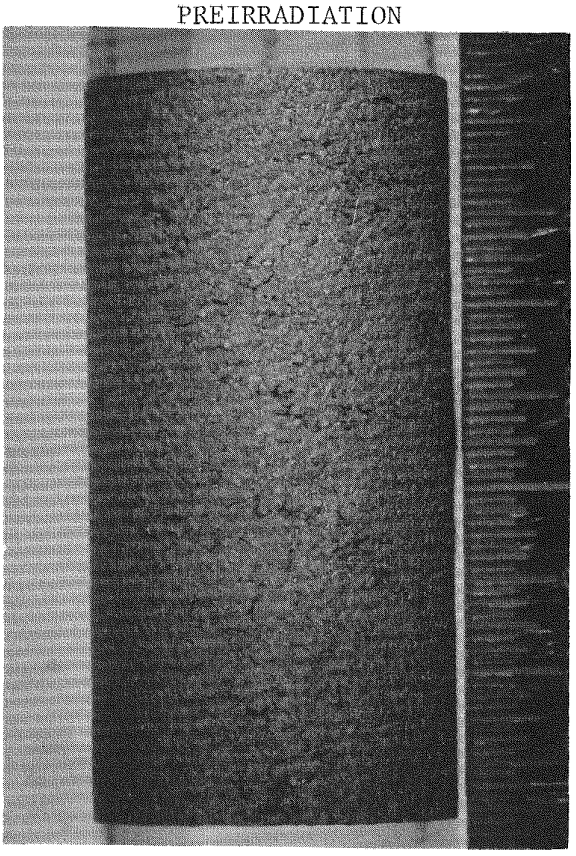

M38343-2 4X

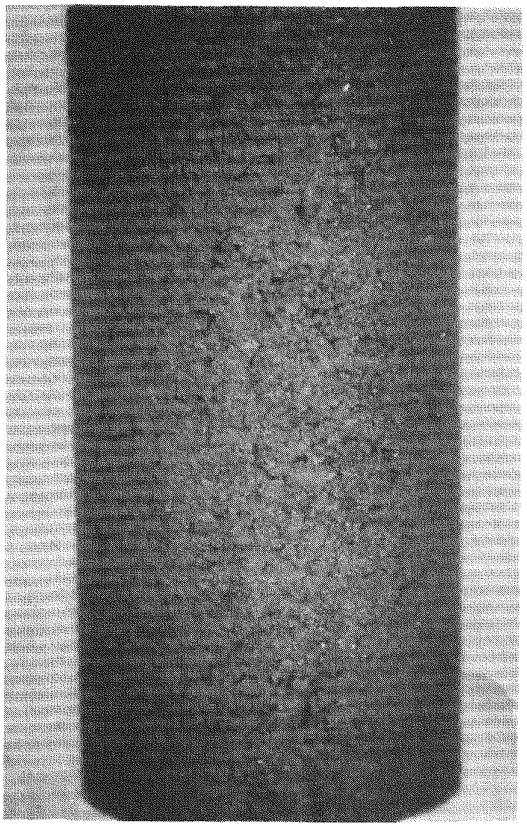

S7328-9 4.2X

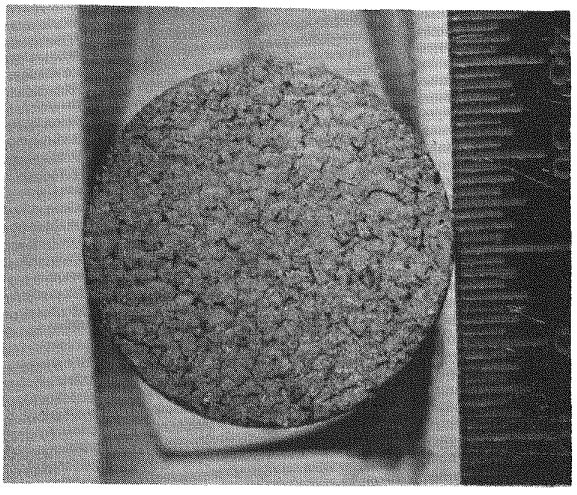

M38343-3 4X

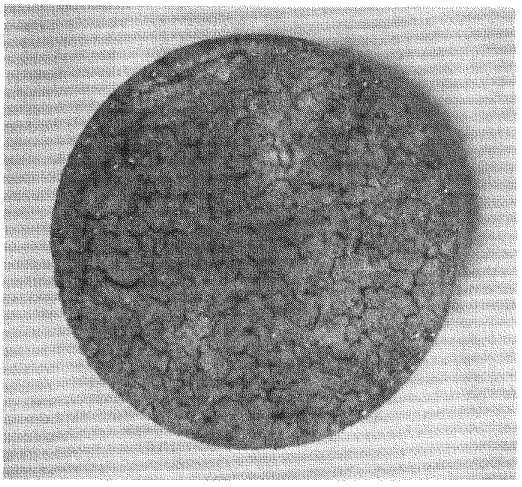

S7328-12 4.2X

Fig. 9-36. Fuel rod 4C-153 before and after irradiation in capsule HRB-5 to 1.1 x 10^{21} n/cm^2 at 1250°C (design). Rod 4C-153 was fabricated by the admix-compaction process using uncoated RC4 shim and isotropic graphite filler and was high-fired in H-327 graphite tubes to simulate in-block curing. This rod contained TRISO UC_2 (resin) fissile, BISO ThO_2 fertile, and BISO carbon inert particles.

PREIRRADIATION

POSTIRRADIATION

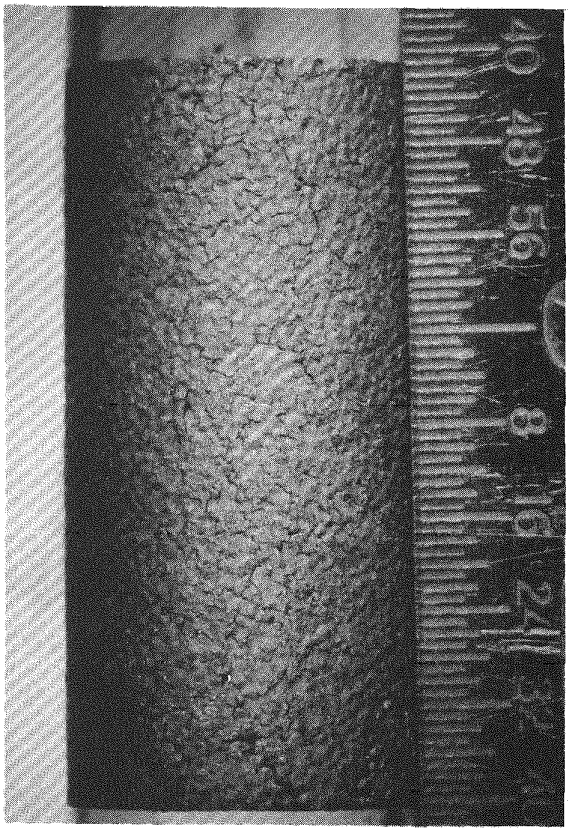

M38354-4 4X

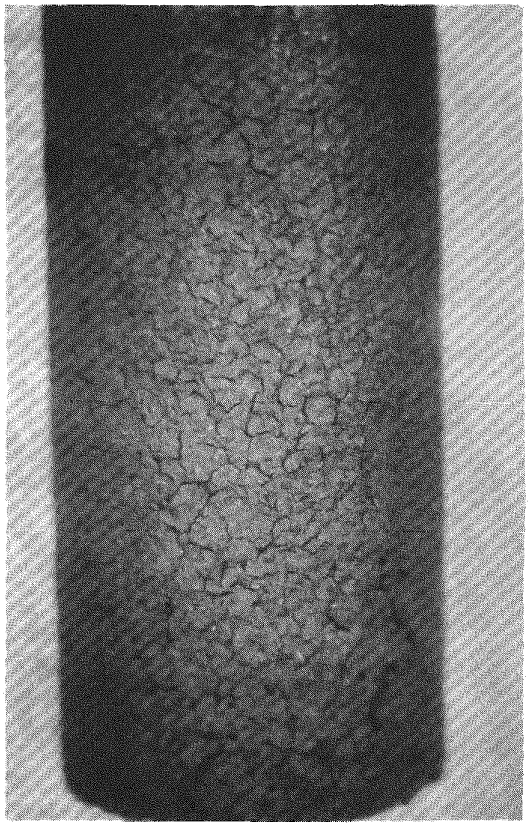

S7328-18 5X

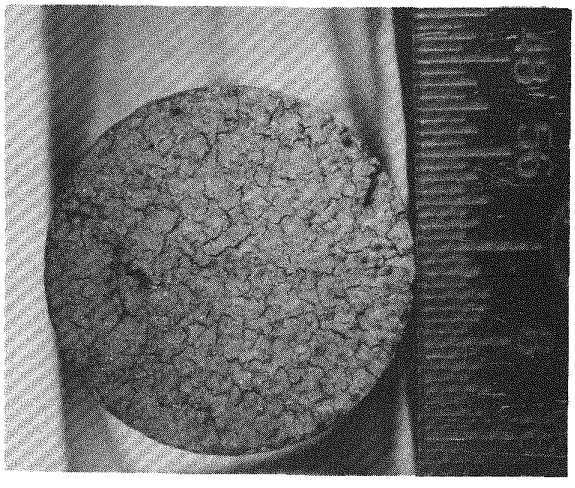

M38354-2 4X

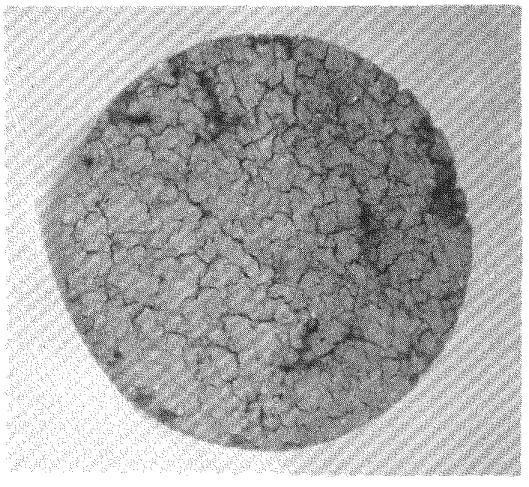

S7328-19 5X

Fig. 9-37. Fuel rod 4B-181 before and after irradiation in capsule HRB-5 to 1.5 x 10^{21} n/cm^2 at 1250°C (design). Rod 4B-181 was fabricated by the admix-compaction process using uncoated GLCC 1099 shim, GLCC 1089 isotropic graphite filler, and Thermax powder and was high-fired in H-327 graphite tubes to simulate in-block curing. This rod contained TRISO UC_2 (resin) fissile, BISO ThO_2 fertile, and BISO carbon inert particles.

in good condition after irradiation. Very little matrix cracking other than that which existed prior to irradiation was observed. A slight amount of particle debonding occurred on the edges of all six rods.

Dimensional change measurements and postirradiation fission gas release measurements (TRIGA activation) were completed; the data are reported in Table 9-6. The dimensional measurements revealed that all rods shrank both radially and axially and that the degree of shrinkage was similar in both directions. The final fission gas release sample taken at the end of irradiation, which represents an average release for all fuel in the capsule, indicated an R/B of 4.7×10^{-5} for Kr-85m. The fission gas release data reported in Table 9-6 for each rod confirm this low release value and indicate relatively good integrity for the several different types of fuel rods irradiated in capsule HRB-5.

Capsule HRB-6

HRB-6 was inserted in the removable target position of the HFIR in early March 1973. Descriptions of fuel rods fabricated at GGA for HRB-6 were given in the previous Quarterly Progress Report (Gulf-GA-A12515). The capsule is being monitored for fission gas release and, from the beginning, release rates of 1×10^{-2} have been observed. Preirradiation fission gas release rates in the six GGA rods included in the experiment yielded a release rate less than 10^{-6}. After observation of the high release rate in HRB-6, ORNL performed fission gas release tests on archive rods from their HRB-6 fuel rod fabrication effort and attributed the high release to rods fabricated in the ORNL U-233 facility. The experiment is continuing to operate with high values for fission gas release.

Capsules HT-12, HT-13, HT-14, and HT-15

The current HT-series (HT-12, -13, -14, and -15) was designed to permit examination of the irradiation behavior of unbonded particle samples of close-to-reference design, BISO coated, 500-μm diameter, sol-gel ThO_2 kernels

during irradiation in the target position of the ORNL HFIR. The coating variables being examined are buffer and OPyC thickness, as well as OPyC density and OPTAF. Each experiment includes particles from seven batches of GGA-coated product and a comparable quantity of ORNL-coated material. A brief description of the GGA particles irradiated in this capsule series was presented in an earlier Quarterly Progress Report (Gulf-GA-A12222).

Capsule HT-12 has completed its irradiation; preliminary observations made while the capsule was unloaded at ORNL were reported in an earlier Quarterly Progress Report (Gulf-GA-A12422). Particles were exposed to fast neutron doses ($E > 0.18$ MeV) of $\sim 4 \times 10^{21}$ n/cm^2 at 1500°C and $\sim 2.5 \times 10^{21}$ n/cm^2 at 1150°C. Further postirradiation examination of these particles at GGA has not been conducted, but density gradient column studies, radiography and metallography are planned for selected particle batches.

Capsule HT-13 completed irradiation and was withdrawn from the HFIR-HT facility in January 1973. A description of the particle samples, estimated irradiation conditions, and results of a visual examination of the HT-13 particle samples is given in Table 9-7. All five particle samples with an OPyC coating density in the range of 1.95 to 2.02 g/cm^3 exhibited complete coating failure during irradiation at 1500°C. The two samples with OPyC coating densities in the range of 1.82 to 1.83 g/cm^3 had slightly lower OPyC failure fractions during irradiation at 1250°C and 0% OPyC failure fractions at 1150°C. The five samples with higher density OPyC coatings exhibited failure fractions ranging from 8 to 100% during irradiation at 1150°C.

The initial results of capsules HT-12 and HT-13 indicate a correlation between OPyC coating density and particle survival during irradiation. In both tests samples with medium-density (1.80 to 1.85 g/cm^3) OPyC coatings performed better than samples with higher OPyC densities. However, some of the particle batches had high density and anisotropy gradients in the OPyC coatings. These large gradients in coating density and OPTAF undoubtedly

TABLE 9-6
DESCRIPTION OF FUEL RODS BEING TESTED IN CAPSULE HRB-5

Sample No.[a]	Coated Particles[b]						Uncoated Shim Particles[d]		Matrix[e]			Particle Packing Fraction[g] (%)	Loading Uniformity[i]		Fission Gas Release[j]	Thorium Contamination[k] (g Th/g Th)	Irradiation Conditions		Postirradiation Examination			
	Fissile[c]		Fertile		Inert[c]				Total Filler[f] (wt %)	Apparent Density[g] (g/cm^3)	Macro-porosity[h] (%)		Uranium	Thorium			Design Temp. (°C)	Estimated Fast Fluence x 10^{-21} (n/cm^2) (E > 0.18 MeV)	Fission Gas Release[j]	Dimensional Change (%)		Visual Appearance of Fuel Rod
	Type	Batch No.	Type	Batch No.	Type	Batch No.	Type	Density (g/cm^3)												Diam.	Length	
HRB-5-2A-123	UC_2-TRISO	4167-01-010	ThO_2-BISO	4252-02-010	C-BISO	4351-00-010	GLCC-1099	1.90	40.21[l]	0.920	32.6	57.53	1.045	1.055	7.116×10^{-6}	$<1.5 \times 10^{-5}$	1250	3.3	4.4×10^{-6}	-2.6	-2.2	Good
HRB-5-4A-115	UC_2-TRISO	4167-01-010	ThO_2-BISO	4252-02-010	C-BISO	4351-00-010	GLCC 1099	1.90	40.21[l]	0.929	32.6	57.38	1.025	1.035	3.098×10^{-6}	$<1.5 \times 10^{-5}$	1250	1.9	2.3×10^{-4}	-2.6	-2.3	Good
HRB-5-2B-184	UC_2-TRISO	4167-01-010	ThO_2-BISO	4252-02-010	C-BISO	4351-00-010	GLCC 1099	1.90	50.45[m]	1.027	24.1	56.62	1.053	1.006	1.947×10^{-6}	$<1.5 \times 10^{-5}$	1250	3.3	4.5×10^{-5}	-2.0	-1.9	Good
HRB-5-4B-181	UC_2-TRISO	4167-01-010	ThO_2-BISO	4252-02-010	C-BISO	4351-00-010	GLCC 1099	1.90	50.45[m]	1.043	24.1	56.72	1.025	1.038	8.013×10^{-6}	$<1.5 \times 10^{-5}$	1250	1.5	4.8×10^{-4}	-2.1	-1.8	Good
HRB-5-2C-149	UC_2-TRISO	4167-01-010	ThO_2-BISO	4252-02-010	C-BISO	4351-00-010	Speer RC4	1.86	40.29[n]	0.907	25.0	57.63	1.024	1.079	3.088×10^{-6}	$<1.5 \times 10^{-5}$	1250	3.2	8.2×10^{-5}	-2.8	-2.6	Good
HRB-5-4C-153	UC_2-TRISO	4167-01-010	ThO_2-BISO	4252-02-010	C-BISO	4351-00-010	Speer RC4	1.86	40.29[n]	0.907	25.0	57.94	1.015	1.020	2.542×10^{-6}	$<1.5 \times 10^{-5}$	1250	1.1	6.3×10^{-6}	-2.2	-2.2	Good

[a] All fuel rods are nominally 0.49 in. in diameter by 1.00 in. long.

[b] Particles coated in production-scale equipment, except where noted.

[c] Particles fabricated at ORNL by the Metals and Ceramic Division; ORNL fissile particle batch No. 52A, ORNL inert particle batch No. 1815.

[d] All shim particles were screened to a final mesh size of -24 +60 (250-μm to 700-μm particle size). Both shim materials are isotropic graphites.

[e] Fuel rods were fabricated by ad-mix compaction using Ashland type A240 petroleum pitch binder and were cured in H-327 graphite tubes (0.495 in. i.d. x 0.850 in. o.d. x 2.0 in. long) at 1800°C.

[f] Measurements made on companion rod from same batch.

[g] Calculated from fired fuel rod dimensions and weights, and mean particle parameters.

[h] Determined from metallographic cross section of a companion fuel rod from the same batch.

[i] Ratio of maximum count rate to mean count rate obtained from γ-ray spectroscopy of both ends of rod (indicative of loading uniformity).

[j] Release rate/birth rate for Kr-85m at 1100°C.

[k] Determined by hydrolysis test. Measurement made on sample to be irradiated. Value indicates amount of exposed thorium.

[l] Nominal filler content; 40 wt % GLCC type 1089 isotropic graphite flour.

[m] Nominal filler content; 40 wt % GLCC type 1089 isotropic graphite flour + 10 wt % Thermax powder.

[n] Nominal filler content; 40 wt % Speer type RC4 isotropic graphite flour.

TABLE 9-7
DESCRIPTION AND RESULTS OF VISUAL EXAMINATION OF GGA SAMPLES IRRADIATED IN HT-13

Batch No.	Diam. (μm)	Buffer		OPyC			Total Particle Diameter (μm)	Capsule Container Number	Irrad. Temp.,[a] (°C)	Calculated Fast Fluence x 10^{-21}[b] (n/cm^2) (E > 0.18 MeV)	OPyC Failure Fraction[c] (%)
		Thickness (μm)	Density (g/cm^3)	Thickness (μm)	Density (g/cm^3)	OPTAF					
4252-02-015	508	83	1.08	75	1.83	1.07	825	40	1150	7.1	0
								27	1500	9.0	88[d]
4252-03-012	501	92	1.00	67	2.00	>1.5[e]	820	43	1150	6.4	100
								30	1500	8.9	100
4252-06-012	514	80	1.10	74	1.82	1.14	819	10	1150	6.4	0
								23	1500	8.9	80
4252-07-016	485	46	1.03	50	1.96[f]	1.20	677	49	1150	4.9	42
								36	1500	8.3	100
4252-08-014	499	39	1.08	119	1.95	1.14	821	2	1150	4.4	94
								15	1500	8.0	100
4252-01-071	495	64	1.11	75	2.02	1.16	811	46	1150	5.7	34
								33	1500	8.6	100
4252-00-013	405	81	1.26	76	2.00	1.14	717	7	1150	5.7	8
								20	1500	8.6	100

[a] Particle temperatures of 1150° or 1500°C estimated on the basis of graphite particle holder temperature of 900° or 1250°C, respectively.

[b] Fast neutron exposures calculated by ORNL.

[c] High-temperature samples contained 75 particles; low-temperature samples contained 53 particles. OPyC failure fraction determined during visual examination conducted at GGA.

[d] Failure fraction determined at ORNL; portion of sample was lost during examination at GGA.

[e] Maximum value measurable by Quality Control instrument is 1.5.

[f] OPyC could not be separated from the buffer layer for a density determination. The value shown was obtained from a grab sample taken during coating.

contributed to the particle failure in some of the samples and will partially obscure correlations between coating thickness, density, and OPTAF.

Capsules HT-17, HT-18, and HT-19

Coated ThO_2 particles from seven particle batches were sent to ORNL for irradiation in experiments HT-17, -18, and -19. The series of particles sent will provide information on the effect of OPyC coating rate, OPyC density, and particle design on the irradiation performance of BISO coated ThO_2 particles to fast neutron exposures of 4×10^{21}, 8×10^{21}, and 12×10^{21} n/cm^2. Samples of TRISO coated ThO_2 particles that will also be irradiated in this series will provide well characterized samples for measurement of the rate of generation and composition of fission gases in ThO_2.

TASK XI
GRAPHITE RESEARCH

INTRODUCTION

Work continued during the quarter to fabricate and prepare capsule OG-1 for the ORR by June 1973. Capsule OG-1 will provide irradiation space primarily for moderator graphite specimens, but will also contain smaller quantities of pyrolytic carbons, silicon carbide, boronated graphites, and fuel stick matrix materials.

CAPSULE DESIGN AND FABRICATION

A description of capsule OG-1 was given in an earlier Quarterly Progress Report (Gulf-GA-A12422). The capsule will operate at 600° to 1400°C to fluences of 0.5 to 3.5 x 10^{21} n/cm^2 (E > 0.18 MeV). Capsule irradiation is scheduled to begin in the C-3 position of the ORR in late June 1973.

All capsule components have been fabricated, and the samples are loaded in the crucibles. The capsule heat transfer gaps were set based on calculations using materials data for the average conditions between beginning and end of life.

Fabrication of a set of containment tubes by ORNL was completed and the tubes are ready for shipment to GGA. Additional lead tube components are still in final preparation at ORNL.

Capsule assembly has begun and will continue through May 1973.

A container is being designed and fabricated to meet the anticipated June shipping date.

The Quality Assurance Plan for operation of capsule OG-1 has been written and is being reviewed for approval. A design report will be issued in May. Procedures required for fabrication and assembly are nearing completion.

GRAPHITE IRRADIATION STUDIES

Several new graphites are under study along with Grade H-327, which is the current reference graphite for HTGR design. A description of these graphites was given in Table 11-1 of the previous Quarterly Progress Report (Gulf-GA-A12515). Additional values of tensile strength and modulus of elasticity have been obtained on specimens from a second log of H-451 and graphites 2020, 9567, and P_3JHAN. The new data are presented in Table 11-1.

The new tensile data were obtained on specimens 0.50 in. in diameter by 4.0 in. long, except for the P_3JHAN specimens, which were 0.25 in. in diameter by 0.90 in. long. The specimens of P_3JHAN were smaller owing to the small amount of material on hand. The procedure was identical except for specimen and specimen holder sizes.

The values for H-451 from the second log were slightly lower than those obtained from the first log tested. The values for 2020 graphite were above 2000 psi in both orientations and well above the purchase specification. Grade 9567 (an oriented extruded needle-coke material) had acceptable strength values in the parallel direction. The P_3JHAN did not meet the guideline specification. These data do not agree with earlier published data* which gave values of 1650 psi in the radial direction and 2120 psi longitudinally. A full log of P_3JHAN is available for further testing of this material.

---

*Mottet, P., J. Rappeneau, J. Love, and P. Cornuault, "Physical and Mechanical Properties of Nuclear Graphites. Their Applications in High Temperature Reactors," in Carbon '72, International Carbon Conf., Baden-Baden, W. Germany, 26-30 June, 1972, p. 183.

TABLE 11-1
STRENGTH AND MODULUS OF ELASTICITY OF NUCLEAR GRAPHITES

Material	Log No.	Orientation	Location in Log	Average Tensile Strength (psi)	Average Modulus of Elasticity x 10^{-6} (chord 250-500 psi) (psi)	Diameter and Length of Specimen (in.)
H-451	II	∥	Mid-length center	1656	1.2	0.5 x 4.02
	II	⊥	Mid-length center	1338	0.96	0.5 x 4.02
	II	⊥	Mid-length edge	1600	0.95	0.5 x 4.02
2020	II	∥	Center	2061	0.99	0.5 x 4.02
	II	∥	Edge	2753	1.09	0.5 x 4.02
	II	⊥	Center	2704	1.40	0.5 x 4.02
	II	⊥	Edge	2737	1.47	0.5 x 4.02
9567	II	∥	Center	1820	1.38	0.5 x 4.02
	II	∥	Edge	2568	1.63	0.5 x 4.02
	II	⊥	Center	1081	0.71	0.5 x 4.02
	II	⊥	Edge	1076	0.65	0.5 x 4.02
P_3JHAN	--	∥	--	1249	1.44	0.25 x 0.90
	--	⊥	--	1241	0.85	0.25 x 0.90

An effort is currently under way to measure Poisson's ratio of H-327 and H-451 graphites using strain gage techniques. Work has been directed toward obtaining test and recording equipment, constructing strain gage completion and calibration units for use with bi-axial gages, and developing techniques for bonding the gages to graphite specimens.

A Poisson's ratio of approximately 0.15 was obtained on a specimen of H-451 graphite.

PYROLYTIC CARBON IRRADIATION STUDIES

The dimensional and density changes of unrestrained pyrolytic carbon and silicon-doped carbons irradiated in piggyback positions in capsule P13M have been measured and analyzed. The data are consistent with previous data obtained from other irradiation capsules in that the high-density LTI carbons ($\rho > 2$ g/cm^3) have expanded in volume somewhat and have large dimensional changes, while the low- and intermediate-density LTI carbons have densified with lower dimensional changes. As reported previously for data from other capsules, the dimensional changes of the silicon-doped carbons are less than those of the pure carbons. Specimens were also irradiated restrained on sapphire spheres, a situation where all of the dimensional changes have to be accommodated by creep and elastic strains. Only the silicon-doped carbons survived the irradiation without fracturing.

The dimensional changes of unrestrained pyrolytic carbons irradiated in piggyback positions in capsule P13N have been measured and are now being analyzed.

APPENDIX

PROJECT REPORTS PUBLISHED DURING THE QUARTER

Scott, C. B., "Thermochemical Stability of Irradiated HTGR Fuel Particles," USAEC Report Gulf-GA-B12409, Gulf General Atomic, May 1, 1973.